REFRACTORY COATINGS FOR CONTAINMENT OF MOLTEN REACTIVE METALS AND THEIR ALLOYS

Hui Su

B.E. Northeast University of Technology, Shenyang, China, 1984
M.E. Northeast University of Technology, Shenyang, China, 1987

A dissertation submitted to the faculty of the
Oregon Graduate Institute of Science & Technology
in partial fulfillment of the
requirements for the degree
Doctor of Philosophy
in
Materials Science

October 1996

The Dissertation "**Refractory Coatings for Containment of Molten Reactive Metals and Their Alloys**" by Hui Su has been examined and approved by following Examination Committee:

Milton R. Scholl, Thesis Advisor
Assistant Professor

James T. Stanley, Thesis Advisor
President, Material Software

David G. Atteridge
Professor

Jack H. Devletian
Professor

ACKNOWLEDGMENT

I would like to express my sincerest appreciation to my thesis advisors, Dr. Milton Scholl and Dr. James T. Stanley, for their guidance, support and patience through this work. I also wish to thank the other members of my dissertation committee, Dr. David Atteridge and Dr. Jack H. Devletian for their time and effort spent as committee members and examining my dissertation and sharing their professional opinions.

I am grateful to Dr. Don Mc Murchie for his invaluable help in the plasma spraying laboratory. I would also like to acknowledge Dr. Jack Mccarthy and Mr. Steven Brooks for their help and cooperation in SEM and TEM analysis and melting experiments. I would like to express my appreciation to Dr. Paul Clayton, my four year SPC chairman, for his invaluable advice and help in my course curriculum. I also would like to thank Department Head Dr. Bill Wood for his help, especially for the final year financial support.

I would like to thank my fellow students at OGI: Hua Li, Youping Gao, Xihong Wang, Shiliang Ding, Lu Fang, Xiaoyen Su, W.Y. Shen, Jun Ding, Nong Jin, Badih J. Rask, Cangsang Zhao, Dawei Shen, Wei Su, Xiao Chen for their help and friendship.

I would like to thank Oregon Metallurgical Corporation and the Oregon Metal Initiative for sponsoring this projects.

Finally I would like to thank my wife Ding Ding for her love, never ending support, encouragement and patience, and my parents for their spiritual and emotional support.

TABLE OF CONTENTS

LIST OF TABLES

LIST OF FIGURES

ABSTRACT

REFRACTORY COATINGS FOR CONTAINMENT OF MOLTEN REACTIVE METALS AND THEIR ALLOYS

Hui Su

Supervising Professors: Milton Scholl
James T. Stanley

The primary difficulty with continuous casting of reactive metals, specially titanium and its alloys, is the inability of current crucible materials to withstand the rigors of prolonged exposure to the high temperatures and reactive environment necessary to process reactive metals. Crucible material selection and crucible fabrication will be critical to successful continuous cast technology of reactive metals. Thermodynamic analysis was employed to choose the potential crucible compounds for molten reactive metals and to explain the experimental results. Plasma spraying technology was used to build multi-layer crucibles. Resistive and induction melting techniques were used to investigate the actual high temperature thermodynamics and interface reactions between molten reactive metals (titanium and titanium aluminide) and crucible coatings.

Experimental results and thermodynamic analysis showed that Y_2O_3 has the highest stability and lowest oxygen contamination for contact with molten titanium, which confirmed the importance of Y_2O_3 as a containment material. Its disadvantage was a low thermal shock resistance. The complex oxide, $SrZrO_3$, was identified as another potential candidate that showed real potential for containment of molten titanium. At 1760°C for 30 minutes, a low zirconium content but no detectable strontium was found in titanium, and titanium oxygen contamination was the second lowest .

CaO-stabilized ZrO_2, Y_2O_3-stabilized ZrO_2, $CaTiO_3$, and $CaZrO_3$ crucibles were eliminated for containment of molten titanium because these compounds severely contaminated titanium. Of three degradation mechanisms of the ceramic coating: dissolution, reaction and erosion, dissolution was the main mechanism observed. A general thermodynamic procedure was developed to choose the potential crucible compounds for molten reactive metals using the compound free energy and the oxide solubility in molten reactive metals as the most primary factors for selection.

CHAPTER 1

INTRODUCTION

Reactive metals, as a group, have advanced to become a major contributor to the competitive manufacturing technology base, varying from the field of medicine to key materials of the aerospace transportation infrastructure. These metals, including titanium, zirconium, and niobium, due to their unique properties such as high temperature stability, outstanding strength-to-weight ratios, and high corrosion resistance, achieved both in pure and alloyed forms, continue to serve as key enabling structural materials. Contributions continue to improve mechanisms and systems for advanced medical diagnostics, more efficient and reliable aircraft transportation, and security for the environment from toxic byproducts of today's complex production activities. As a group, these metals and their alloys hold tremendous potential for a growing array of critical developments that will make major contribution to the nation's industrial competitive future.(1)

However, the applications of reactive metals and their alloys in any form in other industries, such as automobile industries, are often limited by cost considerations. It is well known that application of titanium to automobile engines holds great promise for longer life, high performance and enhanced fuel efficiency. Reactive metals and their alloys are the expensive structural materials. Although titanium is the world's fourth most abundant structural metal, in the cast form, titanium costs several times more than stainless steel and is about equal in cost to highly alloyed nickel-base alloys. Reduced manufacturing costs are essential if the full potential of titanium is to be realized.(2) The cost impact of application is tied to ensuring that properties needed for the task are satisfied. The development of a processing capability is very necessary, which will provide improved cost effective manufacturing technology for reactive metals in diverse non-aerospace application.

Some structural alloys also have a high requirement for purity. The superalloys used for gas turbine disks, blades and vanes in jet engines require strength at high temperatures and corrosion resistance, and also must provide various properties such ductility, castability, formability and weldability. A strict parts per million order value of impurity elements and inclusions in these alloy was set to insure strength and life under the conditions in which they are used. Effects are made to further lower the impurities content. This is because creep and other various characteristics of the alloy changes greatly even with the slightest change in the impurity content, mainly with oxygen, nitrogen and sulfur.(3)

In electronic industry, there are also many requirements for extremely low gas, homogeneous, clean and high purity advanced metals and alloys. The applications include sputtering targets for high density magnetic recording media and head materials such as Co-Cr, Co-Ni, Tb-Te-Co, Mn-Sb, Fe-Al-Si, Ni-Fe, Co-Nb-Zr, superconductor mother alloys for in-situ Cu-Nb wire and also high temperature Cu-Ba-Y and Cu-Ca-Sr oxides. The principle materials used for high density magnetic recording are ferromagnetic alloys used in recording films and high permeability soft magnetic alloys used in the read/write heads. Many of these alloys contain reactive elements such as Sm, Nd, Tb, Dy and Gd as well as refractory metals such as Cr, Nb, Mo Ta and V. High vapor pressure elements such as Mn, Sb and Bi, and precious metals such as Pt, Re, Rh and Ru are also sometimes included.(4)

Magnetic characteristics have a preference in the development of these materials. The alloy behavior, however, present new challenges due to reactivity and segregation. Arc melting and electron melting are two methods which first come to mind in the production of these alloys, but both present some drawbacks with respect to alloy control. Another conventional fabrication method is powder sintering, but with this method, the target will contain a great deal of oxygen contamination due to its porosity.(4)

The specific reactive metal used as the basis of the development work was titanium. Of the reactive metals, melting titanium and its alloys is a challenging task because of its high melting point and marked affinity for interstitial atoms (i.e. oxygen and carbon). This research focused on containment of molten titanium and titanium aluminide.

In recent years, titanium and its alloys have been under intense development for critical application in the aerospace, chemical and related industries.(5) Its superior strength- to-weight ratio has resulted in important advances to air frame and jet engine design. Undoubtedly titanium, in the form of designed high purity alloys, has achieved a great contribution in jet turbine technology.(1) It's excellent high temperature properties and creep resistance have enabled jet turbines to achieve 90,000 lbs of thrust.

Nevertheless, other applications have evolved that utilize properties important to jet engine and additional qualities such as corrosion resistance. Titanium is strongly resistant to oxidizing environments and, where properly alloyed, to mild reducing environments. As a consequence, titanium exhibits exceptional resistance to a broad array of acids, alkalis, and a range of industrial chemicals and byproducts. Titanium is immune to sea water and overall corrosion attack in the marine environment. This property combined with its superior erosion, cavitation and wear resistance, and its high strength to weight ratio make it an excellent choice for marine applications. The combination of all these properties has driven key applications in the marine, energy and chemical, and environmental industries. Specific component application examples include heat exchangers, condensers, pump systems, ball valves, chemical process piping and storage systems, nuclear waste storage systems, medical implants, food processing equipment and recreational/sports equipment. Use of large amounts of titanium and its alloys has been realized in spite of costly limitations in processing and specifically melting technology.(5)

As with most metals, a high degree of ductility is required for any structural application of titanium.(6) Relatively low levels of interstitial impurities such as oxygen, nitrogen, hydrogen, and carbon cause significant degradation in the ductility of titanium and its alloys. Finlay and Snyder(7) reported that less than 0.1% of either nitrogen or oxygen in high-purity alpha titanium, although doubting the reported strength of pure titanium, reduced its ductility by approximately 50%.

If titanium is to be a useful structural material it must be fabricated readily. Few materials are as difficult to melt satisfactorily as titanium and its alloys due to its high affinity for impurities and the extremely high temperatures required for processing. In addition, molten titanium is highly reactive and will reduce most common refractory materials such as oxides, carbides, and nitrides.(5) Therefore the processing of titanium in the molten state is a major source of interstitial contamination. Every conventional known crucible material is attacked to some degree by molten titanium, so that crucible melting can be used only when contamination can be tolerated.(6)

A number of arc-melting practices that avoid molten titanium contacting other materials have been developed to solve the problems caused by the extreme reactivity of titanium, sensitivity to interstitial elements and lack of an inert crucible and mold.(8) These processes can be divided into two distinct types: nonconsumable electrodes of graphite or tungsten and consumable electrodes of titanium.(6) Consumable electrode arc melting in water-cooled copper molds using inert atmospheres is utilized for all large ingots. This process requires precise electrode fabrication to avoid ingot inhomogeneity (because only a fraction of the metal is molten at one time), and solidification patterns are sensitive to electrode characteristics. Thus, remelting is necessary to assure homogeneous and flaw-free ingots, adding significantly to the cost.(8) The process has also been modified by "skull melting," wherein a layer of titanium is frozen against the copper crucible and acts as the inside wall in contact with the molten metal. Because of rapid heat loss by conduction from the titanium through the solid metal and crucible wall, the power required for melting is high and the amount of molten metal is relatively small. This condition is not conducive to homogeneity when alloys are being produced. In addition to the technical difficulty the arc-melting process using a water-cooled copper crucible is hazardous due to close proximity of the water to the molten metal. This design favors a build up of hydrogen gas due to electrolysis of water from minute fissures.(6) Other disadvantages of this process include splattering of molten metal, difficulties in controlling total power input, and potential crucible perforation due to arc-wandering.(9) While skull melting provides an almost completely molten charge, it is severely restricted because of lack of superheat control and size limitation.(8) Electron beam skull melting, which allows greater superheat control than the consumable electrode process, is limited by the requirement for larger crucibles, more expensive equipment, and lower power efficiency.(9)

Current triple VAR (Vacuum Arc Remelting) processing for aerospace application results in high manufacturing costs due to multi-remelting, heat treatment and forging etc. The expense of titanium and its alloys has limited broader utilization, even when appropriate life cycle costing analysis is applied.(1) One cost-driver in consumable arc melting is that scrap recycling is low because of the difficulty and added operations involved in recycling revert into a fabricated or compressed arc electrode. A new melting technology is eagerly needed by the titanium industry to reduce the cost of titanium substantially.

Continuous cast processing has radically changed the steel, and nickel industries and it is beginning to profoundly affect the aluminum industry. Development of an effective continuous cast process translates to quantum reduction in processing costs, improved energy efficiency, quicker response rates, improved alloy quality and greater targeting of desired alloy properties. To obtain bar, sheet or plate stock, titanium must be then forged or rolled to final shape. Because of the high strength and high melting temperature of titanium, forging is an energy and time intense process which adds significant cost to the final product. Addition, the forging process results in an extremely low yield of between 40 and 60%. The continuous casting process is expected to eliminate all the steps after production of the titanium sponge. The ability to continuously cast thin cross section titanium and other reactive metals will have a significant impact on the reactive metals industry.(1)

Based on the example of steel, nickel and aluminum and OREMET's (Oregon Metallurgical Corporation) projections of the effect of new casting technology on the reactive metals industry, the following primary benefits will result from the successful conclusion:(1)

> <u>Critical reduction in costs</u> - Firstly, there will be a critical reduction in costs associated with the manufacturing of the material. This reduction in cost will come from reduced energy use, improved yield and improvements in efficiency.
>
> <u>Long term and short term, there will be improvement in properties</u> - Secondly, based on the experience of the steel and nickel industry, the quality of cast titanium will be improved over the short term with improved homogeneity,

reduced grain size and better chemistry control. In the long term, again based on the experience of the nickel and steel industries, it is expected that new alloys with improved or targeted properties will result from an increased market and associated competitive cost advantages.

Titanium will be able to compete in the commercial sector of the market - Representatives of the automotive industry indicate that the projected cost of continuous cast titanium would open significant new areas for exploitation by the titanium industry. Examples include fasteners and valve heads. This is just one sector of many industrial sectors wherein the competitive use of titanium will expand rapidly with the adoption of continuous casting technology.

Continuous cast technology has more advantages than current VAR processing. Nevertheless only in a limited manner, has the reactive metal industry pursued the idea of continuous cast technology. A number of attempts to develop a continuous casting technology for titanium have been tried in the last decade. The attempts could be classified into two types. The first type used current vacuum induction cold crucible melt technology with some type of electromagnetic stirring to maintain reduced contact between the metal pool wall and the molten material.(10) Although there has been limited success with alloy control and ingot quality, the energy requirements associated with the technique were extreme and scalability has been difficult or impossible. The second type of technology was based on a variation of the rapid solidification technology of spin casting. While this technique had some potential for thin sheet material, there were a number of problems with its use as a commercial process which has severely limited its application.(11) These problems stemmed from the difficulty with control of the molten metal stream. If, indeed, there was a straight translation between continuous cast steel and nickel to the reactive metals industry, there would be pilot scale plants in operation today. However, reactive metals offer forbidding challenges to continuous casting technology. Specifically, there are several problems which must be addressed before continuous casting can become a reality for the reactive metals industry.

The primary difficulty with reactive metals is the high reactivity they possess in the molten state. Liquid titanium has been described as the "Universal Solvent" for its ability to dissolve and/or react with most common materials. This reactivity makes it extremely difficult to design effective inexpensive mold materials to contain the molten material. All current methods for melting titanium use technology where the molten titanium does not come into contact with any material other than solid titanium. A typical example is the use of a cold hearth crucible for skull melting. In this technique, a cold copper crucible is used to contain the titanium which is heated by a central heat source such as a plasma torch or electron beam. The extreme thermal gradients in the melt pool allow the outer material to remain solid while the inner molten material is refined and processed.

The reactive metals, in general, melt at relatively high temperatures over 1700°C opposed to the 1300 to 1500°C temperatures required for processing steel or 600°C for aluminum alloys. The high temperatures put severe thermal mechanical stresses on any crucible material which may be able to withstand the corrosive effect of the molten metal.

The viscosity of the molten reactive material near the solidification temperature is high and therefore prevents easy flow of the material into the mold. It is possible to cast titanium and the other reactive metals by ingenious use of sharp thermal gradients and other techniques. However, the high viscosity of the molten metal at the solidification temperature makes it extremely difficult to translate these techniques to continuous cast technology. It is necessary to maintain a high superheat at the throat or transition region between the crucible and the mold to allow a continuous flow of material: a critical barrier to development of a continuous cast technology for the reactive metals industry.(1)

The primary difficulty with continuous casting of titanium and all other reactive metals is the inability of current crucible materials to withstand the rigors of prolonged exposure to the high temperatures and reactive environment necessary to process titanium. Crucible material selection and crucible fabrication will then be critical to continuous cast technology of titanium. Obviously, an inert material developed for crucible application could also be used as mold or mold facing, allowing much higher mold temperatures to be used in precision casting. An inert crucible is also useful for melting and remelting of high purity reactive metals and alloys other than titanium.

In this study, the results of past work in this area were reviewed and used along with thermodynamic and other considerations to generate a list of materials for experimental evaluation. Crucible fabrication technologies were compared and chosen, and building procedures were decided. The interaction between reactive metals and the candidate materials in resistive and induction melting experiments were then evaluated. Thermodynamic principles were employed to analyze the experimental results and to explain mechanisms of crucible (coating) degradation.

The objectives of this study are:

- To give a general thermodynamic procedure to choose the potential crucible compounds for molten reactive metals and discuss the effects of the most important factors on compound selection.
- To investigate the interactions between molten titanium (or titanium aluminide) and ceramic coatings and study the mechanisms of coating degradation using microstructural and composition microanalysis and thermodynamic analysis.

- To explore new potential crucible compounds for titanium melting using bothexperimental and theoretical approaches.

CHAPTER 2

LITERATURE REVIEW

In this chapter, the requirements of reactive metals for crucibles will be described; the previous experimental results in both ceramic crucibles and coated crucibles are reviewed, specially in titanium melting; the main conclusions and progress are summarized, and existing problems are pointed out.

TITANIUM CHARACTERISTICS AND CRUCIBLE REQUIREMENTS

Working with molten titanium is a great technical challenge. Titanium has a high melting point (~1668°C) and is highly reactive at high temperatures. In addition, titanium absorbs large amounts of oxygen, nitrogen and carbon, while only a small fraction of these interstitial elements can be detrimental to mechanical properties. Consequently, refractory materials such as oxides, carbides and nitrides, when dissolved, contaminate the metal, causing loss of desired properties. An adequate container material, then, should have the following properties:(5,8)

(a) inert or nearly inert to molten titanium. If reaction (reduction, etc.) occurs, the elements involved should not deleteriously affect the engineering properties of the metal;

(b) sufficient thermal shock resistance to survive repeated usage and thermal gradients during heating. This will ensure that the crucibles can be reused many times;

(c) essentially unaffected by air and moisture at room temperature so no specific requirements are needed for storage of crucibles;

(e) non-toxic. It is safe to workers and community;

(f) a potential of reasonable availability, durability, and cost in order to be accepted by reactive metals industry;

(g) a low vapor pressure so that it can be used for high vacuum conditions;

(h) the crucible should also be hard and dense for continuous casting technology to withstand a large volume of flowing molten metals.

CERAMIC CRUCIBLES FOR MELTING OF TITANIUM AND ALLOYS

Weber, et al.(6), have summarized research up to 1957 on molten titanium reactivity with container materials. They note experimental work on ThO_2, W, Mo, Mo_3Al and other carbides, oxides, nitrides, sulfides, borides, silicides, fluorides, complex oxyfluorides and intermetallics. Eastwood and Craighead(12) examined a large number of oxides, carbides, nitrides, silicides, and refractory metals (Mo and W) and concluded that, with the possible exception of zirconia, all were reactive. None of the materials appeared to be much better than carbon. Stabilized zirconia was the only refractory not wetted by the titanium melt. Oxygen was absorbed, however, to produce a high titanium hardness, but the Zr content of the ingot was generally low, possibly indicting that the ZrO_2 was partly reduced and that the lower oxides of zirconium might be useful. Repeated melts could not be prepared in the same stabilized zirconia crucible because of failure as the ingot cooled.

Weber, et al.(6) examined oxygen-deficient zirconia as a crucible material and developed a number of compositions modified by titanium. The 12 atomic percent Ti-ZrO_2 composition was shown to be inert to molten titanium for short times (< 1 minute) with little superheat, suggesting the reaction resistance may be caused by a Ti saturated ZrO_2 phase.

Eisenberg and Stavrolakis(13) investigated the usefulness of fluoride and complex oxyfluoride refractories. The lack of stability of the synthesized refractories severely limited their resistance to molten titanium. Several of the complex oxyfluorides were considered to be superior to stabilized zirconia, but hardness tests indicated a high degree of contamination as a result of reaction with the crucible material.

Intermetallic compounds in the systems Zr-Si, Zr-Al, Mo-Al, and Mo-Zr were investigated by Crandall et al. (14) Although most of the intermetallics were too reactive with molten titanium, Mo_3Al showed some promise when the contaminants introduced by the crucible could act as alloying ingredients in the melt.

Several reports have been issued by Chapin and Friske(15) of the Naval Research Laboratory on oxides, carbon, graphite, carbides, and sulfides. It was generally concluded that all the materials investigated lacked the desirable inertness as all reacted with Ti in varying degrees of severity. The melts were contaminated by reaction products which caused hardness increases, embrittlement, and duplex microstructure.

Cubic CaO-stabilized ZrO_2 remained stable at all temperatures. Both cubic and monoclinic phases were observed at room temperature in Ti-modified ZrO_2 compositions. The cubic phase formed only under special sintering conditions. The specimens were not homogeneous, and free metal was evident in polished sections. The occurrence of solid solution between the metal and the oxide has not yet been established.

Excellent thermal-shock resistance was exhibited by all Ti-ZrO_2 compositions, even though the reversible monoclinic-to-tetragonal transformation occurred.(16)

Since Weber et al's work(6,16) on titanium-modified zirconia, little experimentation on refractory ceramic materials for melting has been reported. Garfinkle and Davis(17) investigated the type of CrB_2, TaB_2, $MoSi_2$, and CeS and found CeS to be the most resistant material to attack, although dissolution of the sulfide was observed. Eastman et al.(18) also reported that CeS and ThS crucibles can be used as containers for all molten metals (with the exception of platinum) which melt at temperatures below 1800°C. However their data on titanium indicted that considerable reaction between CeS and titanium occurred as the melting temperature reported was as low as 1500°C.

Data from weight-change measurements, chemical analyses, metallographic and petrographic analysis, microhardness studies, and electron probe analyses indicated that Ti contents up to 4 atomic % were retained in substitutional solid solution in ZrO_2. Data from metallographic analyses, microhardness sties, lattice parameter measurements, and electron probe analyses indicated that Zr and O from ZrO_2 contents up to approximately 10 mole % were retained in solid solution in Ti. In this case, the Zr entered the Ti lattice substitutionally and the oxygen entered interstitially. There also was evidence that the amount of solid solution on both sides of the diagram increased with increasing temperature. No evidence of compound formation was observed at any composition.(19)

In reaction couple tests shown in Table 2.1 and Figure 2.1,(8) metallographic and microhardness traverses indicted a reaction with CeO_2 and Eu_2O_3. Y_2O_3, Er_2O_3, Ho_2O_3 and Dy_2O_3 were least reactive with a questionable reaction of La_2O_3, Tb_4O_7 and Pr_6O_{11}. The latter two oxides were reacted in the fully oxidized form and could be expected to lose oxygen in vacuum until a M_2O_3 stoichiometry was reached. The higher hardness levels observed for these oxides might be due to this decomposition. Several hardness traces were shown in Figure 2.1 to illustrate the various reactions.

Based on the reaction couple test results above, the reactivity of Y_2O_3, Dy_2O_3, Gd_2O_3, Pr_6O_{11}, Ce_2O_3, oxygen-deficient Y_2O_3, 5Ti-ZrO_2, HfC, and pyrolytic BN was evaluated in the liquid metal-oxide interaction tests. For melting studies, a consumable/nonconsumable arc melting furnace and porous refractory compound disks were utilized. Metallographic evaluation indicated extensive reaction with Ce_2O_3, BN, 5Ti-ZrO_2, and HfC. In all cases the lowest hardness values were greater than 200 VHN as measured furthest from the reaction interface. The interface typically showed extensive dissolution of the materials and severe interstitial hardening; Figure 2.2 illustrates a typical hardness variation with distance for the reaction of Ti-modified ZrO_2 and Ti. The interface was quite brittle, cracked, and irregular and the oxide shows grain-boundary reduction to an oxygen-rich zirconium metal. This phenomena was also observed in the reaction couples of yttria stabilized zirconia, where titanium acts as an "oxygen sink" with reduced grain boundaries in the zirconia. In the latter case, yttrium first precipitated in the grain boundaries as a zirconate, tentatively identified as $Y_2Zr_2O_7$, which in turn decomposed with increasing time.

Table 2.1 Reaction couples(8)

A - detectable hardness gradient or ∂ - case

B - no gradient, average metal hardness < 200 VHN

C- significant oxygen hardening > 200 VHN

oxide	Temp (°C)	Time (hour)	Reaction Type, (Average DPH)
Y_2O_3	1000	12, 15	B (174)
	1200	20	B (177)
CeO_2	1000	12, 15, 62	A

(Table 2.1 continued)			
	1200	20	C (329)
Nd_2O_3	1000	12, 126	C (206) (251)
	1200	24, 57	C (270) (341)
Pr_6O_{11}	1000	20	B, C (199)
	1200	20	B (171) (173)
Er_2O_3	1000	20, 62	A
	1200	20	B (180)
Ho_2O_3	1000	15	B, C (213)
	1200	20	B (180)
Eu_2O_3.	1000	12, 62	A
La_2O_3	1000	62	B (188)
	1200	20	C (261)
Yb_2O_3	1000	100	B (194)
	1200	20	A
Dy_2O_3	1000	15	B (175)
	1200	16	B (172)
Tb_4O_7	1000	12	B (191)
	1200	20	B (262)
Sm_2O_3	1000	15, 24	B (184) (162)
	1200	24	B (184) (162)
10 mole% Y_2O_3-ZrO_2	900	24, 120	A
	1000	24, 120	A

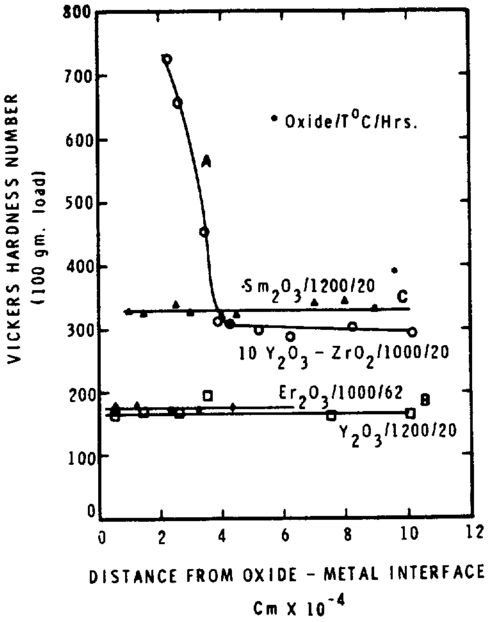

Figure 2.1 Typical variation of hardness with distance for the three reaction types.(8)

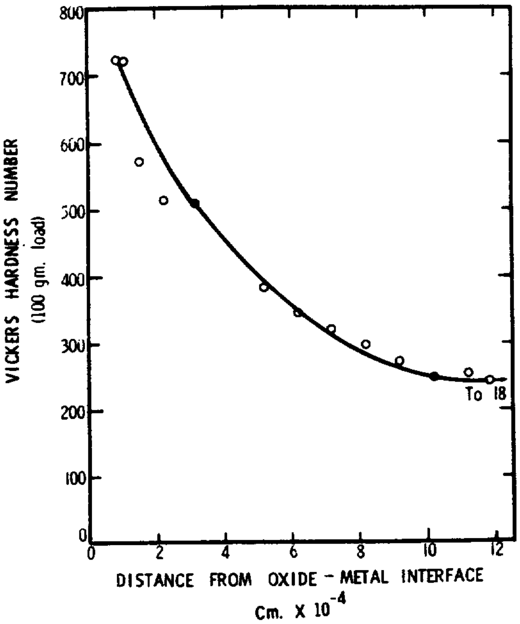

Figure 2.2 Variation of hardness with distance for 5 atomic percent Ti-ZrO2 under arc melting condition (5 minute exposure).(8)

Comparative melts with Pr_2O_3, Gd_2O_3, and Dy_2O_3 showed slight reaction. Some dissolution occurred as evidenced by the precipitation of small dendrites or particles closely adjacent to the interface. Though no significant hardness increase was noted over the base composition, unlike the first two, submicron alpha grains, perhaps indicating more solid solubility for Dy in Ti. Therefore, caution must be exercised in the interpretation of hardness values for metal in contact with these more stable oxides. Precipitation of the oxides reduced the total interstitial level of the metal significantly, while at the same time the presence of fine oxide particles might increase the apparent hardness.

Yttrium oxide showed less reaction than Dy_2O_3, Gd_2O_3, Pr_6O_{11}, Ce_2O_3, oxygen-deficient Y_2O_3, 5Ti-ZrO_2, HfC and pyrolytic BN. When exposed for the same time at equivalent power levels no dendrite precipitation was observed. A few submicron particles were present, adjacent to the interface, but no interface degradation was observed. With increased exposure and consequent heating of the yttria, reaction and dissolution did occur, leading to flower-like yttria dendrites and particles within the grains and prior beta grain boundaries. On cooling, no precipitation of fine particles in alpha grain boundaries or within alpha grains was observed. Precipitation of large dendrites and dendrite-like particles in prior beta grain boundaries indicated formation near or above the solidus temperatures. After precipitation, metal hardness values fell in the 140 to 170 VHN (124 BHN, 500 kg) range, approximately equivalent to Ti-50A titanium. Lattice parameters measurements for such titanium indicated some oxygen increase in solution. One specimen containing numerous dendrites (approximately 0.7 x 0.5 x 0.2 in.) was cold rolled to a 0.020-in. strip and two small tensile coupons removed; (gage dimensions - 0.5 x 0.01 x 0.125 in.). The specimens were encapsulated in Vycor, annealed at 400°C for 60 hours and exhibited tensile ultimates of 52,670 and 51,680 psi, a 0.2 percent yield of 42,970 and 37,580 psi with 15.4 and 20.9 percent elongation, respectively. Considerable necking was observed. Therefore, even though dissolution might occur at high superheats, the precipitation of the oxide as yttria occurred, leading to matrix tensile properties equivalent to or lower than those of Ti-50A.

Two crucible melts were made with substoichiometric yttria: 1780°C for 10 minutes and 1730°C for 2 minutes. The former contained an estimated 2 percent or less second-phase yttria particles as dendrite flowers and small elongated particles (Figure 2.3). Hardness was Rb81. The second, as expected, showed significantly less yttria as a second phase and was free from the flower-like dendrites. Cold-wall induction melting condition was also utilized for yttria crucibles, and holding time was 1/2 to 1 minute after visible melting. As expected, darkening of the oxidized yttria occurred at the metal oxide interface and in most cases wetting was apparent. Typical metal cross sections exhibited no dendritic yttria but several fine Y_2O_3 particles adjacent to the interface (Figure 2.4). Metal hardness was 143 ± 4 VHN (113 BHN, 500 kg). From the darkened zone it was obvious that titanium was locally reducing the yttria to a lower oxygen stoichiometry, though the total oxygen entering the metal was minor. Diffusion and melting experiments indicated potential for the use of nonstoichiometric yttria as a container for liquid titanium.

Experiments had shown that substoichiometric (reduced) Y_2O_{3-x} offers more resistance to attack by molten titanium, due to lower oxygen potential, but was subject to increased uptake of yttrium into solution. Yttria reacted with and contaminated molten titanium having greater than 100°C superheat and where the crucible temperature was equal to or exceeds the melt temperature. The yttrium taken into solution, however, scavenged oxygen from the titanium solution and precipitated as Y_2O_{3-x}, reducing interstitial to acceptable levels. Normal cold-wall induction melting, using greater metal

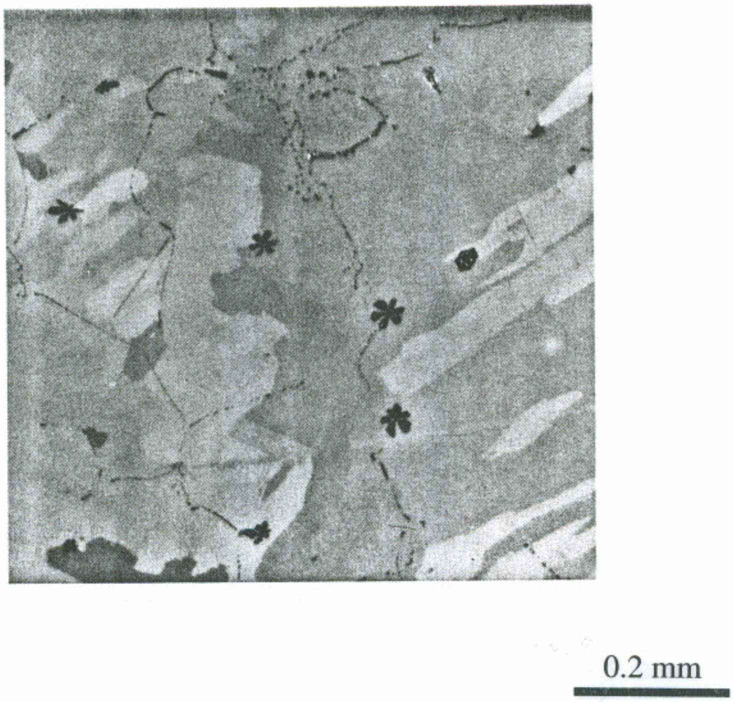

Figure 2.3 Titanium microstructure after melting at 1780°C for 10 minutes. Dark second phase is yttria as flower-like dendrites or particles on prior beta grain boundaries.(8)

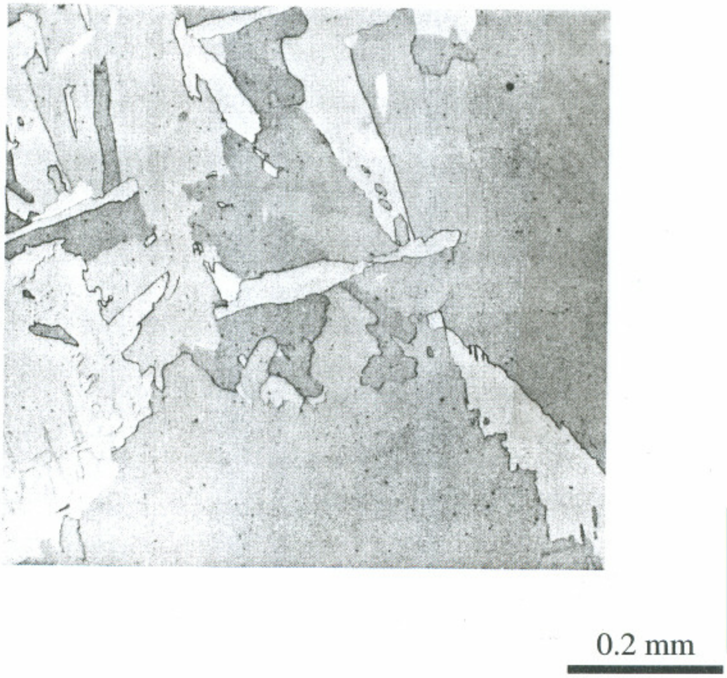

Figure 2.4 Titanium microstructure after induction melting (~1 minute, melt time).(8)

mass to contact area in a substoichiometric yttria crucible yielded high quality titanium metal, comparable to some grades of present commercially pure metal.(5)

Helferich and Zanis's experiments concluded that molten titanium partially dissociated yttrium oxide, resulting in limited interstitial oxygen contamination of the titanium and in the formation of a titanium-yttrium-oxygen eutectic phase in the cast microstructure. Variation in the density of the crucibles over the range of 70% to 97% of theoretical had no measurable effect on the extent of melt contamination. Although up to 1.93% yttrium and 0.56% oxygen were picked up from the crucible, comparison of the results of this investigation with previous studies on refractory oxides indicated that yttrium oxide appeared to be the best candidate crucible material for melting titanium, even though the yttrium oxide melts were superheated to higher temperatures and held for longer times. Table 2.2 compares the results obtained in this investigation to the results of earlier studies using similar size thorium oxide and beryllium oxide crucibles. These data indicated that the yttrium oxide crucibles displayed lower levels of melt contamination than the other oxides, even though the yttrium oxide melts were superheated to higher temperatures and held for longer times. It should be noted that prior to their investigation, thorium oxide was generally considered the most stable refractory oxide in contact with molten titanium.(9)

Schuyler and Petrusha had reported that for low-melting (near 1430°C) titanium alloys such as Ti-13Cu-1.5Al and Ti-2.8Be. A melt of the Ti-2.8Be control alloy made in the candidate ceramic crucibles displayed the contamination levels shown in Table 2.3. The crucible materials are arranged according to their total contamination level with the best performing system (least contamination) listed first. It is readily apparent that Y_2O_3 base compositions performed best in limiting contamination of the low-melting titanium alloy. Based on chemical analysis, ThO_2, CeS, pyrographite, and CaO also displayed reasonably low reactivity. However, multiple melts made in CaO showed a wide range of results and this material was considered too erratic for continued work.

Table 2.2 Comparison of crucible performance for yttrium oxide crucibles to that of thorium and beryllium oxide crucibles.(9)

	Melting Parameters			Titanium Contamination		
Crucible Materials	Atmosphere	Superheat Temp. °C	Holding Time minutes	Oxygen, wt%	Calculated Oxide, wt%	Average Titanium Hardness
Yttrium Oxide	Vacuum	50	5	0.2 to 0.56	0.7 to 2.5 (Y_2O_3)	130 HK
Thorium Oxide	Argon/ Vacuum	25	4	0.4 to 1.2	3.1 to 10.6 (ThO_2)	245 DPH
Beryllium	Argon/ Vacuum	25	1	2.4 to 8.8	3.6 to 13.6 (BeO)	650 DPH

Table 2.3 Contamination of Ti-2.7Be melts made in ceramic crucibles (2)

* Alloy held molten at 1577°C (2870°F) for 10 minutes
* Results are an average of multiple tests and given as the amount above base alloy content (typical pre-melt oxygen level in alloy was 0.168%)

Nominal Crucible composition	oxygen (wt %)	Crucible elements (wt %)	Total (wt %)
Y_2O_3	0.13	0.17	0.30
Y_2O_3.15Ti	0.25	0.17	0.42
REO (60% Y_2O_3)	0.47	0.16	0.63
Y_2O_3.8Ti	0.68	0.08	0.76
REO (60% Y_2O_3). 8Ti	0.63	0.16	0.79
CaO.15Ti	1.06	1.01	1.07
CaO	0.94	0.22	1.16
ThO_2	0.57	0.63	1.20
Dy_2O_3	0.95	0.48	1.43
REO (60% Y_2O_3). 15Ti	1.70	0.07	1.79
REO (75% CeO_2)	3.10	0.03	3.13
MgO	3.41	0.01	3.42
La_2O_3	Deteriorated--	unable to test	
Pyrographite	0.02	0.58	0.60
CeS	0.03	0.75	0.78
SiC	0.02	13.34	13.32

Microstructural examination indicated that melts made in pyrographite and CeS developed extensive second phase networks compared to scattered blocky inclusions developed in melts made in Y_2O_3, ThO_2, Dy_2O_3 and REO crucibles. This tendency to form extensive second phases eliminated pyrographite and CeS from further consideration for use as melting crucibles. Experimental results of melting of Ti-10Cu, Ti-16Cu and Ti-9Fe alloys in Y_2O_3, Y_2O_3-15Ti, ThO_2 and Y_2O_3 based REO crucible systems again indicated high Y_2O_3 materials were superior in limiting contamination of low melting alloys. In addition, results of these melt runs show that temperature was of considerable importance in controlling melt contamination.

At the conclusion of laboratory melt runs, Y_2O_3 was clearly the best material for minimizing reaction with low-melting titanium alloys. However pure Y_2O_3 crucibles displayed a poor thermal shock resistance (TSR) as evidenced by their gross cracking on cooling to room temperature, whereas similar cracking as not observed with titanium modified Y_2O_3 crucibles. Y_2O_3-15Ti was therefore selected as the primary melting crucible material based upon its superior TSR and capability for multiple melts in the casting activity. A Y_2O_3 + potassium-silicate composition was identified as the best material for fabricating a low reactivity mold facecoat system. The presence of Y_2O_3 inclusions in low-melting titanium alloy casting did not appear to adversely influence tensile properties; axial high-cycle-fatigue tests showed no tendency for failures to initiate at Y_2O_3 inclusions.(2)

Koch et al's result(20) showed that small titanium and zirconium casting can be made successfully in rammed zircon sand ($ZrSiO_4$) mold. Zirconia mold and core washed (water or isopropyl alcohol bases) are very effective for inhibiting metal-mold reactions for the largest castings produced. Zircon sand ($ZrSiO_4$) is considered to the most refractory of the common foundry sands (fusion point 2426°C) and produces a superior finish on heavy-walled ferrous castings. The quantity of sodium silicate (waterglass) binder used had a very important effect on the quality of the casting produced. 93 - 95 wt % zirconia and 5 - 7 wt % sodium silicated solution was used for the mold.

Thermodynamically calcia (CaO) is one of the most stable oxides. Its reactivity to various molten metals is extremely low and it is therefore an excellent candidate for a crucible material. Degawa et al(21) reported that the oxygen contamination of Ti using calcia crucible was caused by the reaction of molten Ti and low grade oxides especially Fe_2O_3 and SiO_2. The application of high purity fused calcia crucibles enabled the melting of titanium with less contamination by reducing the oxygen content in titanium below 0.2%. Contamination from the crucibles (Ca, Fe, Si and Mg) was minimal. Despite the problems of scaling and handling in melting Ti and precision casting, calcia was expected to become useful in the future.

Single crystal CaO substrates has a better non-wetting characteristic than MgO, Y_2O_3 stabilized ZrO_2 and Al_2O_3. The CaO-polycrystalline substrates show almost the same excellent non-wetting characteristics as the single crystal CaO, especially in the high purity Ar atmosphere (99.999%). For all the tested ceramics, higher the purity of Ar, the better the non-wetting characteristic. The oxygen content in Ti drops with the increasing purity of Ar, which confirms that Ar with purity more than 99.999% was needed to obtain an excellent Ti casting with low oxygen content.(22)

Attempts to use calcia as melting refractory were conducted as early as the 1870's in Europe but the first well documented work with successful results was W. A. Fisher et al in the 1950's when they employed a calcia crucible in an equilibrium test with molten high carbon steel. In the United States, in the latter half of the 1950's, calcia crucibles were used to melting uranium alloys.(4) Currently, calcia is seldomly used as crucible material due to its two essential drawbacks: hydration in air and slagging with acid oxides. Because of these drawbacks, manufacturing and storage of calcia crucibles are difficult, limiting its use mainly to the laboratory. In recent years, refractory technologies including hydration resistance and sintering methods, were developed and improved for the practical use of calcia.

Calcia crucibles are expected to be useful for Vacuum Induction Melting (VIM) and precision casting molds.(23) The metal refine technology using the calcia crucibles with VIM is defined as the "Calcia Refining Process" because the calcia crucible can provide effective refining such as deoxidization, desulphurization, denitrization and the removal of inclusions.

Intermetallic compounds with the unique combination of hardness, strength, high temperature resistance and low density are being studied as future materials, and many of the compounds contain large amounts of highly reactive elements such as Al and Ti. In the TiAl binary there are three kinds of intermetallic compounds, Ti_3Al, TiAl, and $TiAl_3$. In particular TiAl is now drawing attention as a light-weight heat resistant alloy because it provides a specific strength larger than that of Ni-base superalloys. By employing calcia crucibles, alloys were cast with an oxygen content under 1000 ppm. There is a significant difference in UTS among samples with different Ti and Al ratios, but no dependence on oxygen content. However, there is a strong oxygen content dependence of elongation below 2000 ppm for any composition of TiAl, the lower the oxygen content, the higher the elongation. 2000 ppm oxygen should be considered the maximum allowable content for the minimum ductility design specification of TiAl casting. There were no inclusions in a TiAl matrix with up to 3000 ppm oxygen, and the major composition of inclusions observed is the same as the crucible materials such as Al_2O_3 and ZrO_2. The oxygen content has a more significant effect than inclusions on hardness of TiAl ingots. The surface condition of TiAl precision cast parts, which includes contamination layer depth and smoothness, is very important for ductility, even though the contamination is not serious. The shape memory alloys, NiTi has been mainly melted in graphite crucibles, but contamination such as carbon and oxygen, and nonuniformity were a problem. By using a calcia crucible, a clean NiTi with low oxygen and carbon contents is obtainable, and an improvement in corrosion resistance and fatigue characteristics is expected.(4)

CERAMIC CRUCIBLES FOR MELTING OF OTHER REACTIVE METALS

With the calcia refining process, an effective refining reaction occurs from the calcia crucible wall, providing optimum conditions for the production remelting of Ni-base superalloy. An example of re-melting a Ni-base superalloy is shown in Table 2.4. It can be seen that by using the calcia refining process, not only is the gas and sulfur content lowered but that there is little contamination caused by calcia. Further prospects for practical uses are expected not only with calcia but with calcia-magnesia crucibles.(4)

Chromium is an excellent anti-corrosion and anti-oxidation metal. Because metallic Cr has a high melting point (near 1990°C) and is very brittle, its application has been limited. By appropriately using a calcia crucible it has become possible to develop corrosion resistant materials of pure Cr and high Cr alloys. Various satisfactory high Cr alloys such as Cr-Fe, Cr-Al , etc. have been produced by using the calcia crucibles.(4)

Using calcia crucibles, low gas content clean and homogeneous target alloys can be obtained. Tables 2.5 and 2.6 show summarized results of gas contents in various target alloys, which clearly show the superiority of calcia refined targets. For Ni-Fe and Fe-Al-Si melt in calcia crucibles, the permeable magnetic percentage values rose 2-3 time compared to alloys melted in the conventional manner. Another great advantage is that

Table 2.4 Chemical composition of remelted Mar M-247 using various crucibles held at 1323 k for 20 minutes at a 1.3 x 10^{-2} Pa vacuum(4)

	Contaminant Elements (mass ppm)					
Crucibles	O	N	S	Si	Zr	Ca
MgO	6	10	9	290	600	< 1
Al_2O_3	6	9	6	310	600	< 1
ZrO_2	16	9	6	430	5600	--
CaO	< 5	< 5	3	190	600	< 10

Table 2.5 Gas content in target alloys for recording film using the calcia refining process(4)

Compositions	gas	MES Calcia Refining Grade	Commercial Grade
Co-Ni	O	< 10 ppm	50 - 100 ppm
	N	< 10	20 - 50
Co-Cr	O	< 10	50 - 200
	N	< 10	20 - 100
Fe-Tb-Co	O	200 - 500	900 - 1300
	N	20 - 50	100 - 200

Table 2.6 Impurities in target alloys for read/write head using the calcia refining process(4)

Compositions	impurity	MES Calcia Refining Grade	Commercial Grade
Fe-Al-Si	O	< 10 ppm	20 - 50 ppm
	N	< 5	20 - 50
	S	< 1	30 - 50
	C	< 10	30 - 50
Ni-Fe	O	< 10	50 - 100
	N	< 10	10 - 50
	S	< 5	30 - 100
	C	< 10	150 - 2000
Co-Zr-Nb	O	50 - 100	150 - 2000
	N	< 20	30 - 100

Table 2.7 Comparison of size distribution of inclusions distribution in a 3.5 GPa Maraging steel between normal and calcia melting(4)

<table>
<tr><td></td><td colspan="7">Number/mm^2</td><td></td></tr>
<tr><td></td><td>Total</td><td colspan="6">0.5 1.0 2.5 4.0 6.5</td><td>Volume (%)</td></tr>
<tr><td>By Calcia Melted</td><td>0.35</td><td>0.06</td><td>0.09</td><td>0.16</td><td>0.03</td><td>0.01</td><td>0.00</td><td>0.018</td></tr>
<tr><td>Conventional Melted</td><td>5.17</td><td>0.26</td><td>1.03</td><td>2.85</td><td>0.59</td><td>0.47</td><td>0.07</td><td>0.435</td></tr>
</table>

batch uniformity is super, which is especially important in magneto-optical use. Compared with targets such as powder sintered alloy, the magnetic stability was increased remarkably.

High cleanliness and low gas content are the main characteristics of calcia refined alloys. These characteristics are especially effective in improving the quality of the Maraging steel. A size distribution of inclusions is given in Table 2.7 while Figure 2.5 shows the results of increased fatigue strength with a decreased deviation by using the Calcia Refining Process. It is now of being utilized for high quality springs in computer equipment, especially in high speed line printers.

Vacuum-induction melting (VIM) of uranium and its alloys commonly utilizes graphite crucibles and components that are typically coated with crucible/mould washes of yttria and zirconia. Carbon contamination 33 ± 15 ppm by weight of the uranium and/or alloys can be detected. The carbon /carbide contamination has very undesirable effects on metallurgical properties. A new material (Tribocor 532N, an alloy produced by Fansteel, Inc., of 50 wt% niobium, 30 wt% titanium, 20 wt% tungsten nitrided at >1800°C) has been shown to be relatively inert with uranium and its alloys, thus, is an ideal candidate material for a noncarbon crucible/susceptor. The Tribocor 532 N material is a heavily nitrided metal and thus has a very hard outer layer consisting mostly of titanium nitride. The hard, abrasion-resistant surface of Tribocor 532 N prevents gouging and puncturing upon loading heavy uranium parts. A main source of the uranium-graphite reaction as contribution to carbon pick-up.

Testing with the Tribocor 532N crucible showed that even if the painted wash-coating (yttria or zirconia) is gouged, the hardness of the nitrided surface will prevent the crucible from being gouged. The general unreactiveness of the nitrided surface of

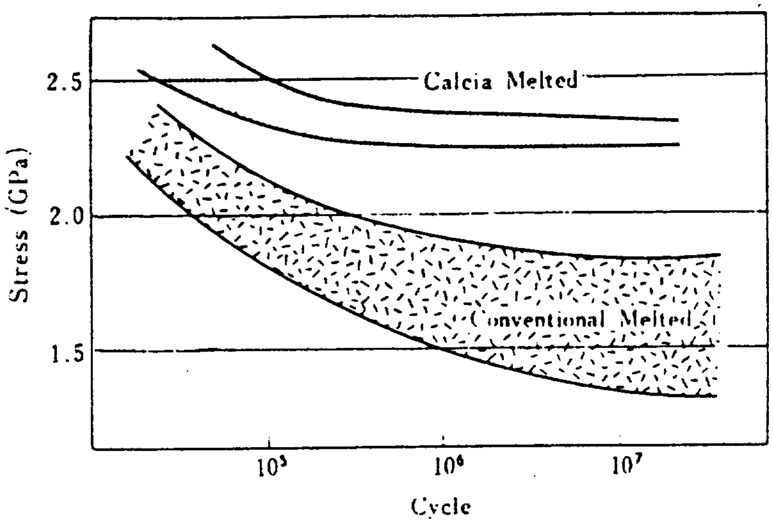

Figure 2.5 Fatigue life of calcia and conventional melted maraging high strength steel.(4)

Tribocor 532N to uranium and its alloys will prevent any appreciable attack. Even if the nitrided outer portion of Tribocor 532N were punctured to the un-nitrided region of the material, the components of Tribocor (Nb, Ti and W) are only dissolved and form higher-melting alloys with uranium as they dissolve (essentially a self-sealing effect). Chemical analysis indicated no pick-up of any of the Tribocor components. Also, carbon levels could be kept unchanged (at or below 50 w. p. p. m) after casting.

Nickel aluminides can be melted by air-induction melting. The recovery of chromium, zirconium, and boron is 100% and 95% for aluminum. The aluminum in these alloys acts as an deoxidizer. It forms a continuous Al_2O_3 film during melting and protects the melt from any loss to or pick up of any element from the atmosphere. The oxygen content of the air-melted ingots is generally ≤ 50 ppm by weight. At Oak Ridge National Laboratory, air-induction melting of nickel aluminides was carried out using ZrO_2 crucibles. No interaction between the melt and ZrO_2 crucibles was observed. However, because of poor thermal shock resistance, ZrO_2 crucibles generally cracked after eight melts. Commercially, nickel aluminides have been successfully melted using Al_2O_3 crucibles. The molten metal from either the air or vacuum melting has been successfully cast into graphite molds. Although air-melted material is of acceptable quality based on chemical analysis, its hot workability and fatigue properties can be further enhanced by vacuum-induction melting (VIM), vacuum-arc remelting (VAR), and electroslag remelting (ESR). The nature of VAR and ESR processes results in high surface quality and relatively porosity-free ingots. Furthermore, the grain structure of VAR and ESR ingots allow their ease of flow during various hot- and cold-deformation processes.(24)

A series of refractory metal plasma sprayed coatings, W, Ta-W and Re-W applied to graphite crucibles, were tested as containment barriers for melt processing Al_2O_3-

ZrO_2, Al_2O_3-Y_2O_3 and Al_2O_3. The molten ceramics migrated along the plat boundaries into the porosity of the coatings. Despite the undesirable wetting of the coatings, there did not appear to be any chemical attack of the tungsten or tantalum by the oxides. Conversely, the Re-W coatings reacted with molten Al_2O_3-Y_2O_3 and Al_2O_3. However, it appears necessary to decrease the porosity of the coatings in order to reduce the penetration of molten oxides. This could accomplished by low pressure plasma spray and/or post-deposition heat treatment.(25)

COATED CRUCIBLES FOR TITANIUM AND ITS ALLOYS

Zanis and Helferish(26) investigated the feasibility of using refractory metals (Mo, Ta and W) and yttria-coated graphite crucibles for induction melting titanium. They found that the vacuum-sintered metallic coatings were not sufficiently dense to resist rapid dissolution by the molten titanium. The concept of coating graphite crucibles with refractory metals was concluded to be severely limited due to the unfavorable reactivity of the metals with carbon. Specially, the reactivity of the refractory metals with carbon prevents the attainment of sintering coating with adequate densities to resist rapid dissolution by molten titanium. Hafnium and niobium are considered to be the most promising coating materials for graphite on the basis that their melting points are decreased by only 1% to 5% as a result of reaction with carbon. Another shortcoming of coated graphite crucibles lies in the fact that melting of the titanium will favor transformation of the refractory metal to a carbide and thus continuously reduce the effective thickness of the coating. Evaluation of a yttria-coated graphite crucible indicated that yttria reacted with carbon at temperatures near the melting point of titanium was therefore not considered suitable as a coating for graphite crucibles intended for induction melting of titanium. They also reported that induction melting titanium in a graphite crucible resulted in significant carbon contamination of the melt due to dissolution of the crucible by molten titanium.

To improve TSR (Thermal Shock Resistance, inherently poor for yttria refractories) a refractory laminate of tungsten/yttria/tungsten/yttria was prepared by plasma spraying with alternate layers of the materials. While the titanium strongly wet the laminate crucible, no delamination of layers occurred nor did any thermal shock problems appear. The TSR of yttria was significantly improved with a W/Y_2O_3 laminate crucible. The reactivity of yttria with titanium would cause 0.7-0.9 wt pct contamination with yttria precipitates, with the matrix titanium containing a relatively low level (estimate 1000 wppm) of yttrium in solid solution.(27)

Some work has been done on the evaluation of stability of rare earth oxides as face coats for investment casting of titanium.(28) The intensity profiles of oxygen, normalized with respect to titanium, were similar to microhardness profiles. The gradation of oxides, based on the oxygen profile, increasing order of their stability was $ZrO_2 \rightarrow Nd_2O_3 \rightarrow Y_2O_3$. Based on the bulk hardness and oxygen analysis of 20-mm cast rods in investment molds, the oxides could be graded in order of increasing stability as

$$CeO_2 \rightarrow ZrO_2 \rightarrow Ge_2O_3 \rightarrow \text{didymium oxide} \rightarrow Sm_2O_3 \rightarrow Nd_2O_3 \rightarrow Y_2O_3$$

The grading did not fully follow the free energy data on the formation of these oxides. A better correlation with experimental findings was obtained when the solubility of the metallic species in titanium was also taken into consideration. In more severe conditions, where titanium was heated above its melting point in contact with face coat oxides, the observed contamination levels suggested a slightly different sequence of stability for the oxides:

$ZrO_2 \rightarrow Sm_2O_3 \rightarrow Gd_2O_3 \rightarrow La_2O_3 \rightarrow$ didymium oxide $\rightarrow Nd_2O_3 \rightarrow Y_2O_3$

The fact that the oxygen contamination was much higher than that of the metallic constituent of oxide confirmed that refractory oxides were not completely leached by liquid titanium. Oxygen was preferably transferred to the liquid titanium, leaving behind the metallic components as lower oxides in the mold.

COATED CRUCIBLES FOR OTHER REACTIVE METALS

Uranium and uranium alloys are typically induction melted in graphite crucibles under vacuum. Due to the chemical reactivity of uranium and most alloying elements with carbon, a protective coating is generally applied to the crucibles. Standard coatings for graphite crucibles have generally been zirconia based such as magnesium oxide, calcia-stabilized zirconia and magnesium zirconate, applied either as a wash or by flame or plasma spraying. These materials are suitable for melting unalloyed uranium and alloys requiring less 1400°C. However, for alloys such as uranium-6 niobium, uranium-7.5 niobium-2.5 zirconium and uranium-10 molybdenum, undesirable carbon levels and poor alloy control generally result when these coating are utilized. Yittria provides superior protection above 1300°C but becomes less satisfactory above 1450°C when applied directly on graphite. The utilization of a protective niobium-zirconia bilayer coating between the yttria and the graphite results in improved performance at 1500°C. Yttria has been satisfactorily applied both by plasma spraying and by brush application of a stable suspension. When the protective niobium layer is used, coating adherence after melting is excellent and multiple uses of coatings is practical. The coatings adhere to graphite with a high coefficient of thermal expansion (CTE) (~7 $\mu m\ m^{-1}\ C^{-1}$) much better than to standard crucible grade graphite (~4 $\mu m\ m^{-1}\ C^{-1}$). A single Nb/Y_2O_3 coated high CTE graphite crucible has been used for seven melts at 1450°C without repair or increased carbon contamination.(29)

Melting of zirconium is normally accomplished either by vacuum-arc skull melting using consumable electrodes or by a vacuum-induction melting, which is limited to small castings using water-cooled copper crucibles. An alternate process of vacuum-induction melt large castings in a coated graphite crucible is proposed. The laminated coating would consist of plasma-sprayed layers of metal ceramic that are designed to withstand temperatures approaching 2000°C while maintaining enough integrity to prevent contamination of the melt with carbon.

Melting temperatures approaching 2000°C present a difficult challenge in reference to thermal shock and compatibility of materials. A number of initial experiments were conducted using available ceramic crucibles and coating materials to determine which of these ceramics was most compatible with molten Zr. The following conclusions are based on the experimental results.

Zirconia was the least reactive refractory for melting Zr. Indeed, Zr can be melted without carburizing the melt or introducing large carbides using a calcia-stabilized ZrO_2 crucible. The difficulties in using a ZrO_2 crucible are size limitations and poor thermal-shock resistance. Both TiN, which can be plasma sprayed onto graphite, and TRIBOCOR indicate some degree of compatibility with molten Zr and are candidates for further investigation. The application of zirconia paint to a plasma-sprayed zirconia coating provides a releasing mechanism for removing the solidified melt and has potential applications for both the coated crucible and the mold. Because of the presence of calcium inclusions, a nonstabilized ZrO_2 paint may be difficult. Even with a release coating, a two-piece mold design appears necessary for this application.

A graded or composite coating between the metallic layer and the ceramic layer improves the overall integrity of the coating system by countering mismatches in thermal expansion properties between metals and ceramics. The metallic layer that provides the most resistance carbon and/or carburization of the Zr melt is Mo. Both the thin and thick layers appear to be effective barriers to carbon diffusion. Tungsten applied as a thick layer may be adequate, but it is not recommended for thin-layer applications. The reasons for the apparently better performance of Mo over W are unknown. The furnace atmosphere contributed strongly to carbon contamination of the melts, primarily from CO gases. Melting in a vacuum and/or covering the melt with coated lids should help prevent this condition. These experimental results indicated that a plasma-sprayed coating system consisting of a metal/ceramic laminate appears feasible for large casting applications.(30)

Deformation processed copper-refractory metals were studied because of their combined properties of high mechanical strength and excellent electrical conductivity. Precursor alloys are typically produced by consumable arc melting techniques and conventional crucible melting. The latter process, however, is subject to melt contamination due to the high melt temperature required for melt homogenization and the strong compound forming tendencies of Group V-VI transitions metals. In addition to the need for alloy purity, it is desirable to form these alloys by rapid solidification in order to develop fine-scale microstructures prior to deformation process.(31) However, the large superheat temperatures required for proper flow during melt processing lead to alloy contamination, crucible degradation and ultimate inability to atomize the alloy due to flow obstruction and mechanical failure to the crucible. A series of uncoated and plasma sprayed graphite crucibles were tested as containment crucibles for Cu-15v/o Cr and Cu-15v/o Nb alloys. The uncoated graphite crucibles physically contained the molten alloys, i.e. no substantial wetting occurred; however, carbon contamination of the melt was observed. Tantalum-based coatings were severely wet by both copper alloys and chemically reacted with the melts. Tantalum was detected in the melt and, where analyzed, chromium and niobium were found within the bulk of the coating. The ZrO_2-

88w/o Y_2O_3 coatings, which were applied over a tungsten bond coat, were not wet by the molten alloys and were chemically stable to the levels discernible.(32)

CONTINUOUS CASTING OF TITANIUM AND ITS ALLOYS

A number of rapid solidification processes have been developed over the last three decades attempting to produce rapidly solidified titanium alloys. In 1983, RIBTEC developed a rapid solidification process called melt overflow (Figure 2.6). Molten metal overflows a reservoir onto the surface of a rotating chill block. The melt streams is not extruded through an orifice to contact the chill block like melt spinning techniques. The melt pool overflows a reservoir and is channeled by a tundish or hearth to contact the moving chill surface.

The melt overflow process is ideally suited to direct casting of reactive metals and alloys using skull melting techniques. Two different melting methods are currently used with melt overflow to cast titanium alloys: induction skull melting and transferred plasma arc skull melting. The induction skull melting system uses a separate tundish while the plasma arc system uses a tilting water cooled copper hearth to deliver liquid titanium to the chill block.

The induction skull melting furnace operated by the Duriron Company, shown in Figure 2.7, was designed for casting investment molded titanium pump parts. The melt overflow machine is loaded into the charging chamber of the furnace and raised into position. The furnace is sealed, evacuated, then filled with a partial pressure of argon. The titanium alloys are melted by electric induction in the segmented copper crucible and the liquid titanium is poured into the funnel. The funnel discharges liquid titanium into the tundish which spreads it against the rotating chill block to cast thin strip. The liquid titanium forms a skull against the graphite tundish and graphite funnel to protect the remaining liquid from interstitial carbon. The temperature of the graphite funnel and tundish are kept below the melting point of titanium to ensure that a skull will form.

Transferred plasma arc melting of titanium alloys can result in low gaseous and foreign object impurities, and high alloy recovery. The capital cost, maintenance costs and labor costs are relatively low compared to other directed energy sources like laser or electron bean. A wide variety of feed plasma arc melting with melt overflow has been applied to directly cast titanium alloy fiber, filament, ribbons and strip.

Many different plasma torches have been designed for melting reactive and refractory metals. Two plasma melt overflow furnaces using two different plasma sources have been built and operated at RIBTEC Company. The first plasma furnace was designed to melt roughly 100 grams of titanium alloys. The second furnace uses a vortex stabilized, hollow copper anode torch that is designed to melt 2 kilograms of titanium alloys. In a laboratory bench scale plasma melt overflow furnace, the water cooled chill block measures 5 cm wide by 19 cm diameter. Chill block materials include, but are not limited to, copper, brass, steel and molybdenum. The water cooled copper hearth has a cavity 5 cm diameter by 2.5 cm deep for skull melting roughly 100 grams of titanium alloys. The system features a turbo molecular pump for a vacuum cycle that is rapid and clean. The laboratory scale plasma melt overflow furnace is capable of casting fiber, filament and ribbons (up to 2.5 cm wide).

In a pilot production scale plasma melt overflow furnace, the chill block measures 30 cm wide by 25 cm diameter. The chill block can be either solid or water cooled. The water cooled copper hearth has a cavity that measures 20 cm diameter by 8 cm deep. The hearth is has a cavity that measures 20 cm diameter by 8 cm deep. The hearth is designed to melt 2 kilograms of titanium alloys. The 75 cm long plasma torch can be manipulated in X-Y-Z directions during melting. The pilot production scale plasma melt

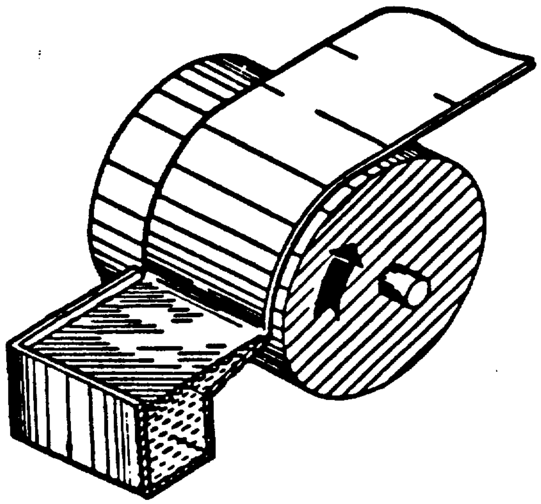

Figure 2.6 Schematic of melt overflow technique.

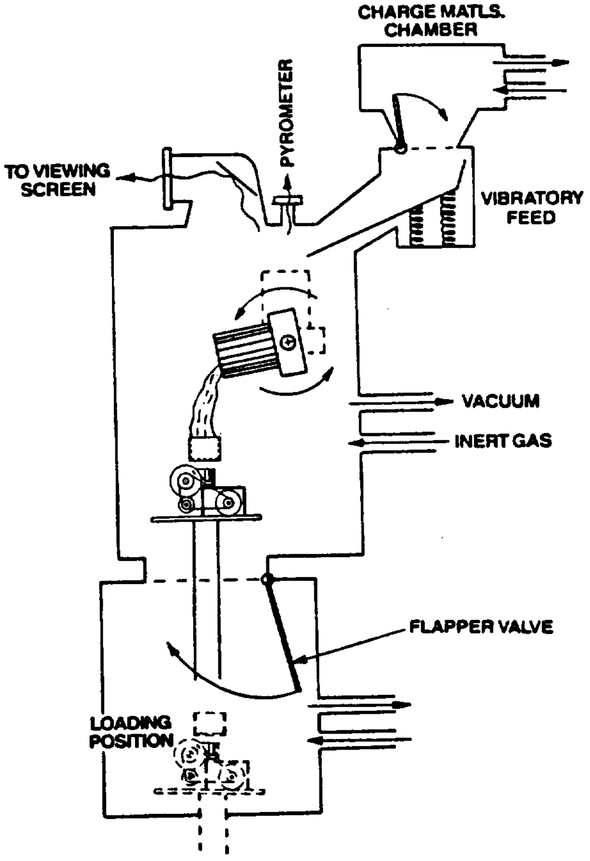

Figure 2.7 Schematic of induction skull furnace.

overflow furnace is capable of casting fiber, filament, ribbons and strip (up to 20 cm wide).

The induction skull melting system is best suited for casting strip over 10 cm wide because the crucible must be emptied within w seconds or less. In contrast, the plasma arc skull melting systems have been most successful in casting titanium fiber, filament and ribbon. The small volume of liquid titanium delivered by plasma skull melting techniques have limited the width of strip or ribbon that have been cast.

The Ti-6Al-4V and Ti_3Al-Nb (alpha II) titanium alloys have been cast into strip by melt overflow. Strip up to 18 cm wide has already been cast and work is continuing to cast strip up to 30 cm wide. The thicknesses of cast strip range from 0.1 to 0.5 mm. The process parameters that affect strip thickness are casting speed, substrate material, substrate surface texture and the physical properties of the liquid alloys.

Increasing casting speed decreased the strip thickness, all other factors being equal. A 67% increase in surface speed resulted in a 30% in as-cast strip thickness during experiments with a yellow brass chill block with grooves machined on the periphery. The copper chill block produced thicker strip than the yellow brass chill block, all other factors being equal. This appears to hold true regardless of the tundish position against the chill block. A knurled casting surface produced wider and slightly thicker alpha II alloy strip than a grooved casting surface.

The Ti_3Al-Nb alloys produced thicker, narrower strip than the Ti-6Al-4V alloy, all other factors being equal. This difference is attributed to the difference in the viscosity and surface energy of the two liquid alloys. Both viscosity and surface energy depend upon temperature, alloy composition and the wetting characteristics of the system. The oxygen content of Ti-14Al-21Nb alloy strip cast by melt overflow was measured using a Leco Model TC-136 oxygen/Nitrogen Analyzer. The average oxygen content of the samples is 630 ppm with a standard deviation of 70 ppm.

Based on the experimental results above, Gaspear and Hackman(11) believed that both induction skull melting techniques and plasma arc skull melting techniques have been successfully adapted to cast titanium alloy strip using the melt overflow process. Titanium alloy fiber, filament and ribbons can also be cast using melt overflow. The oxygen content of alloys is relatively low, considering the large surface area of the strip. Therefore, the melt overflow process shows considerable promise for producing strip from titanium alloys that are difficult or impossible to obtain in thicknesses below 0.5 mm.

In "Cold Crucible Continuous Casting" (4 C) process used by CEZUS Company in Ugine (France), induction melting was employed for reactive materials. For suitably chosen frequency, Ti-6Al-4V ingots (15 cm diameter and 2.5 m length) with excellent surface quality were produced. Typical withdrawal velocity was 3 meter per hour. Even with high withdrawal velocity the skin of the ingot is crack free: it should be noticed that a poor choice of frequency value was usually responsible for the presence of cracks. There was no increase in oxygen and nitrogen contents, nor in copper. This latter information that the crucible was not physically or chemically attacked is very important for the industrial use of this slagless process. Moreover melting with an argon atmosphere prevents the loss of volatile elements such as aluminum. This is an advantage of this technique compared to arc or electron beam process. Not only circular cross section but also square and rectangular sections can be produced by this technique.(10)

The Melt Spinning technique was tried for the ribbon production of gamma titanium aluminides (Ti-55Al and Ti-48Al-2Cr-2Ta). The alloys are tungsten-inert gas arc melted in a tilting, water-cooled, copper hearth, shown in Figure 2.8. The molten metal is introduced to a rapidly spinning, 25 cm diameter molybdenum wheel at the three o'clock position by tilting the hearth and allowing the metal to be extracted through a V-notch in the crucible. In contrast to the as-cast ingot alloy, the melt ingots, the melt-spun alloys, Ti-55Al and Ti-48Al-2Cr-2Ta, are uniform in composition and structure. The experimental work indicates that ribbon thickness and grain size are controlled principally by wheel speed, and the process models indicate that both cooling rate and growth rate are functions of wheel speed.(33)

SUMMARY OF PREVIOUS RESEARCH

Previous experiments show that a large variety of refractory materials including pure metal, intermetallic compounds, borides, carbides, sulfides, nitrides, and oxides had been studied for reactivity with titanium.(28) Most of the intermetallics in the systems Zr-Si, Zr-Al, Mo-Al, and Mo-Zr were too reactive with molten titanium.(13) Borides of Cr, Ti, W, and Zr were found to severely contaminate the titanium melt(12). Among the Cr, Mo, Ta, and Ti borides, TaB_2 caused the least amount of contamination of molten titanium.(17) In general, borides do not offer much promise as a crucible material or mold e coat material and, thus, have not been actively pursued.

Titanium carbide formation was observed in all castings using crucibles made of carbides of elements B, Mo, Si, Ta, Ti, W, Cr, and Zr.(12,17) It appears that the affinity of titanium for carbon triumphs even over the most stable carbides. NbC performed satisfactorily while in contact with molten titanium, probably because of a slower rate of carbon diffusion. Nitrides of refractory elements were also found to severely contaminate the melt.(12) As regards the performance of sulfides, computer calculations have shown significant advantages in the use of sulfides as mold coatings for titanium casting. Sulfides of calcium and magnesium were not satisfactory since appreciable pressure of

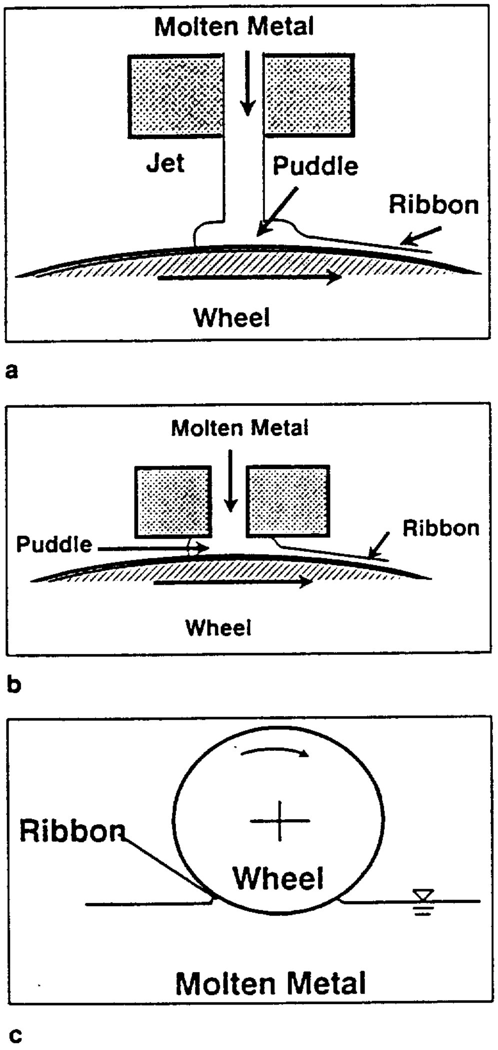

Figure 2.8 Generic types of melt spinners. (a) Free-jet melts spinning, (b) Planar-flow melt spinning, (c) Melt-extraction melt spinning.

metallic elements develops in equilibrium with molten titanium. The rare earth sulfides (CeS and ThS) were found to perform better,(12,18) although dissolution of the sulfide was observed, and the data on titanium indicated that considerable reaction between CeS and titanium occurred as the melting temperature reported was as low as 1500°C.

Earlier work showed that the lack stability of the synthesized fluoride and complex oxyfluoride refractories severely limited their resistance to molten titanium.(13) Oxyfluorides have recently been investigated, and some have proven effective. Neodymium oxyfluoride(34) and lanthanum oxyfluoride(35) have been patented as the major constituents in a mold coating. However, oxysulfides or oxyfluorides need to be prepared carefully to ensure purity and correct stoichiometry.

In search of suitable crucible material, the oxide family of materials has received the most attention. In an early study, zirconia was found to be the least reactive of the various oxides examined. Later investigations indicated that Y_2O_3 or HfO_2-stabilized ZrO_2 had performed better than CaO-stabilized ZrO_2. The 15 atomic percent Ti-ZrO_2 (oxygen-deficient zirconia) composition was shown to be inert to molten titanium for short times (< 1 minute) with little superheat. Some works[8,9,10] showed that CaO is a potential material in melting titanium, but the critical thing is how to solve calcia hydration. Pure Y_2O_3 has received considerable attention by investigators with Y_2O_{3-x} and Y_2O_3 + 8 to 15 wt pct Ti performing the best. Rare earth oxides(28) have also been the subject of interest with some positive results, a sequence of stability for the oxides is

$$ZrO_2 \rightarrow Sm_2O_3 \rightarrow Gd_2O_3 \rightarrow La_2O_3 \rightarrow \text{didymium oxide} \rightarrow Nd_2O_3 \rightarrow Y_2O_3$$

Previous experiments showed that the free energy diagram for oxides is useful for comparison of the relative stability of oxides, solution effects also need to be taken into consideration to obtain a more realistic picture.

EXISTING PROBLEMS

The experimental results reviewed show that of all reactive metals and alloys, melting of titanium and its alloys was and still is a challenging task although a great efforts had been expended in the past forty years. An advance in melting technology and knowledge of titanium and its alloys could induce a potentially revolutionary advance in processing technology for the reactive metals industry. However, there exist four main problems: ***Reactivity, Size of Crucible, Thermal Shock Resistance and Cost.***

Because of high reactivity of titanium at elevated temperature, at present there exists no refractory compound that does not react with liquid titanium. Such reactions include the pick-up of oxygen. However, there also are other components of compounds which yield a hardness increase in near surface areas. The thickness of this penetration layer depends on the melting temperature and holding time. The least reactive refractory compound to melt titanium or other reactive metals is unidentified and performance yet unverified. Although there are some interesting compounds such as Y_2O_3, CaO, and CeS, etc., large ceramic crucibles required for melting titanium or other reactive metals are not readily available in industry. Almost all ceramic crucibles have a poor thermal shock resistance, especially Y_2O_3 crucibles. All the interesting refractory compounds such as Y_2O_3, CeS, and rare earth oxides are fairly expensive, which further limits their application in industry.

In this work, several strategies have been proposed to solve the existing problems. High quality graphite is chosen as a base material to build large crucibles, to increase thermal shock resistance and reusability of the crucibles. Surface coating technology was selected for large crucible building, low cost and thermal shock reduction. Static furnace melting, thermodynamic analysis and TEM and SEM microanalysis were used to evaluate the reactivity of several candidate compounds.

SELECTION OF REFRACTORY MATERIALS

Previous experimenters have utilized some form of thermodynamic considerations in the selection of potential candidate crucible materials. Generally, this has consisted of a comparison of free energies of formation of refractory compounds with the corresponding titanium phases (TiO, TiO_2, TiN, TiB_2 and TiC). Based on this approach any oxide having a more negative free energy of formation at elevated temperatures than the appropriate titanium compound would be identified as a candidate, such as Al_2O_3, ZrO_2, HfO_2, ThO_2, BeO, etc. However, the above approach disregards the need to consider solution effects. Many experiments have shown that the level of contamination in liquid titanium from refractory oxides may not only be related to thermodynamic stability of the refractory compound but may be influenced by the solubility of the metallic species in the titanium. As such, another important approach is required to calculate the solubility of the ceramic metal component and the ceramic compound in titanium. Finally for reasons of mechanical stability, the melting point of the ceramic should be higher than the temperature of the superheated titanium, a reasonable minimum melting temperature is 2400°C. The data on melting point, free energy of formation, and solubility for the various refractory compound suggested for study are included in Table 2.8.

SELECTION OF FABRICATION METHOD

General Introduction of Coating Technologies

Ceramic crucibles have difficulty being used in titanium industry due to their expense, poor thermal shock resistance, and incompatibility with induction heating. More importantly, large ceramic crucibles required for melting titanium and its alloys are not readily available in industry. A surface coating technology is targeted to make crucibles; thermal spraying is preferred because it offers the ability to handle diverse materials, achieves high deposition rates and potentially produces high quality, high dense coatings.

Thermal spraying is a microsolidification consolidation process of depositing metallic or nonmetallic coatings onto various substrates. A thermal spray coating is produced by the successive accumulation of molten particles that rapidly flatten and solidify after impingement on the substrate surface.(36) Increased attention is being focused on this materials-processing technique due to its ability to process most materials that have stable melting phases, to process materials in many forms (e.g., powders, rods, wires, and composite mixtures), and to readily consolidate them in order to produce relatively homogeneous, refined micro-structures.(37) The thermal spray process permits rapid application of high-performance materials in thicknesses from a few mils to more than 25 mm (1 in.) on parts of a variety of sizes and geometry. Thermal spraying requires minimal base-metal preparation can be applied in the field, and is a low temperature no delution method compared with techniques such as weld overlay.(38)

Thermal spraying reduces wear and corrosion and greatly prolongs part service life by allowing use of a high-performance coating material over a low-cost base metal. Application areas of the family of processes are:(38,39)

- Wear resistance
- Oxidation resistance
- Corrosion resistance
- Restoration of dimension
- Abradable clearance control
- Thermal barriers
- Electrical conductivity
- Biomedical
- Free-standing shape
- Molding making

Table 2.8 Free energy and solubility Data of various compounds(28,40)

Compound	Melting point (K)	Standard Free Energy of Formation of Oxides $-\Delta G°$(kJ/mol O_2) 2000 K	Maximum Solid Solubility (wt pct) of Element in ß-Ti
TiO	2003	705.8	--
TiO_2	2143	652.7	--
Y_2O_3	2683	891.3	1.0 at 1628 K
ThO_2*	3573	855.9	86.5 at 1463 K
CaO	2873	809.0	0.0033 at 1067 K
$SrO{\cdot}ZrO_2$	2973	788.8	0.011 Sr at 1155 K
$CaO{\cdot}ZrO_2$	2618	779.4	
HfO_2	3085	758.7	complete solubility
ZrO_2	2953	725.5	complete solubility
$CaO{\cdot}TiO_2$	2248	721.4	
ZrO_2-8%Y_2O_3	3023		
ZrO_2-5%CaO	3033		

* radioactive

More than 200 coating materials with different characteristics of toughness, coefficient of friction, hardness, and other properties are available. These materials can be grouped as:

- Pure metals
- Metal alloys
- Cermets
- Ceramics
- Carbides
- Polymers
- Special composite materials

All thermal spray processes rely on three basic operational mechanisms: heating material in either wire or powder form to a molten or plastic state; propelling the molten or semi-molten particles; impact of the material onto a workpiece whereby the particles rapidly solidify and adhere both to one another and to the substrate to form a dense, functional protective coating.

As the molten or semi-molten plastic like particles impinge upon the substrate, one or more of three possible bonding mechanisms cause a coating to build up.(39) Mechanical bonding occurs when the particles splatter on the substrate. The particles interlock with the roughened surface and/or other deposited particles. With some combination of substrates and coating materials, localized diffusion or alloying can occur. Van de Waals forces may cause some bonding as well.

Thermal Spray Processes

The common characteristic of all thermal-spray methods is the use of chemical or electrical energy to develop the thermal or kinetic energy which heats the feed materials to create a stream of molten droplets that are accelerated and directed toward the surfaces to be coated. Currently, thermal-spray processes are differentiated into five major categories by the energy source (combustion or electrical), feed materials (particulate or solid), etc.(37)

- Flame Spray
- High Velocity Oxygen Fuel (HVOF)
- Twin Wire Arc
- D-Gun
- Plasma Spray

Flame Spray(38,41)

The oldest of the thermal spray coating methods. The process utilizes an oxygen-fuel gas flame as a heating source, which melts coating materials in either rod, wire, or powder forms. The gas combustion temperature is only about 5000°F (2760°C), which restricts the use of flame spray. Particle velocity ranges from 24-36 m/s for powder, to 240 m/s for wire and rod. In general, flame sprayed coatings exhibit lower bond strengths, higher porosity, a narrower working temperature range, and higher heat transmittal to the substrate than plasma-arc and electric-arc spraying.(39) Notwithstanding, the flame spray process is widely used by industry for the reclamation of worn or out of tolerance parts.

High Velocity Oxygen Fuel (HVOF)

The HVOF process uses extremely high kinetic energy and controlled thermal energy output to reach sonic or supersonic velocity in the jet plume and to produce very low porosity coatings that exhibit high bond strength, fine as-sprayed surface finish, and low residual stresses.(38,42) The HVOF process has a lower flame temperature, below 5000°F (2760°C). Due to the high gas exit velocity particle velocity is about 1350 m/s (4500 ft/s). In HVOF, powder particles are injected internal to the accelerating nozzles so that the momentum transfer to the particles are substantially higher than in flame spray process.(37) It can produce coatings having great thickness, strong bonds, and high hardness and durability. It is commonly used for coatings in the aerospace industry.(15,42)

Twin Wire Arc Spray(39,43,44)

Twin wire arc spray utilizes a continuous-dc arc between two conductive, consumable wires (as an anode and as a cathode) to melt their tips. A jet of compressed gas, normally air, atomizes the molten metal and projects the particles onto a prepared substrate. Temperatures of the arc can reach up to 12,000 to 20,000 K, and the typical particle velocities, ranging from 300 to 400 m/s, is normally higher than flame spray and lower than HVOF or plasma spray. Unlike the other thermal-spray processes, wire-arc spraying uses cold gas jets to break up the molten droplets of the arc-melted wires; therefore, the component being coated are not heated significantly by the process an advantage for thermally sensitive base materials.(37) It is widely used in wear and corrosion protection. However, the material sprayed by twin wire arc must be electrically conductive and in the form of wire. This severely limits the use of advanced materials such as ceramics.

D-Gun (Detonation-Gun)(45,46)

Detonation produced by igniting mixtures of explosive gases in a long barrel which is harnessed to produce a high velocity, high temperature gas stream which accelerate and heats the powder particles prior to impact on a chosen substrate. The maximum gas temperature and speed are 4740 K and 2930 m/s respectively. The particle velocity generally varies between 800 and 1100 m/s. The extremely dense coating with high bond strength deposited by D-Gun is used primarily for wear resistance. In general, this system can not be used for refractories and ceramics and the deposition rate is relatively low.

Plasma Spray

Pressurized gas is directed through a direct-current arc between a tungsten cathode and a copper anode that makes up the nozzle. Electrical energy is converted into thermal energy in the gas. The increase in temperature provides sufficient energy to ionize the gas, and with increasing temperature come expansion. Plasma-spray processes can heat gases to temperatures of over 25,000 K, producing plasma jets with temperature distributions of 3,000-15,000 K. At these temperatures, the plasma gases (Ar, H_2, He and N_2) dissociate and ionize into an equilibrium mixture of ions and electrons as energy is pumped into them by the confined arc discharge. This plasma state is what give the process its name and, more importantly, gives the process its capability to melt any material with a stable melting point.(37,39,43,47,48)

A plasma-spray device consists of a tungsten cathode, which emits electrons when heated by an electric arc aligned concentrically within a water-cooled copper anode nozzle. Electrons emitted from the cathode flow from the cathode to the nozzle anode under the influence of an applied electric field. Gases are heated to the plasma state by the electric arc and expanded through the nozzle to form a sub- or supersonic jet. The gas exit velocity may exceed 1.5 km/s in some cases, depending on the operating power, nozzle design, gas composition, and gas flow rate.(37)

Nitrogen and argon are gases frequently used as primary plasma gases. Hydrogen is often used as a secondary gas with nitrogen or argon in amounts of 5 to 35 percent. Hydrogen addition raises the arc voltage and, thus the power; it also increases the gas velocity.(43) Helium is sometimes used as a secondary gas mixed with argon when hydrogen embrittlement or hydriding, particularly on titanium substrates, is a consideration.(49)

Plasma spray technology was chosen in this project due to several advantages. First, the plasma spray process produces higher temperatures and is capable of higher powder particle velocities than the other thermal spray processes. High temperature and gas velocities result in coating that are superior in mechanical and metallurgical properties to low-velocity coatings. Plasma spray coatings exhibit higher densities and higher bond strengths, and the oxide content of metal coatings is inherently lower due to the use of inert arc gases. Decomposition of materials is minimized because of the gas velocities produced by the plasma, resulting in extremely short residence time in the thermal environment. The plasma process is particularly efficient for spraying high-quality coatings of ceramic materials, such as zirconia and yttria.(43)

CHAPTER 3

EXPERIMENTAL APPROACH

EXPERIMENTAL PROCEDURE

Experimental Equipment

A 200 KW Plazjet high energy plasma-spray system was used in this project.(50,51) It is operates at high voltages, 300-450 volts, and low currents, 200-500 amps, yielding over 200 kilowatts of power. Most conventional plasma-spraying systems operate at nominally 40-60 volts and up to 1800 amps, yielding power levels of 40 to 100 KW. The high voltage coupled with the gun design and high gas flow rates, generates hot plasma gas exit velocities which can be several times the speed of sound. Shock waves can be observed in the plasma plume.

Experimental Materials

Graphite crucibles

High quality dense graphite was selected as the base material. The thermal and mechanical properties of graphite are given in Table 3.1.(52) Graphite has a high melting point 3730°C, good mechanical strength, excellent thermal shock resistance, compatibility with induction heating, good machinable and relatively low cost. Another of the outstanding properties of graphite is its high-temperature strength. In contrast to most materials, its strength increases with temperature and reaches a maximum

Table 3.1 The thermal and mechanical properties of graphite(52)

Sublimation temperature, °C	3350
Melting point (at pressure > 100 atm), °C	3730
Bulk density, g/cm^3	1.5 - 1.7
Thermal conductivity, cal./cm-sec-°C (transverse)	0.2 - 0.3
Thermal conductivity, cal/cm-sec-°C (parallel)	0.3 - 0.6
Electrical resistivity, microhm-cm (transverse)	900 - 1500
Electrical resistivity, microhm-cm (parallel)	700 - 900
Coefficient of thermal expansion, per °C (transverse)	3 - 5 x 10^{-6}
Coefficient of thermal expansion, per °C (parallel)	2 - 4 x 10^{-6}
Permeability to gases, Darcy units (transverse)	1.5 x 10^{4}
Permeability to gases, Darcy units (parallel)	1.1 x 10^{4}
Young's modulus, psi	1000 - 3500
Compressive strength, psi	4000 - 10,000

at about 2500°C. A typical graphite with a tensile strength of 2000 psi at room temperature would have a strength of about 4000 psi at 2500°C. Because graphite is a light material, its strength to weight ratio is also outstanding and, in fact, is better than any known materials above about 1500°C.

Most metals and oxides react with graphite at high temperature to form carbides. The temperature at which a noticeable reaction first occurs varies widely with the particle size of the reactants. The minimum reaction temperatures with Mo, Nb, W are 1200, 870 and 1500°C respectively, 1600°C for ZrO_2,(53) and 1437°C for Y_2O_3.(54)

High purity, high thermal expansion graphite was purchased from POCO Graphite, Inc. Its coefficient of thermal expansion (CTE) is 8.4 x 10^{-6}/°C.

Bond layer sprayed metals

Molybdenum was used as the plasma sprayed bond layer between the refractory compound and the graphite. It acts primarily as a diffusion barrier to carbon migration into coatings and molten alloy and secondarily as a substrate for adherence of the ceramic coating. Molybdenum was chosen because of its high melting point (2650°C), fair-to moderate coefficient of thermal expansion (CTE, 5.8 x 10^{-6}/°C), self-bonding characteristics, and ability to form carbides at high temperatures. In addition, experimenters have shown that Mo bonds fairly well to graphite.(29,30)

Ceramic powders

Y_2O_3 (CTE is 8 x 10^{-6}/°C), Y_2O_3-ZrO_2 (8 wt yttria stabilized zirconia, CTE is 10.6 x 10^{-6}/°C), CaO(5%)-ZrO_2, $CaTiO_3$, $SrZrO_3$ and $CaZrO_3$ were selected and purchased from Miller Thermal Inc. and Cerac Incorporated. The particle size was a

-150, +325 mesh. The criteria for selection of refractory materials will be presented in detail in the discussion section.

Melting materials

Commercially pure titanium (C_p Ti) and titanium intermetallic alloy based on TiAl with a nominal composition of (Ti-48Al-2Cr-2Nb, in at %) supplied by OREMET (Oregon Metallurgical Corporation) were used in the experiment.

Plasma Spray Process

Spraying was performed with a Plazjet II Plasma spray gun operating at 400-450 volts and 300-350 amps. Nitrogen is used as a primary plasma gas with a working gas pressure of 200 psi. When a secondary plasma forming gas was needed, hydrogen was used with a working pressure of 140 psi. Figure 3.1 shows a schematic of the moldmaking process. A 1" diameter hemisphere was milled into semi-conductor grade graphite. Prior to coating, the graphite crucibles are blasted with 50 µm silica. Graphite crucibles were plasma sprayed with a 800 µm of molybdenum. To mitigate the effects of thermal shock between the metal and the ceramic, an intermediate coating approximately 200 µm thick was plasma sprayed consisting 50:50 blend of molybdenum and the ceramic powder. A final ceramic layer, approximately 400 µm thick, was then plasma sprayed onto the cermet to complete the coating system. Plasma spraying parameters were experimentally determined and are reported later in the results section.

Melting Process

Two fundamentally different melting technologies were used for this study.(55) The first melting procedure used a resistive element furnace to obtain the desired melting temperature. The second melting procedure used inductive heating. Although, the

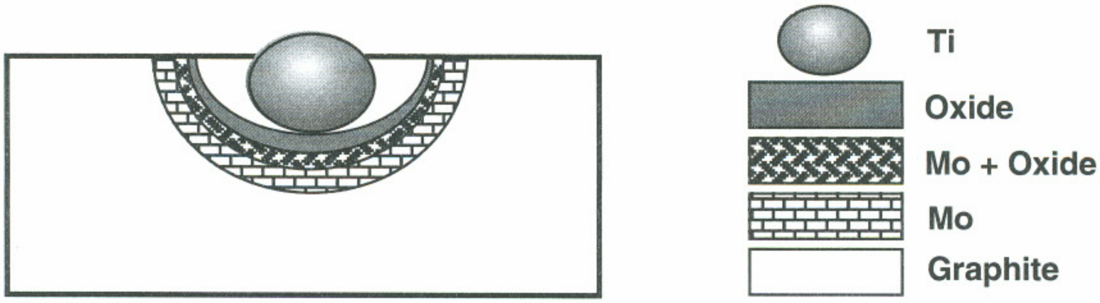

Figure 3.1 Schematic of plasma-sprayed crucible.

goal of the project was to develop coating technologies for inductive heating environments, the complexity of this environment and the difficulty with accurate control capabilities made it difficult to conduct consistent and well characterized experiments.

The melting experiments were conducted in a Brew high temperature, controlled atmosphere furnace with molybdenum resistance heaters. This method was selected for its excellent temperature control, the high purity atmosphere, and the expected quiescent nature of the melt pool. A stagnant melt pool was desired for the first set of experiments because emphasis was placed on understanding the actual high temperature thermodynamics and phase transformations which occur at the a stagnated molten metal/crucible interface. For these experiments, the melting sample and crucibles were placed in the Brew furnace and pumped to 10^{-5} torr using a two stage process (rotary then diffusion pump). The samples were then heated to 1000°C (1273 K) in approximately 15 minutes and held for times ranging from 30 minutes to 4 hours. This process was designed to effectively eliminate oxygen trapped in the graphite or coating material. The sample was then cooled and the chamber filled to 13 inches of vacuum, with an ultra-high purity inert gas (He or Ar). The melting sample and crucible were then heated to the desired peak temperatures, 1710°C (1983 K) and 1750°C (2023 K) (approximately 500

K per hour) for 30 minutes. The temperatures were monitored by an optical pyrometer. The molten alloy was then furnace cooled to room temperature (approximately 900 K per hour) and removed. For TiAl intermetallic compound, a melting temperature 1512°C (1785 K) was used.

Induction heated melting experiments were conducted in an American Induction Furnace with a radio frequency power unit. The experimental set-up was dictated by the high temperatures required and the effect of a cold heat sink in the form of the cold copper coil. Figure 3.2 is a schematic of the final design.

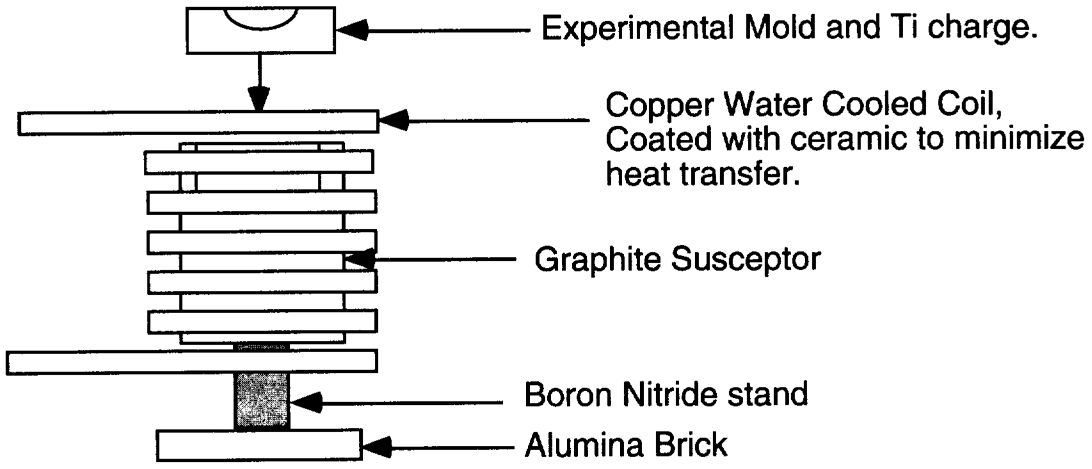

Figure 3.2 Schematic of the induction experiment.

MICROSCOPY ANALYSIS

Optical Microscopy

Following the melting processing evaluation tests, the alloy-containing crucibles are transverse sectioned axially to reveal the crucible-coating-alloy interface. Specimens for optical microscopic examination were ground successively on 400, 600 and 800 grit abrasive papers and then polished with 6 μm and 1 μm diamond pastes. Final polishing was carried out by repeatedly polishing the specimens with 0.05 μm alumina particles suspended in glycerin and ethanol. The examinations were performed on a Nikon optical microscope.

Scanning Electron Microscopy

Scanning electron microscopy was performed in the Zeiss SEM using both back scattered electron (BSE) and secondary electron (SE) imaging modes for microstructural feature identification and characterization. Energy Dispersive Spectroscopy (EDS) with a multi-windowed detector was used to analyze composition distribution in the coating and alloys.

Transmission Electron Microscopy (TEM)

Samples containing the interface between coating and melt alloy were cut to the size 2.5 x 2.5 x 0.3 mm from crucibles. The samples were then manually thinned to 3-4 μm thickness by grinding successively on 400, 600, 800 and 1200 grit papers. Ion mill was used for final polishing. TEM studies of the foils were conducted in a Hitachi H-800 electron microscope operated at 200 kV. Energy Dispersive Spectroscopy (EDS) was used to analyze composition of coating, alloy, and especially precipitates. Desktop Microscopist^{TM}, a software program, was used for identification of complex phases from electron diffraction patterns.

CHAPTER 4

EXPERIMENTAL RESULTS

DEVELOPMENT OF OPTIMUM PLASMA SPRAYING PARAMETERS

As single splat analysis technique(47) was used to obtain optimum plasma spraying parameters for the bond layer metal coating, the graded cermet coating, and the ceramic coating. During spray parameter development, individual splats are collected by rapidly passing a glass slide or metal coupon through the spray pattern at a specific working distance. These samples are then examined under a stereo microscope. Identification of splat characteristics give clues as to which parameters should be adjusted. Poor splat morphologies such as bounce back, star patterns, empty splat centers, lack of small splat, and otherwise misshapen splats, which indicate what is out of balance: particle speed and/or temperature. Individual splats should be flat and round, shown in Figure 4.1 (a–e). The single splat analysis technique works very well however thicker coatings are still required, shown in Figure 4.2 (a–c). As coating thickness increases, substrate temperature increases. Single splat analysis(47) and metallographic examination of the coating cross-section was necessary to properly evaluate the coating quality and allow high deposition rates. Optimal spray parameters are shown in Tables 4.1 and 4.2. Porosity of coating produced by optimum parameters was less than 1 %.

PHYSICAL CONTAINMENT OF MOLTEN TITANIUM

Table 4.3 gives a list of the melt experiments. This table lists the crucible

Table 4.1 Optimized spray parameters for original gun anode

	Molybdenum (Mo) powder	Mo(50% wt) + yttria or calcia stabilized zirconia	Yttria or calcia stabilized zirconia
Primary gas	N_2	N_2	N_2
Secondary gas	Ar	H_2	H_2
Gas flow rate (lpm): N_2	250	'250	250
Gas flow rate (lpm): 2nd	80	100	100
Arc current (A)	350	350	350
Arc voltage (V)	400	400	400
Powder carrier gas	Ar at 20 psi	Ar at 20 psi	Ar at 20 psi
Feed rate (rpm)	12	12	12
Standoff distance (mm)	200	180	150
Coating thickness (mm)	0.8	0.2	0.4

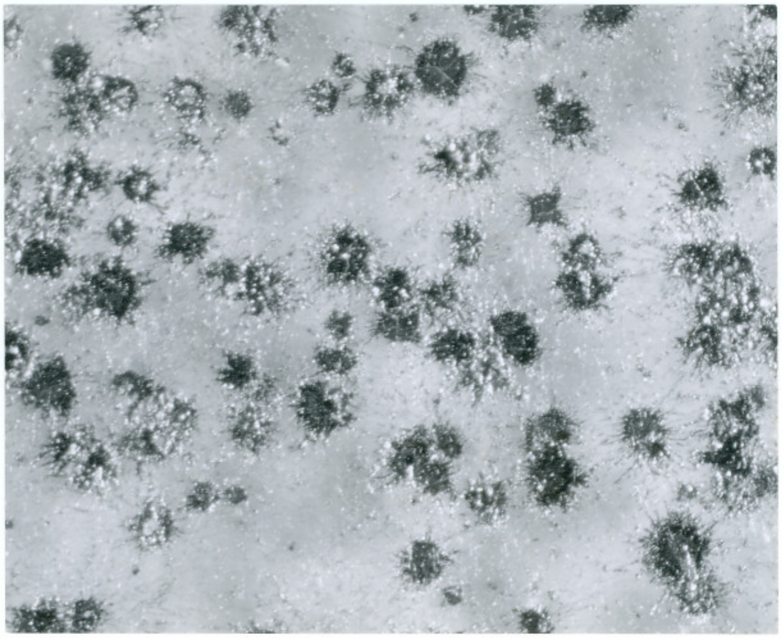

Figure 4.1 (a) Optical morphology of Mo splats.

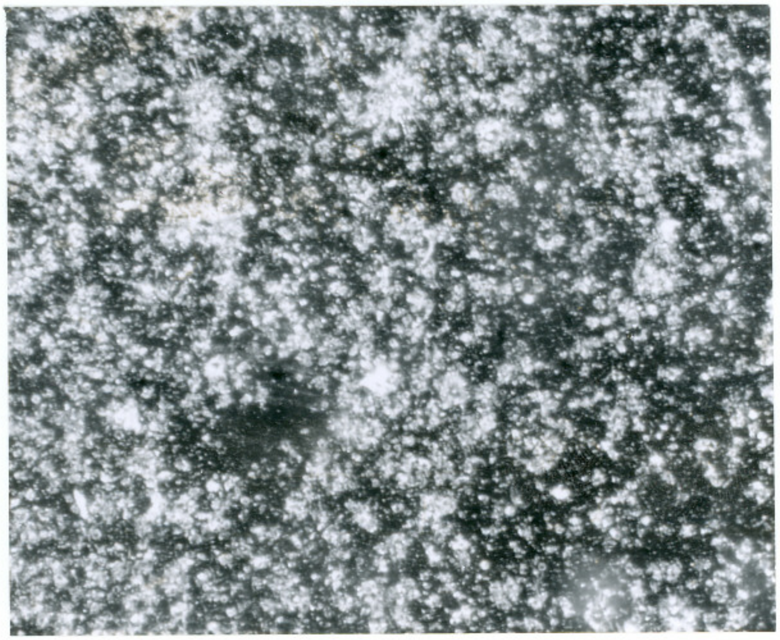

Figure 4.2 (b) Optical morphology of Y_2O_3 splats.

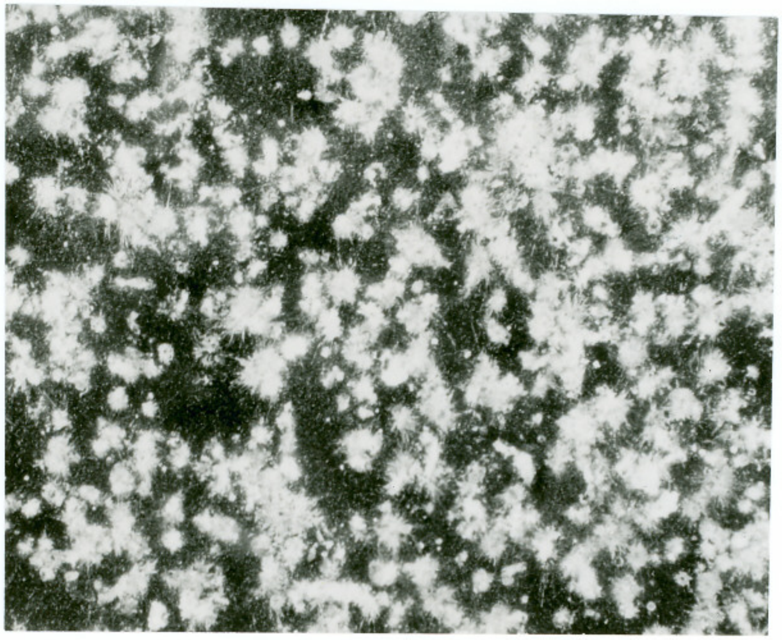

Figure 4.1 (c) Optical morphology of $SrZrO_3$ splats.

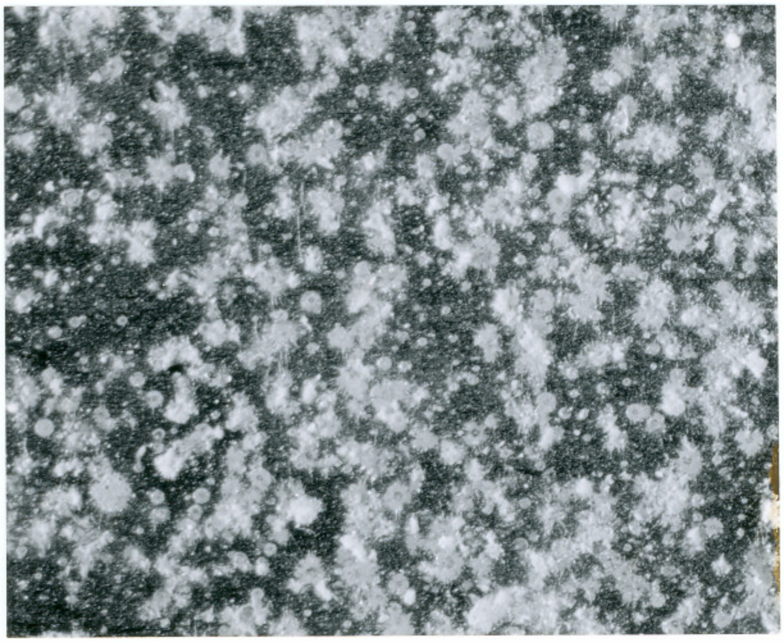

Figure 4.1 (d) Optical morphology of $CaTiO_3$ splats.

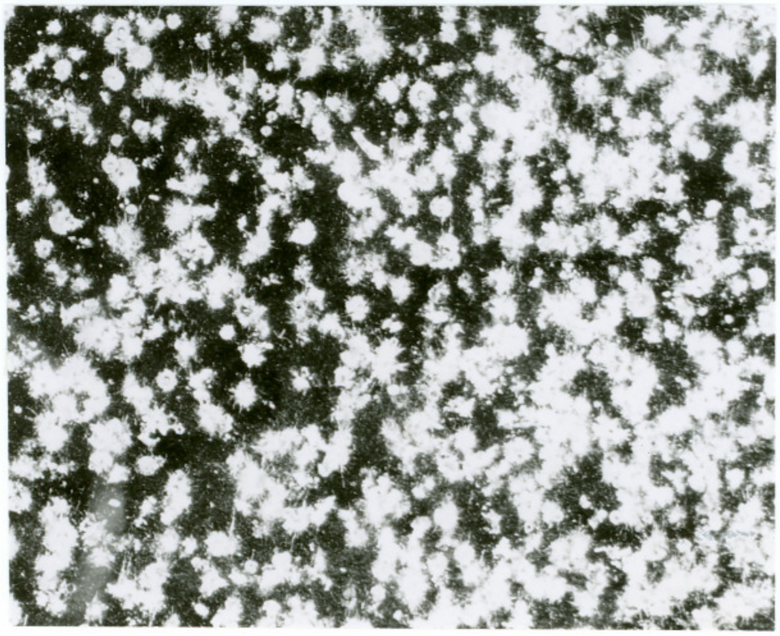

Figure 4.1 (e) optical morphology of $CaZrO_3$ splats.

Figure 4.1 Optical morphologies of different powders, (a) Mo, (b) Y_2O_3, (c) $SrZrO_3$ (d) $CaTiO_3$ and (e) $CaZrO_3$.

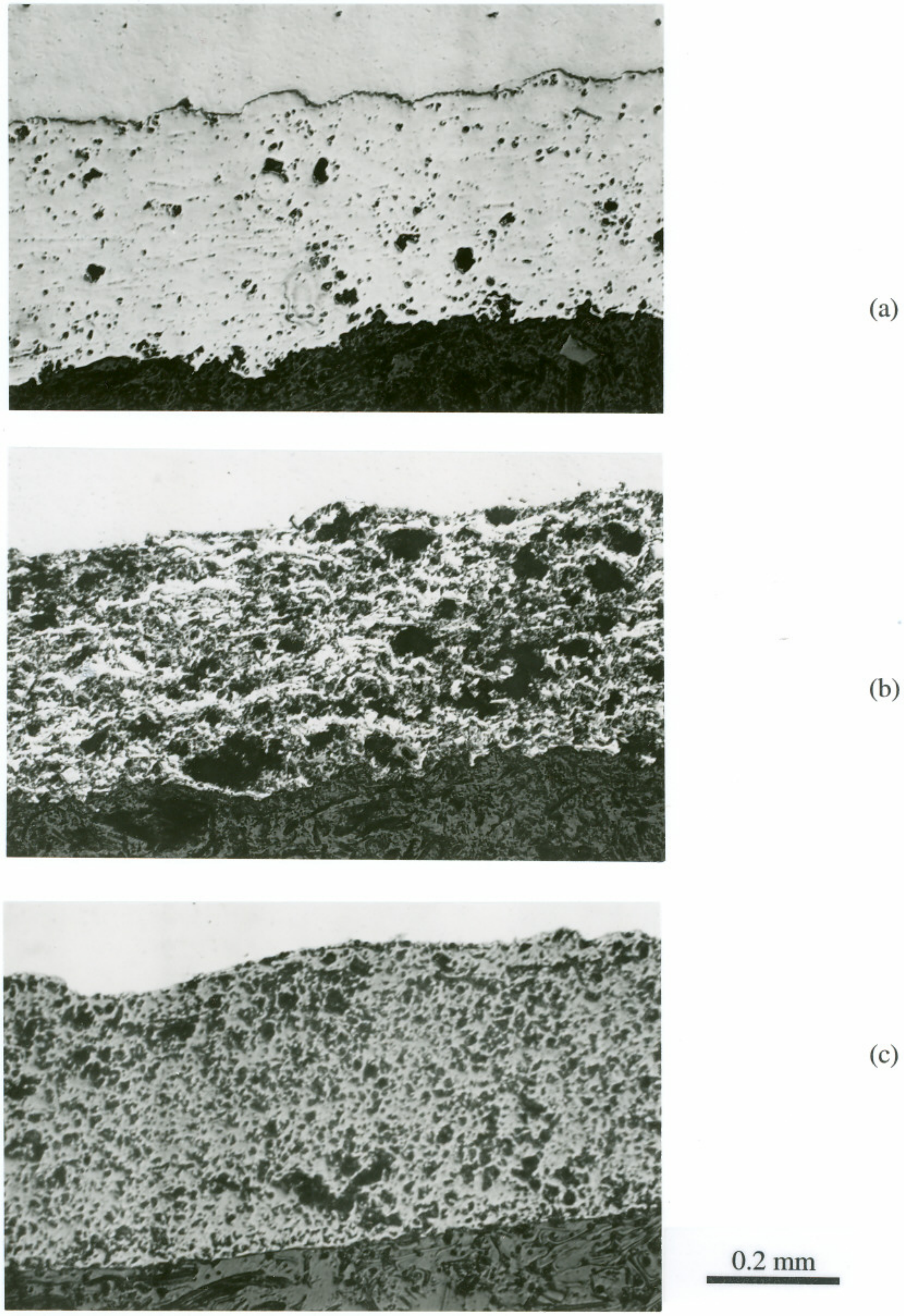

Figure 4.2 Optical micrographs of coatings: cross-section, (a) Mo, (b) 50% Mo + Y_2O_3-ZrO_2 and (c) Y_2O_3-ZrO_2.

Table 4.2 Optimized spray parameters for replacement gun anode

Anode Design B	Mo powder	Ceramic Powder
Primary gas:	N_2	N_2
Secondary gas:	none	H_2
Gas flow rate (lpm): N_2	220	230
Gas flow rate (lpm): 2nd	----	50
Arc current (A):	350	350
Arc voltage (V):	400	400
Powder carrier gas:	N_2 at 20 psi	N_2 at 40 psi
Feed rate (rpm):	10	15.5
Standoff distance (mm):	240 - 250	210
Coating thickness (mm):	0.8	0.4

compounds, melting types, melting temperatures and short notes about crucibles and melts.

Figure 4.3 show six macrographs showing a representative crucible of each of the six compounds. Figure 4.4. shows the crucibles and molten Ti after removal from the Brew furnace. The CaO- and Y_2O_3-stabilized ZrO_2 coatings appeared to maintain minimal contact with the molten titanium, while the Y_2O_3 and $SrZrO_3$ coatings allowed substantial flow of molten titanium over the crucible surface. This is particularly striking in the case of the $SrZrO_3$ crucible where molten titanium flowed out of the crucible and across the top of the mold. It was postulated that in this case, there were flaws in the mold surface which allowed the titanium to reach the Mo and graphite subsurfaces and caused the molten titanium to interact strongly with these constituents encouraging the flow of material. Comparing Figure 4.3 with Figure 4.4, these crucibles

Table 4.3 List of the melt experiments

Crucibles	Melting Type	Temp.	Note
CaO-ZrO_2	Brew furnace	1710°C	excellent melt shape, bright color and smooth surface
Y_2O_3-ZrO_2	Brew furnace	1715°C	bright color of melt, rough surface, darkening coating
Y_2O_3	Brew furnace	1710°C	a part of coating was broken, surface wetting
$CaZrO_3$	Brew furnace	1760°C	surface wetting,
$SrZrO_3$	Brew furnace	1760°C	melt flowed out, surface wetting
$CaZrO_3$	Brew furnace	1800°C	a reaction of melt with coating
$SrZrO_3$	Induction	>1700°C	partially melting
$CaTiO_3$	Induction	1720°C	terrible, a reaction with coating or coating melting
Mo	Induction	>1700°C	surface wetting
Y_2O_3	Induction	1800°C	darkening melt, surface wetting
$CaZrO_3$	Brew furnace	1510°C	melt flowed out
$CaZrO_3$	Brew furnace	1515°C	bright color of melt, surface wetting
$CaZrO_3$	Brew furnace	1600°C	terrible, darkening melt and coating, a reaction of melt with coating

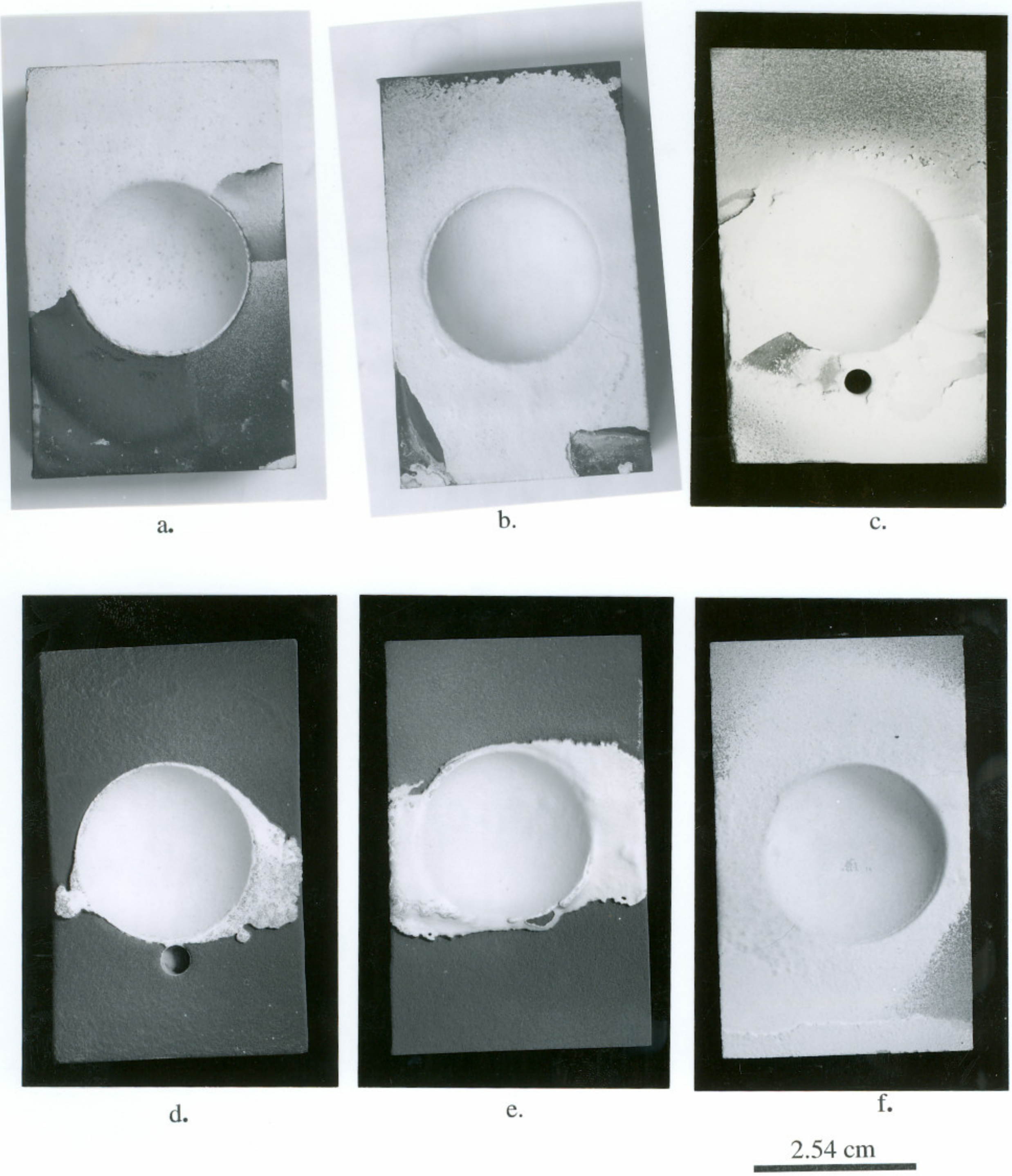

a.

b.

c.

d.

e.

f.

Figure 4.3 Macrographs of representative samples from each of the six different crucible types. Coverage outside of hemisphere is incomplete or non-existent due to either mechanical removal or partial coverage during processing. (a) CaO stabilized ZrO_2, dark spots due to graphite contamination caused by deposition geometry, (b) Y_2O_3 stabilized ZrO_2, (c) Y_2O_3, (d) $SrZrO_3$,(e) $CaZrO_3$ and (f) $CaTiO_3$.

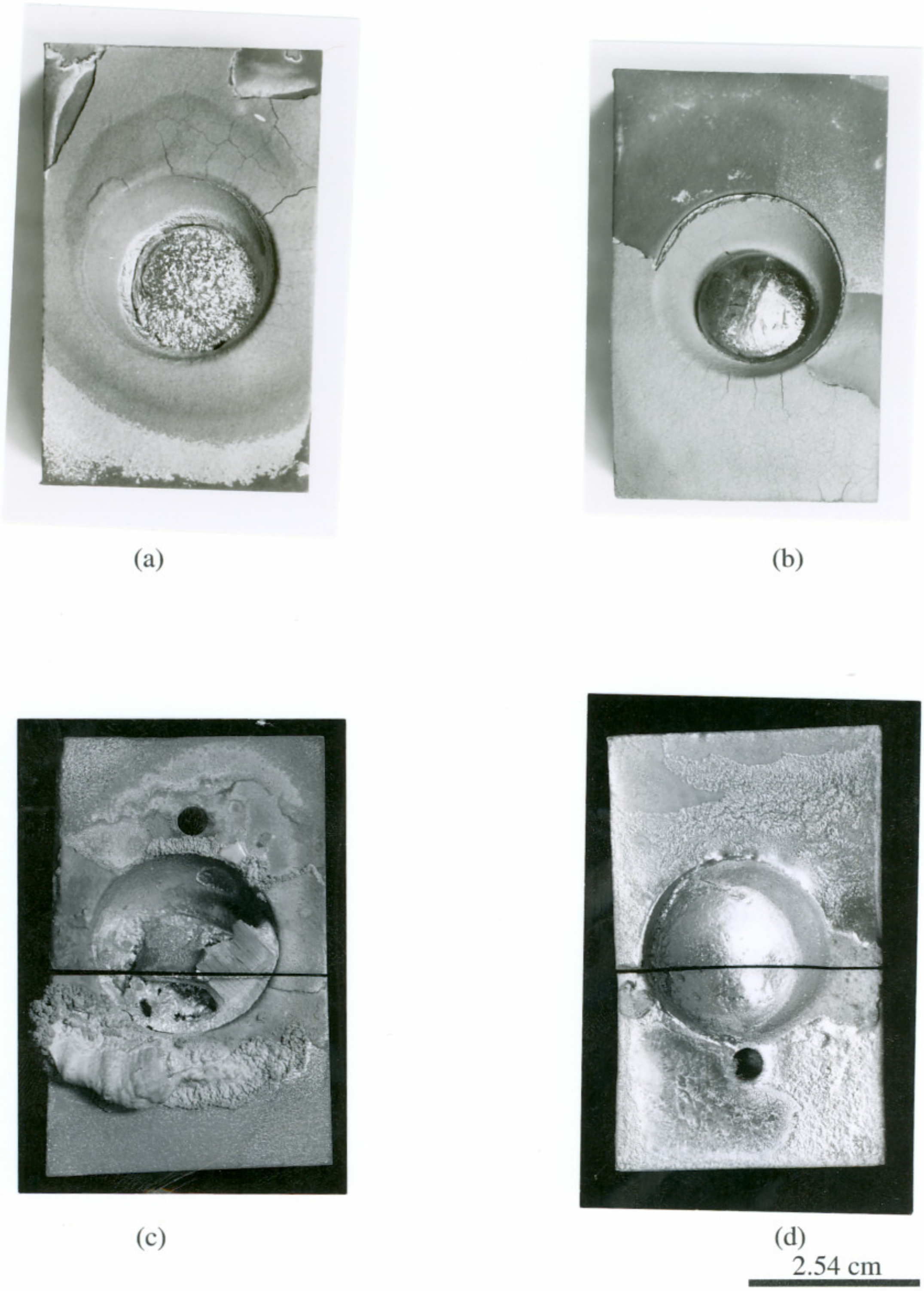
(a) (b) (c) (d)

Figure 4.4 Titanium and crucibles after melting in the Brew furnace for 30 minutes, (a) Y_2O_3-ZrO_2 (1715°C), (b) CaO-ZrO_2 (1710°C), (c) Y_2O_3 (1710°C) (d) $SrZrO_3$ (1760°C).

exhibited a noticeable surface darkening, specially the Y_2O_3 crucible, which had been identified as an indication of oxygen deficiency in the oxide. In the Y_2O_3 crucible, there was a mechanical failure of the coating. Y_2O_3-ZrO_2 coating was attacked by molten Ti.

CHEMICAL COMPATIBILITY OF MOLTEN ALLOYS AND COATINGS

Single Oxide Crucibles

Y_2O_3 stabilized ZrO_2 crucible (1715°C)

When the sample was sectioned, the Y_2O_3-ZrO_2 coating and Ti were separated at the interface. This indicates that the interface between Ti and Y_2O_3-ZrO_2 was quite brittle, which agrees with Alexander's results(56). The Y_2O_3-ZrO_2 coating not in contact with the molten Ti remained homogeneous as shown in Figure 4.5 (a). However, the coating in contact with titanium exhibited obviously detectable reaction with the molten Ti or alloyed with the molten Ti. In the original coating area there were only some Y_2O_3-ZrO_2 clusters (shown in Figure 4.5(b)), which indicates that Y_2O_3-ZrO_2 coatings can not resist the attack by molten Ti and degraded completely. EDS elemental analyses (Figure 4.6) showed that Zr and Mo contents in titanium decrease with the distance and are higher between dendrites than in dendrites; diffusion zone thickness is about 2 mm, shown in Figure 4.7. No yttrium was detected by EDS in the Ti matrix. EDS indicated that the average oxygen content in titanium was about 1.5 - 2.0 wt%, and chemical analysis found that oxygen content in titanium was 2.0 wt%.

CaO stabilized ZrO_2 crucible (1710°C)

In this crucible, EDS elemental analyses (Figure 4.8) found Zr, but not Mo in the Ti matrix; the Zr content near the interface reached 30% and its thickness was about 0.3 mm, shown in Figure 4.9. Ca is only found in ceramic coating, not in the Ti matrix.

However, EDS results indicated that molten Ti has diffused into the Y_2O_3-ZrO_2 coating up to 0.3 mm and optical microscopy observations (Figure 4.10) also supported the results. EDS showed that in the Y_2O_3-ZrO_2 coating the titanium contents are 62 and 33 wt% respectively at 70 and 200 µm from the interface. The oxygen concentration near the interface is about 3 wt%. This means that degradation of CaO-ZrO_2 coating had begun; maybe longer holding times and/or higher holding temperatures will accelerate the process. At top surface of titanium 2.5 wt% of oxygen was found, which was believed primarily due to the effect of secondary contamination from graphite base material and the furnace. In this experiment, the CaO-ZrO_2 coating was little better than the Y_2O_3-ZrO_2 coating although the method of degradation appears to be somewhat different.

Y_2O_3 crucible (1710°C)

Sectioning of a Y_2O_3 crucible (Figure 4.11(a, b)) revealed that some microcracks went through the Y_2O_3 coating. It is believed that these cracks developed during cooling cycle. In this experiment, the actual heating rate (1500 k/h) and cooling rate (3000 k/h) were twice that of the other experiments. However, Figures 7 and 14 lend further emphasis to the weak thermal shock resistance of the Y_2O_3 coating. Upon further examination of the interface between the yttrium oxide and the molten titanium, it was found that the titanium only penetrated about 0.01 mm into the yttrium oxide coating, and most of it went through Y_2O_3 coating porosity. The sharp, well-defined interface between the titanium and the oxide is illustrated in Figure 4.12 (a and b). Sharp interface indicates little reaction between molten Ti and Y_2O_3 coating. So, although visual and optical examination of the Y_2O_3 coating indicated some contamination, microstructural examination suggests that this contamination did not occur from degradation of the mold coating. Only in one region of the sample was the narrow acicular structure (about 0.01 mm) indicative of oxygen contaminated titanium observed. This probably results from

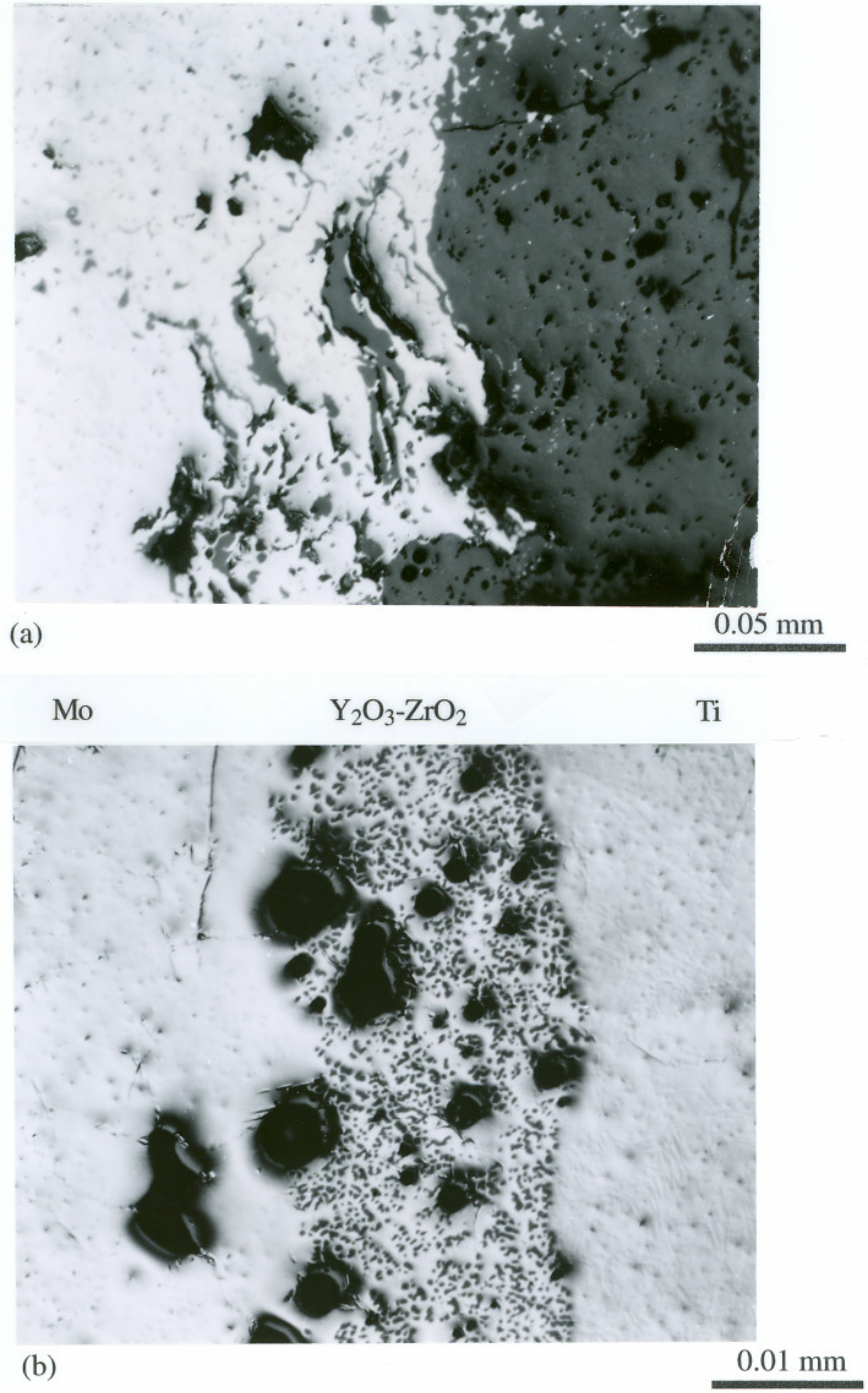

Figure 4.5 Cross-section of Y_2O_3-ZrO_2 crucible (1715°C) (a) the Y_2O_3-ZrO_2 coating which was not exposed to molten Ti, from left to right: Mo, blend and Y_2O_3-ZrO_2; (b) the Y_2O_3-ZrO_2 coating in contact with molten Ti, from left to right: Mo, blend, Y_2O_3-ZrO_2 and Ti.

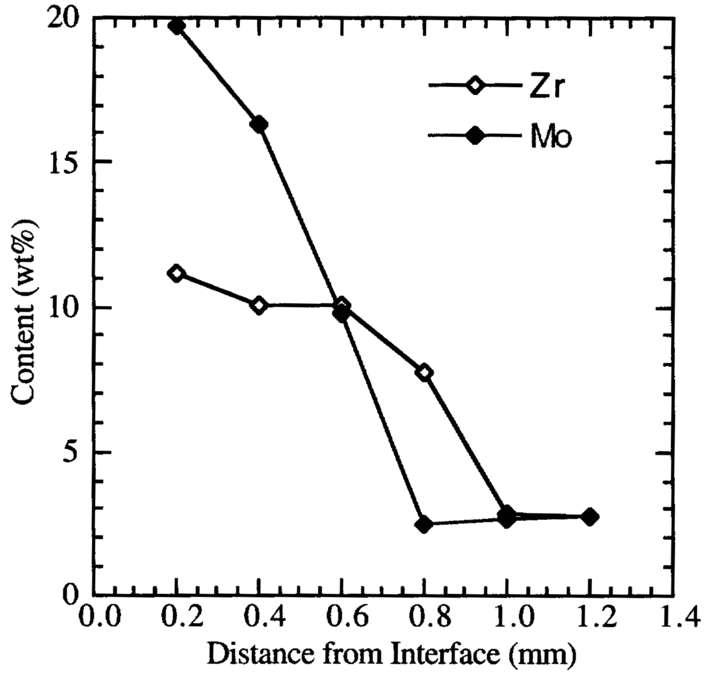

Figure 4.6 Composition profile in the Y_2O_3 - ZrO_2 crucible.

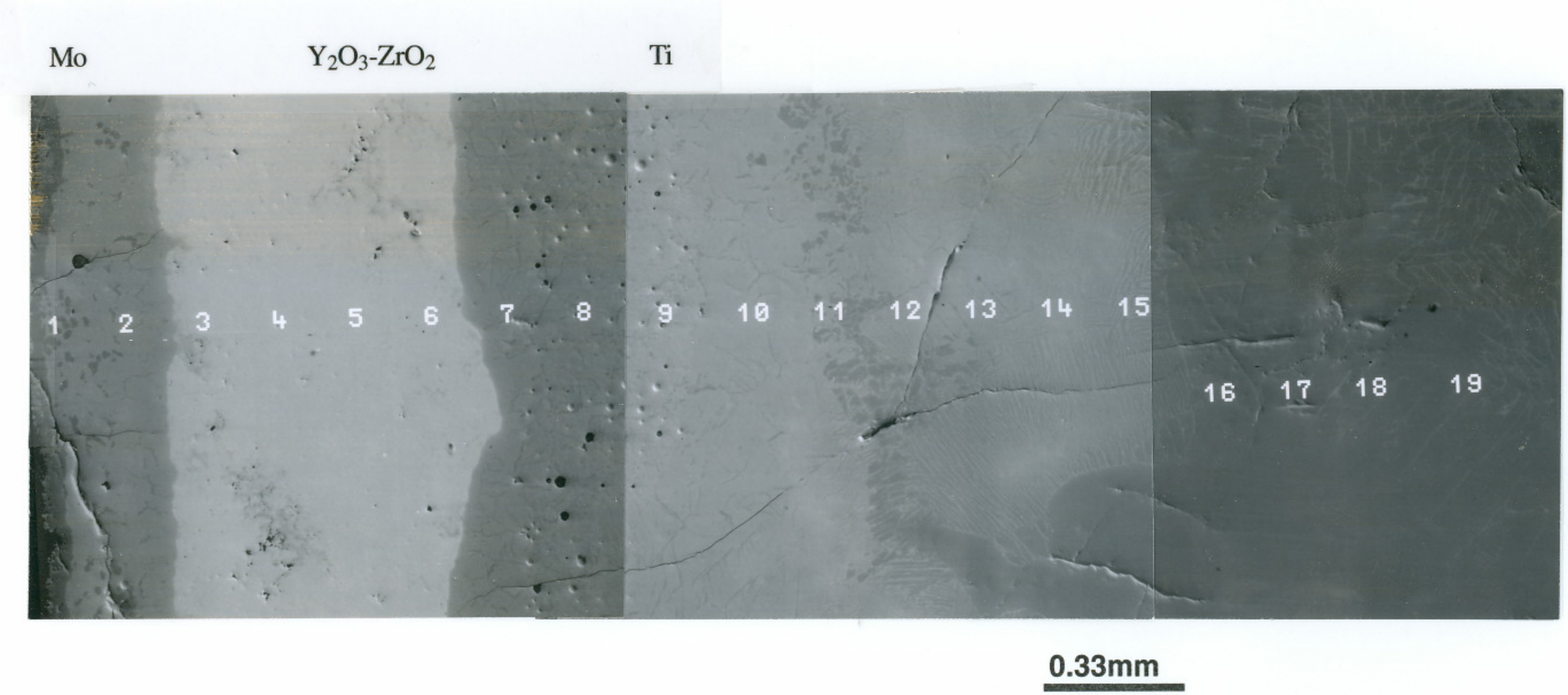

Figure 4.7. SEM micrographs of cross-section of Y_2O_3-ZrO_2 crucible and Ti, from left to right: coating and Ti.

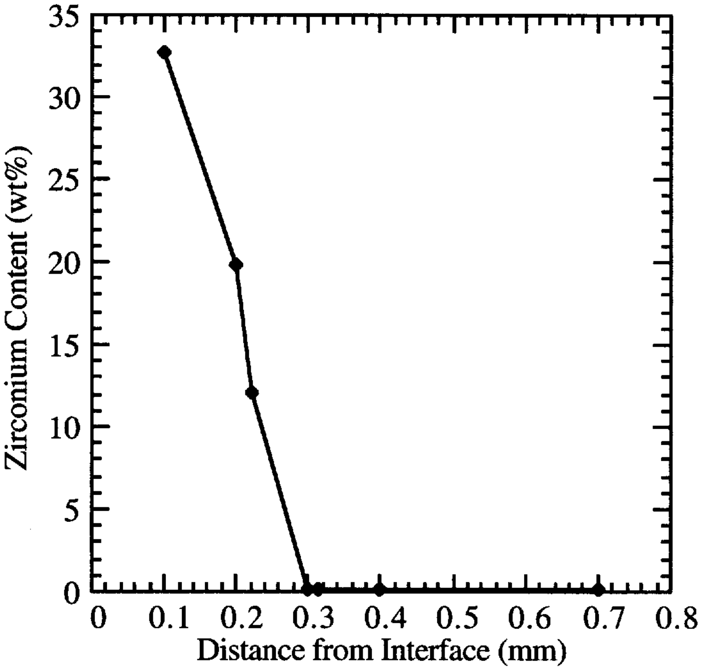

Figure 4.8 Composition profile in CaO-ZrO_2 crucible.

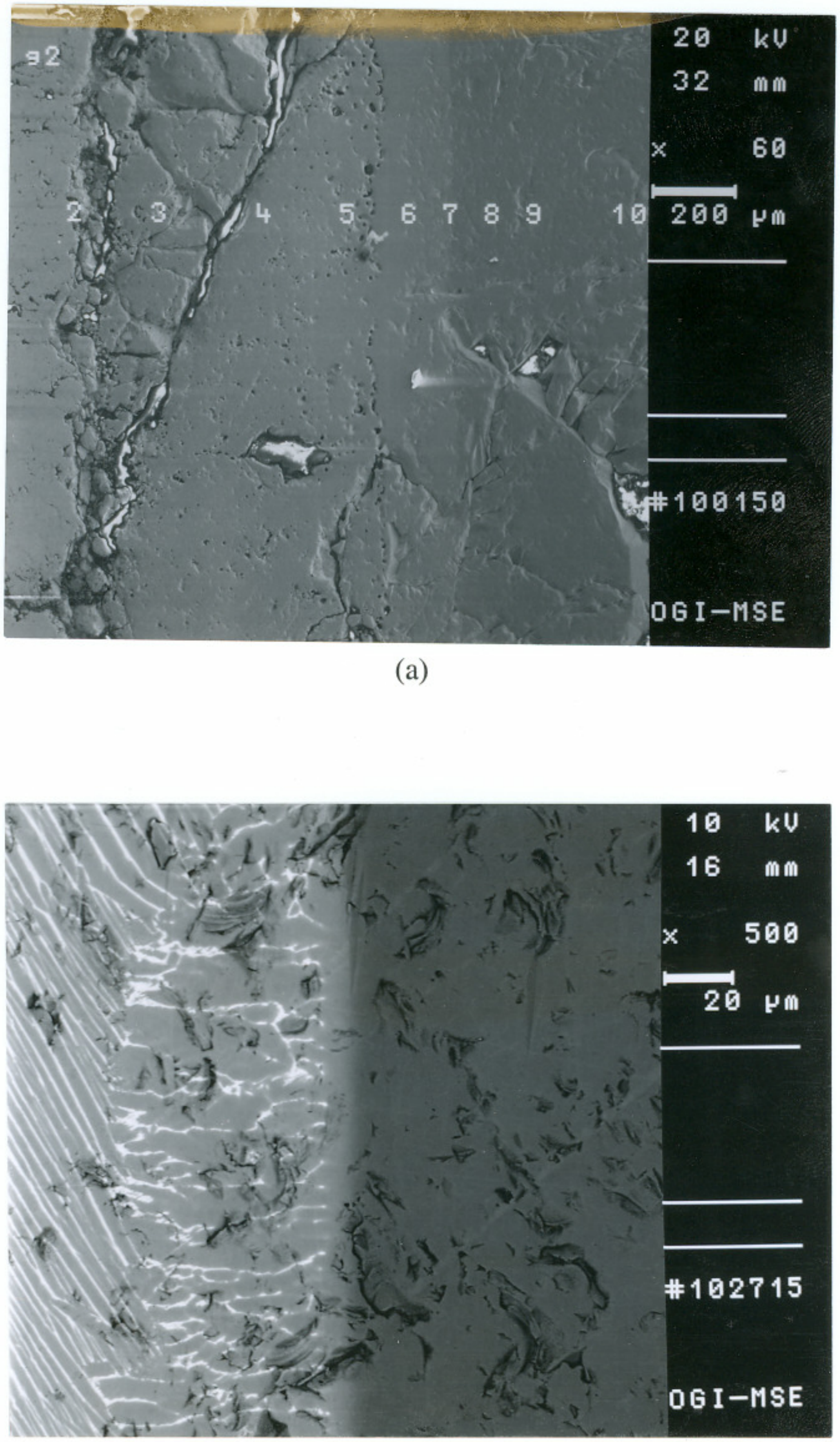

(a)

(b)

Figure 4.9 SEM micrographs of cross-section of Ti and CaO-ZrO_2 crucibles at 1710°C, (a) Coating and Ti, from left to right: Mo, blend, CaO-ZrO_2 and Ti; (b) Backscattered electron image of Ti, showing diffusion thickness in Ti.

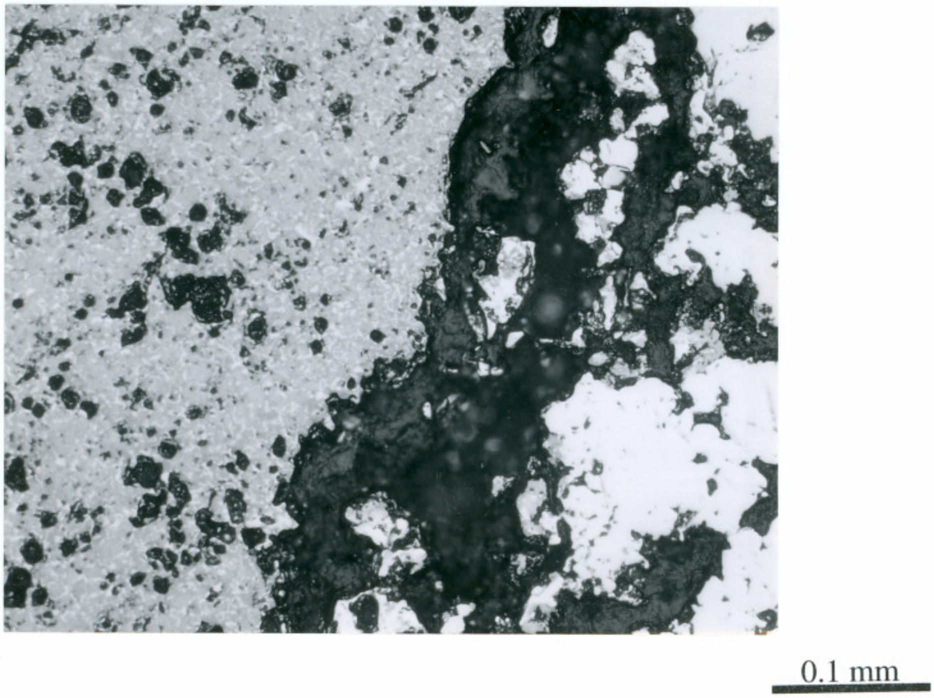

Figure 4.10 Optical micrograph of CaO-ZrO_2 coating.

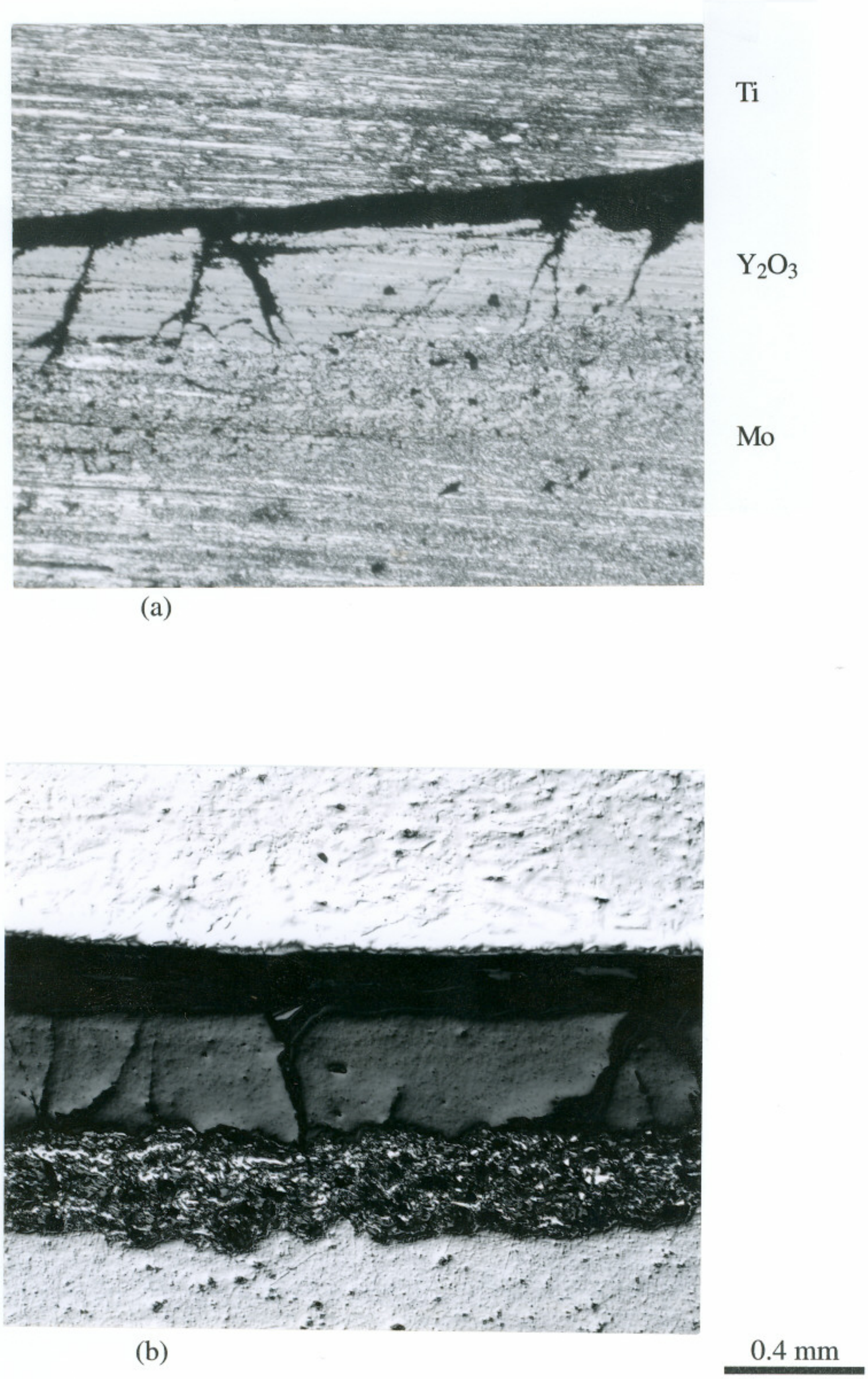

(a)

(b)

Figure 4.11 Optical micrographs of cross-section of Y_2O_3 crucible, (a) before polishing; (b) after polishing, from top to bottom: Mo, blend, Y_2O_3 and Ti.

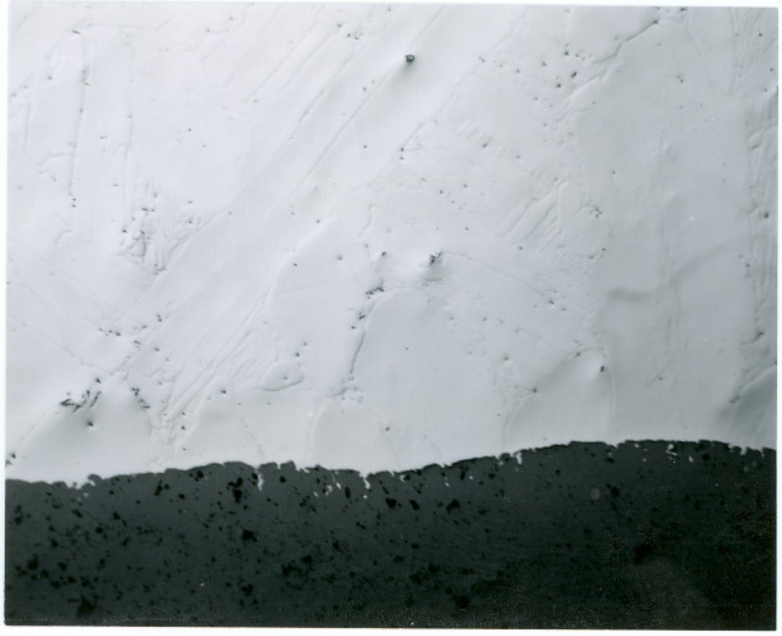
(a)

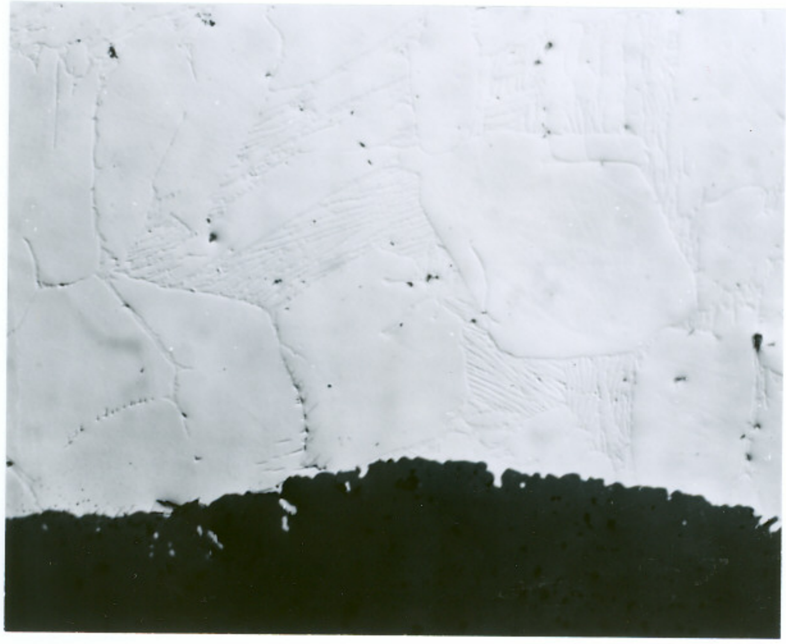
(b)

Figure 4.12 Optical micrographs of Y_2O_3 coating and Ti at different magnifications, from top to bottom: Y_2O_3 and Ti. Brew furnace, 1710°C, 30 min. and He, atm.

compounds , and their composition is approximately 90% Ti, 6% Zr, 2% Mo and 2% O (wt %). EDS results indicate a high Mo content in the Ti matrix, but Ca and Zr were not found in solid solution.

$SrZrO_3$ crucible (1760°C)

Sectioning of a $SrZrO_3$ crucible (Figure 4.15) also revealed that some microcracks went through the $SrZrO_3$ coating. Average heating rate for this crucible was high, about 1600 k/h. Optical microscope and SEM observations showed that Ti only penetrated into the $SrZrO_3$ coating about 0.04 mm, and most of it went through $SrZrO_3$ coating by coating porosity. $SrZrO_3$ coating showed great resistance to molten titanium and improved densification of the $SrZrO_3$ coating may reduce the contamination. Some $SrZrO_3$ compounds began to peel off and diffuse into molten titanium. However, EDS analysis found only 0.309 wt% titanium in the $SrZrO_3$ coating. No strontium (Sr) and its compounds were found in the titanium matrix; only zirconium (Zr) and molybdenum (Mo) as shown in Figure 4.16. An average Mo content of 2% by wt in the Ti probably resulted from molten titanium contact with the crucible surface. EDS elemental analyses showed that zirconium content in the $SrZrO_3$ coating decreases from 63.4% wt (internal side) to 52.2% wt (interface between coating and titanium). This indicates that zirconium diffusion into the molten titanium. The zirconium content of titanium adjacent to interface is 6 wt%, much lower than that in the CaO-ZrO_2 crucible, and no zirconium inclusion was found in the titanium. The oxygen concentrations in titanium measured by EDS are shown in Figure 4.17. The oxygen concentrations near the interface (50 μm) is 2.27 %wt, which is the second lowest to Y_2O_3. The oxygen content at top surface of titanium is 1.5 wt%. Because of the severe wetting experience in this experiment, only an extremely thin Ti layer remained after the experiment, therefore the accurate evaluation of contamination proved difficult. However, the experimental results at such high melting temperature still indicate that the $SrZrO_3$ compound has potential as a refractory material for molten titanium.

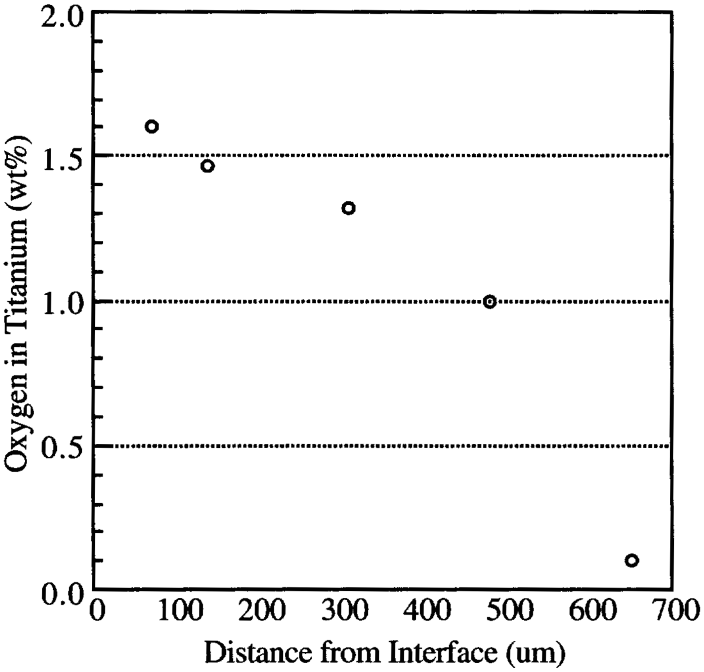

Figure 4.13 Oxygn concentrations in titanium melt in Y_2O_3 crucible (1710°C, 30 minutes).

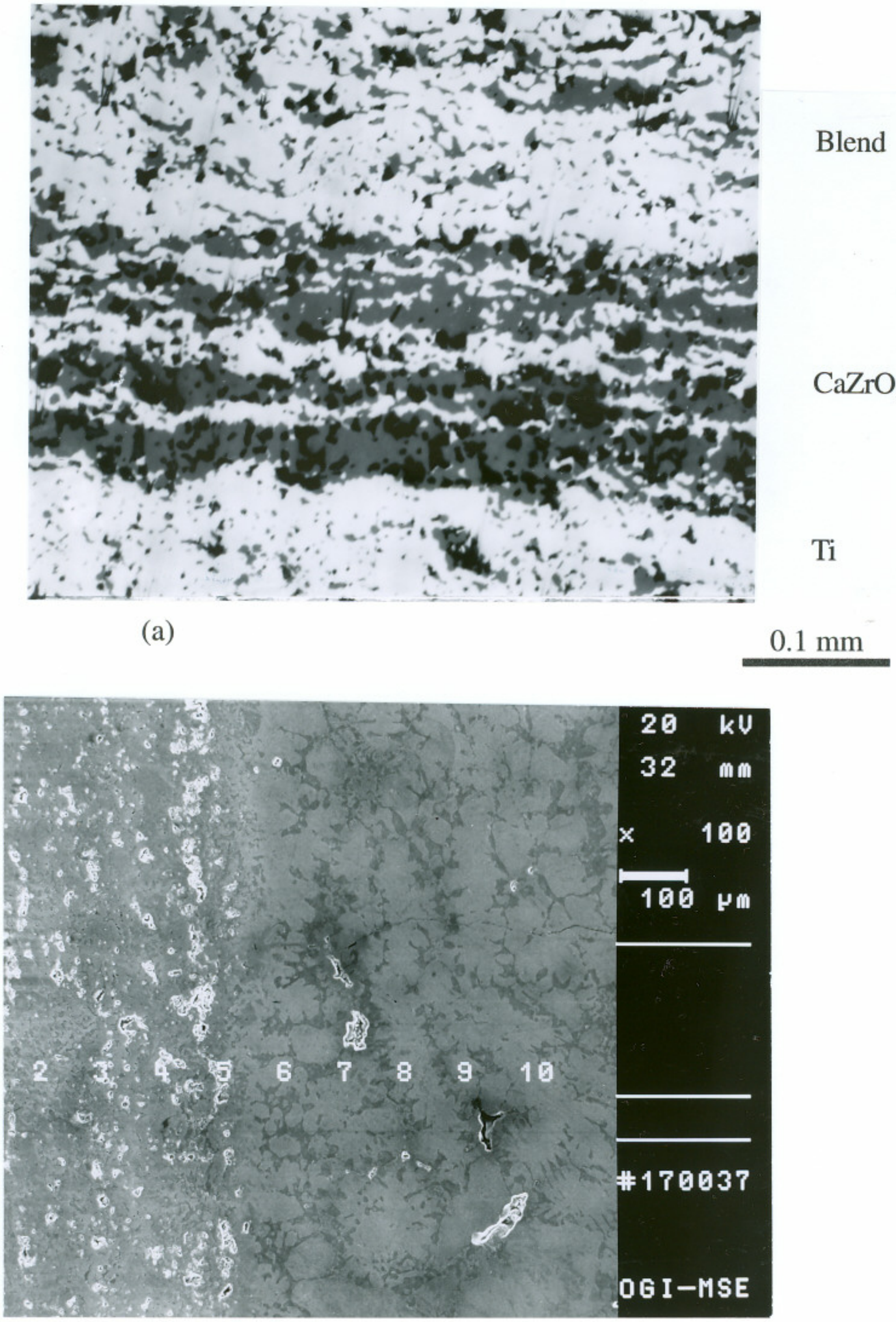

Figure 4.14 Optical and SEM micrographs of a section through a $CaZrO_3$ crucible(brew furnace, 1750°C and He). (a) optical micrograph, from top to bottom: Mo, blend and $CaZrO_3$; (b) SEM micrograph, from left to right: $CaZrO_3$ and Ti.

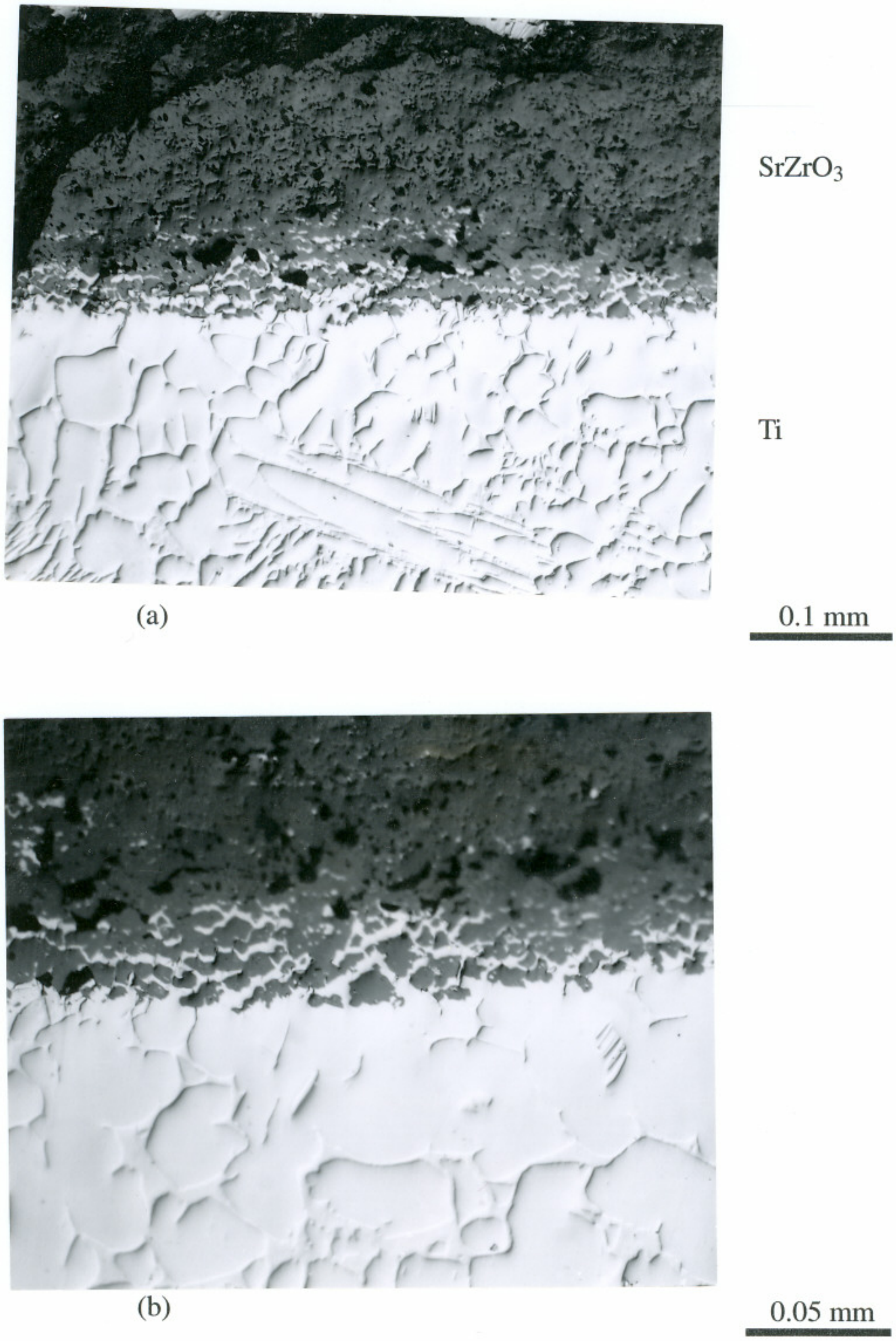

Figure 4.15 Optical micrographs of $SrZrO_3$ coating and Ti at different magnifications, from top to bottom: $SrZrO_3$ and Ti (Brew furnace, 1760°C, 30 minutes and He).

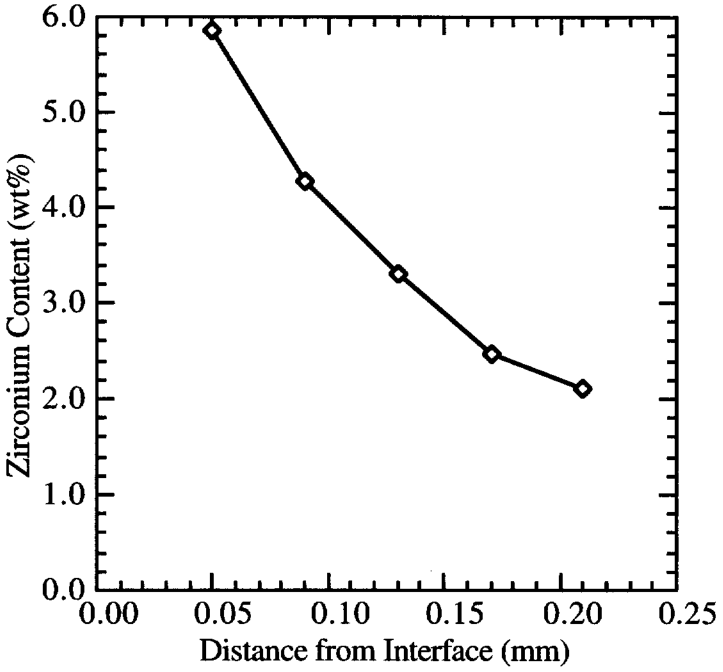

Figure 4.16 Composition profile in $SrZrO_3$ crucible (1760°C and 30 minutes).

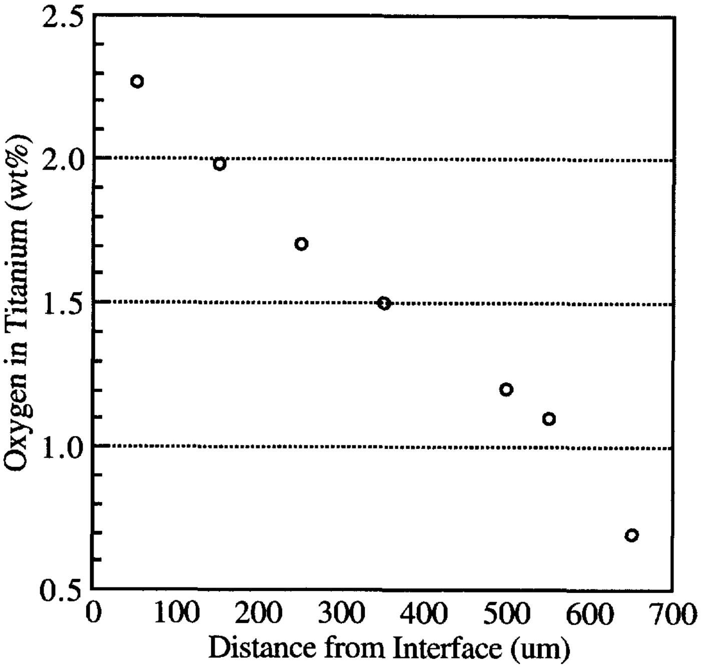

Figure 4.17 Oxygen concentration in titanium melt in $SrZrO_3$ crucible (1760°C, 30 minutes).

INDUCTION MELTING RESULTS

The primary goal of induction melting experiments was to develop an understanding of how a moving metal interface affects the crucible material. It was expected that these experiments will eventually lead to calculation of an accurate erosion rate for the crucible materials under production conditions. Pump out and sample preparation was the same as that used for the Brew furnace. However, accurate temperature control was difficult to achieve due to temperature differences between the crucible and the titanium charge caused by the difference in coupling between the graphite mold and the titanium and skin effect of induction melting. Typical temperature variations were as large as 300°C before melting. At melting temperatures the temperature of crucible is at least 100°C higher than that of the titanium. This increase in surface temperature led to severe stress on the crucible system.

$CaTiO_3$ crucible (1720°C)

Comparing Figure 4.3 with Figure 4.18, the $CaTiO_3$ coating on the crucible looks like it melted and severe carbon contamination occurred. Optical microscope observations (Figure 4.19 (a)) revealed that there was no continuous $CaTiO_3$ coating in the crucible and there was complete mixing of the molten Ti with the $CaTiO_3$ coating. In some areas, there were some $CaTiO_3$ + Ti structures, in other areas, there were some eutectic structures, as shown in Figure 4.19 (b). All these results showed that for this induction melting condition, $CaTiO_3$ coating degraded completely.

Mo crucible

Figure 4.20 revealed that during titanium melting, oxidation occurred. Optical microscope observations showed that it is difficult to find the interface between molybdenum and titanium. Since, titanium and molybdenum are completely miscible above the transformation temperature of pure Ti (882°C), this is a not unexpected result. Therefore, the molybdenum coating can be expected to severely contaminate molten titanium. This result is in-line with previous observations.

Y_2O_3 crucible (1800°C)

Titanium and Y_2O_3 crucible after melting in the induction furnace are shown in Figure 4.21. Optical microscope observations show that Y_2O_3 coatings were broken by the fast cooling. As with the resistive melting experiments, contamination rates between the titanium and Y_2O_3 appeared to be relatively low.

$SrZrO_3$ crucible (> 1700°C)

The $SrZrO_3$ crucible was also used for Ti melting in the induction furnace. Optical microscope observation showed that the interface appears to be intact although a few $SrZrO_3$ inclusions were found in Ti matrix. This result also showed that $SrZrO_3$ compound may have potential for use as a crucible material.

MELTING OF TITANIUM ALUMINIDE COMPOUND

In addition to the extensive studies on Cp titanium, the evaluation of mold material for the containment of a alloy based on TiAl was conducted. These studies were extremely limited and concentrated on a single mold compound $CaZrO_3$.

The $CaZrO_3$ crucibles and the melted TiAl intermetallic compound are shown in Figure 4.22 (a, b and c). For the first experiment, the crucible was filled fully; the maximum temperature was 1515°C; and industrial grade He was used as a protection gas.

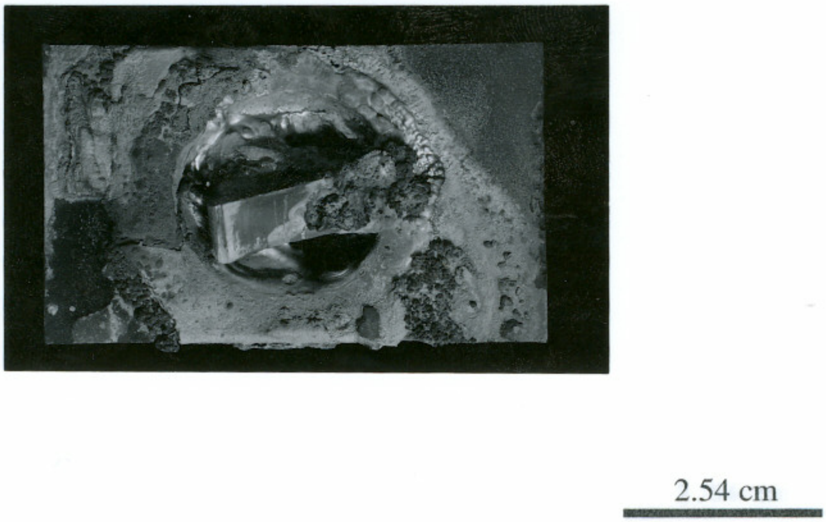

Figure 4.18 Optical macrograph of $CaTiO_3$ crucible and titanium after induction melting (1720°C), showing some melting of $CaTiO_3$ coating.

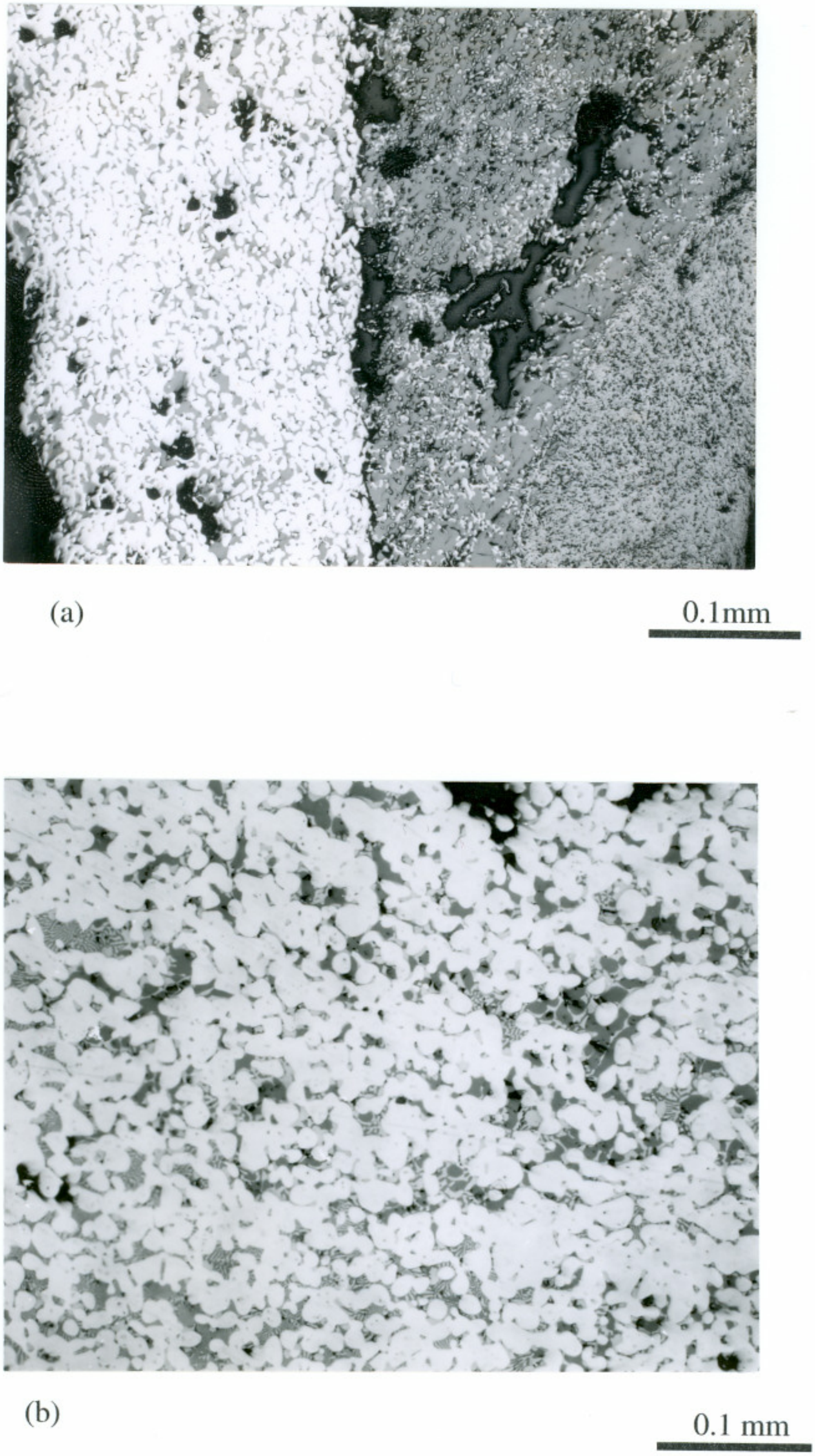

Figure 4.19 Optical micrographs of $CaTiO_3$ and Ti after induction melting (1720°C and He atm), (a) from left to right: Ti and $CaTiO_3$ coating, (b) Ti and eutectic microstructure.

Figure 4.20 Optical macrograph of Mo crucible and Ti after induction melting, showing some contamination of the titanium.

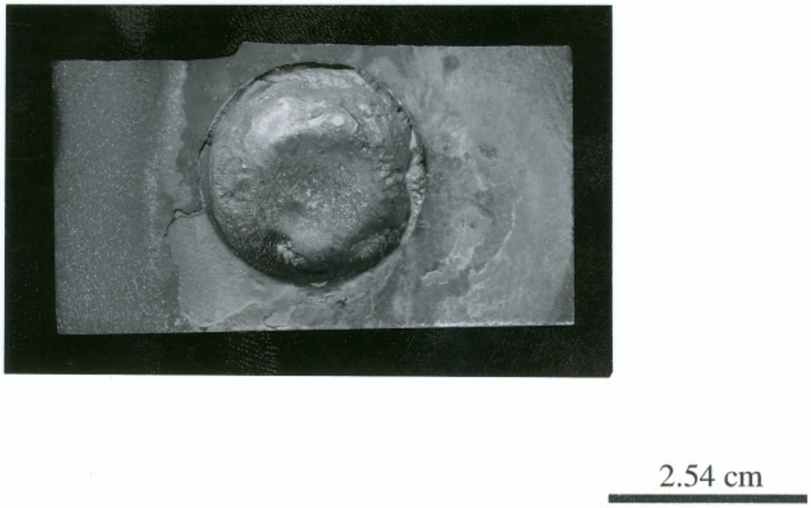

Figure 4.21 Optical macrograph of Y_2O_3 crucible and Ti after induction melting (1800°C).

Most of the TiAl flowed out the crucible, shown in Figure 4.22 (a). Optical microscope observation found that $CaZrO_3$ was still there, but only minute amount of TiAl on the coating (Figure 4.23 (a)). In the TiAl matrix, there are some fine inclusions and molten TiAl has diffused into the $CaZrO_3$ coating, but not extensively (Figure 4.23 (b)).

For the second experiment, only two small pieces of TiAl were put into the $CaZrO_3$ crucible; the maximum temperature was 1520°C and a high vacuum condition were used. The molten alloy flowed extensively over the $CaZrO_3$ coating and the color of the TiAl was brighter than that of first experiment (Figure 4.22 (a and b)). Examination after the experiment revealed that some microcracks had formed in the $CaZrO_3$ coating. Again, in the TiAl matrix there are some fine inclusions adjacent to grain boundaries, tentatively identified as a zirconium, titanium and oxygen compound; and molten TiAl has penetrated into the $CaZrO_3$ coating about 0.13 mm, shown in Figure 4.24 (a and b). Also in the $CaZrO_3$ coating 16.2 wt% of titanium and 2.19 wt% of aluminum were found at 70 μm from the interface. EDS elemental analyses did not find calcium, but zirconium was identified in the TiAl matrix, shown in Figure 4.25. 1.2 - 1.5 wt% of oxygen was found by EDS in titanium aluminide.

For the last experiment, two small pieces of TiAl were put into the $CaZrO_3$ crucible; heated to a maximum temperature of 1600°C and research grade He was used as the protection gas. Again, some of the TiAl flowed out of the crucible, the TiAl was contaminated severely and the $CaZrO_3$ coating was damaged by molten TiAl, shown in Figure 4.22 (b). Sectioning of the crucible showed that some of the $CaZrO_3$ coating was completed eliminated. One possibility for this problem, the $CaZrO_3$ coating was eroded by molten TiAl because the Al ions are very active, even more active than Ti ions at such high temperatures.

BOND LAYER AND INTERMEDIATE LAYER

EDS elemental analysis found a very small carbon peak in the Ti matrix. EDS analysis and optical microscope observations showed that the carbon diffusion zone in molybdenum bond layer was about 0.3 mm at 1710°C and 30 minutes (shown in Figure 4.26 (a)) and about 0.4 mm at 1750°C and 30 minutes (Figure 4.26 (b)). Therefore, a 0.8 mm molybdenum bond layer is thick enough to block carbon diffusion contamination on ceramic coatings for any reasonable extended length tests of a molding material.

The evaluation of an effective design for an intermediate coating is difficult. A intermediate coatings should mitigate the effects of thermal shock between metal and ceramic coatings.(27,43) This whole area of mold design is open to further development. However, the intermediate layer which was used for these experiments did effectively resist separation and cracking for many of the shells and in all cases for the layer itself.

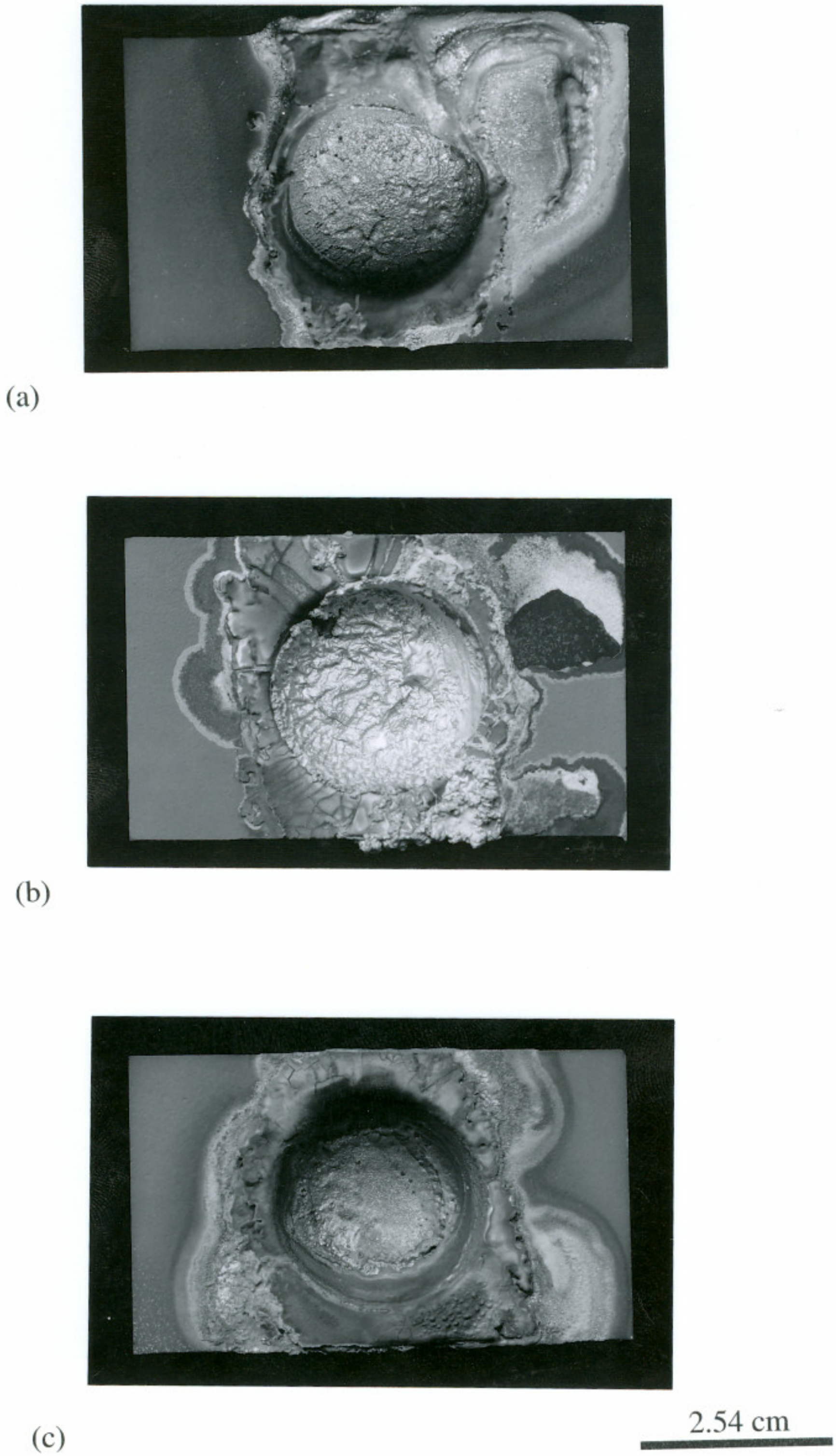

Figure 4.22 Optical micrographs of CaZrO3 crucibles and TiAl after melting at Brew furnace. (a) 1515°C, 30 min., He; (b) 1520°C, 30 min., vacuum condition; (c) 1600°C, 30 min., He atm.

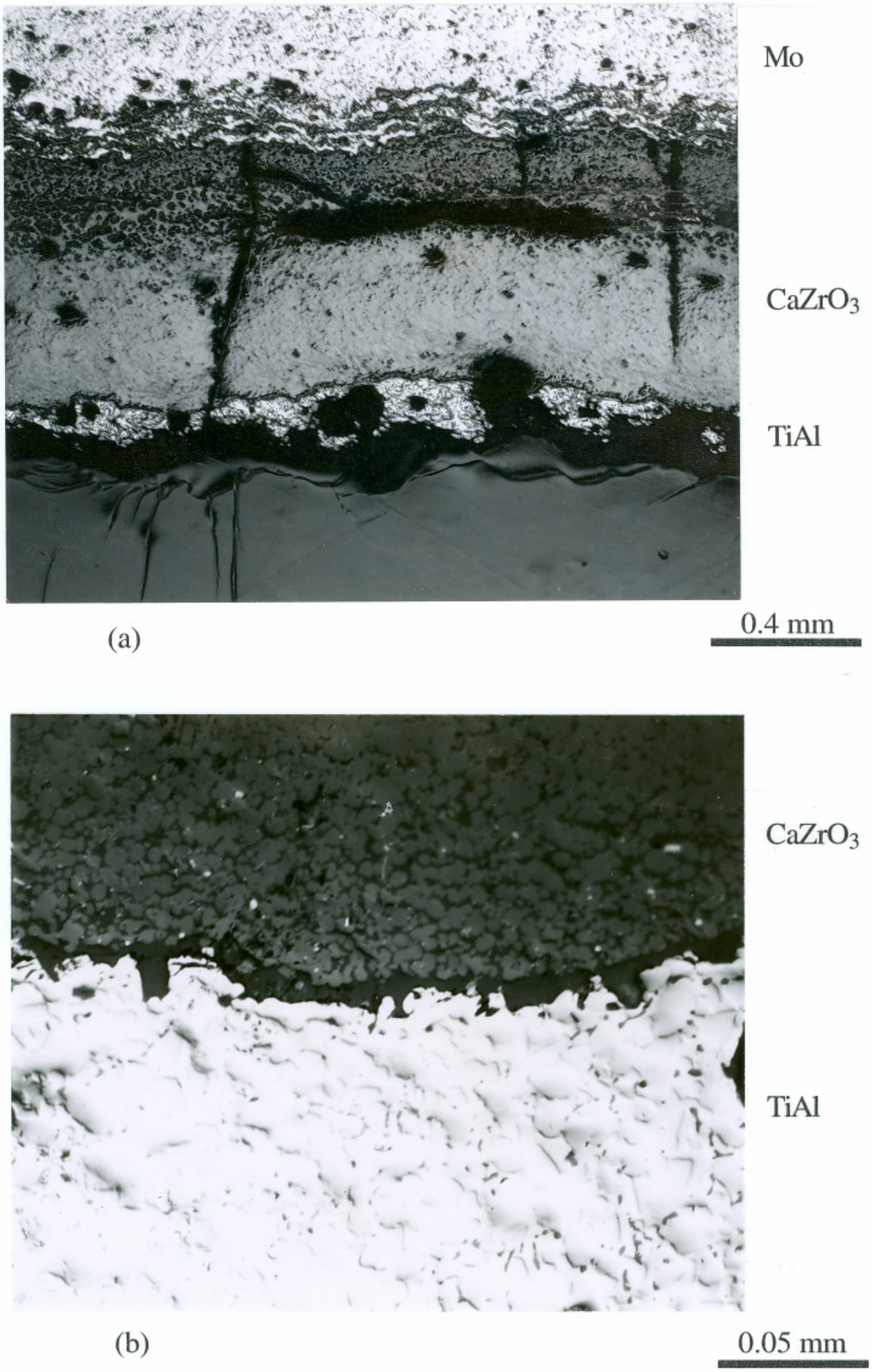

Figure 4.23 Optical micrographs of cross-section of $CaZrO_3$ crucible and TiAl at different magnifications (1515°C and He), (a) from top to bottom: Mo, blend, $CaZrO_3$ and TiAl; (b) from top to bottom: $CaZrO_3$ and TiAl.

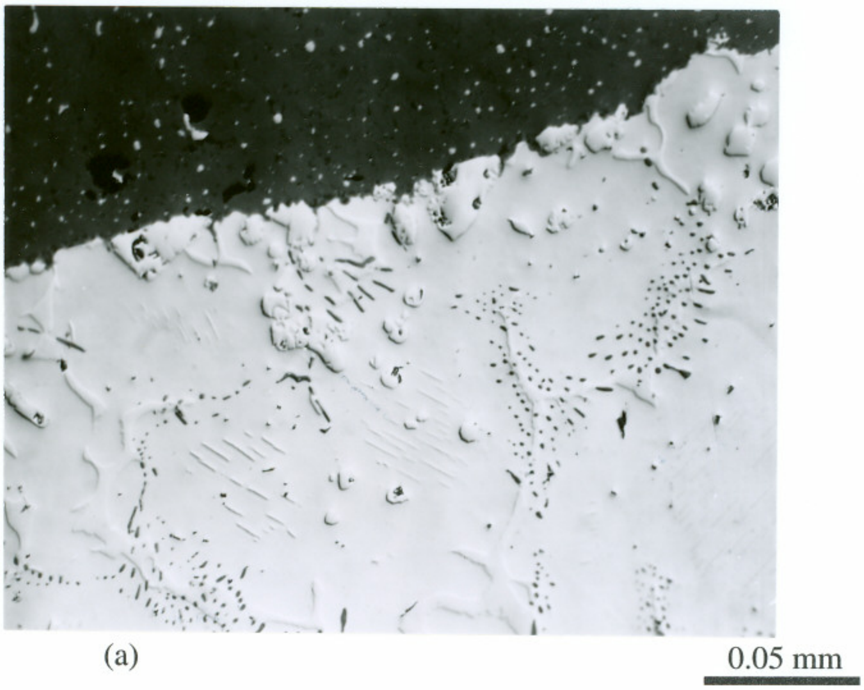

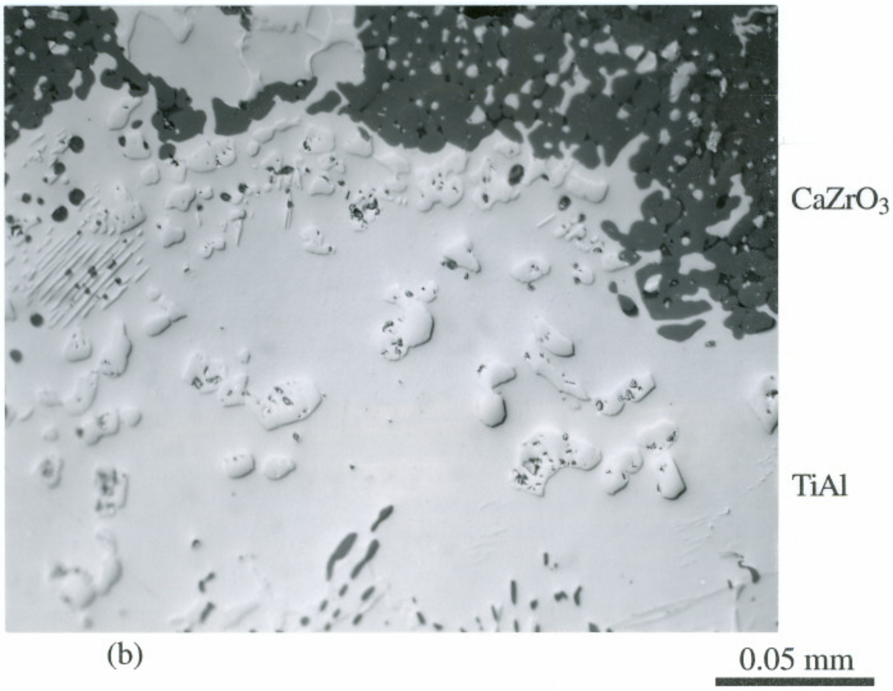

Figure 4.24 Optical micrographs of CaZrO$_3$ coating and TiAl (1520°C and vacuum condition). (a) CaZrO$_3$ coating without degradation; (b) CaZrO$_3$ coating with degradation.

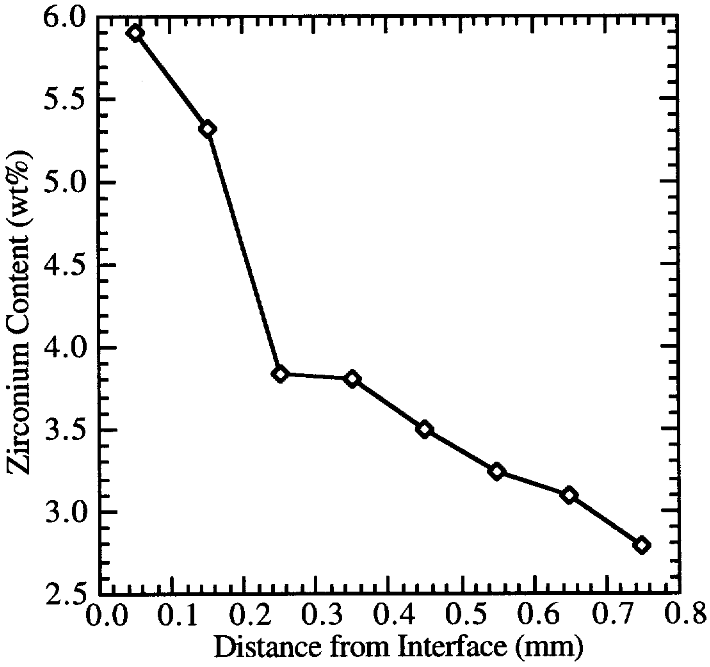

Figure 4.25 Composition profile of TiAl in the $CaZrO_3$ crucible.

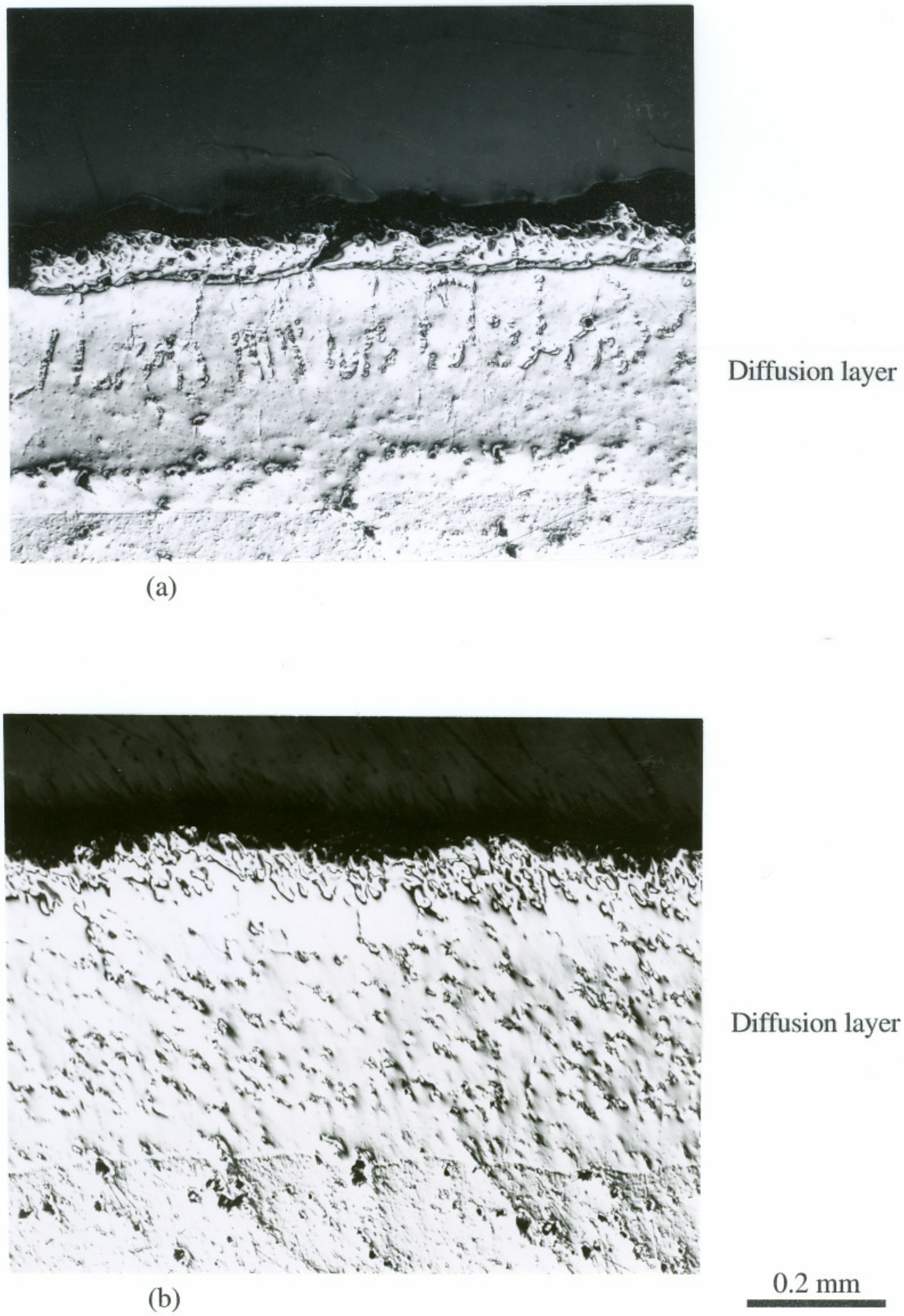

Figure 4.26 Carbon diffusion layer in molybdenum coating, (a) in Y_2O_3 crucible (1710°C, 30 minutes) and (b) $SrZrO_3$ crucible (1760°C, 30 minutes).

TEM ANALYSIS OF COATINGS

$SrZrO_3$ coating

In the $SrZrO_3$ coating, at room temperature, the matrix lattice was identified as orthorhombic, a = 5.792Å, b = 5.813 Å, c = 8.196 Å, $\alpha = \beta = \gamma = 90°$.(57,58) Its diffraction pattern was shown in Figure 4.27. On $SrZrO_3$ matrix, there existed both fine and coarse precipitates. A TEM brightfield micrograph of the coarse precipitates can be seen in Figure 4.28 (a). By using electron diffraction in Figure 4.28 and EDS in TEM the coarse precipitates were identified as $SrZrO_3$, tetragonal, a = b = 8.27 Å, c = 8.25 Å, $\alpha = \beta = \gamma =$ 90°. The following orientation relationships between matrix and coarse precipitate could be revealed (shown in Figure 4.29):

$(001)_m // (010)_p$

$[100]_m // [010]_p$

In the large precipitates EDS technique found higher Mo content had stabilized the high temperature tetragonal phase.

The fine precipitates are shown in Figure 4.30, which have the cubic lattice, a = b = c = 4.10 Å, $\alpha = \beta = \gamma = 90°$. The orientation relationships between matrix and small precipitate are not yet been determined because of their very small size. The fine and coarse precipitates could coexist and exist separately.

$CaZrO_3$ coating

Figure 4.31 represents a bright-field TEM micrograph of $CaZrO_3$ coating after $CaZrO_3$ crucible was heated at 1510°C for 30 minutes. This micrograph clearly shows the microstructure of $CaZrO_3$ and some particles on grain boundaries. The electron diffraction technique identified that the crystal lattice of matrix is orthorhombic, a = 5.792 Å, b = 5.813 Å, c = 8.196 Å, $\alpha = \beta = \gamma = 90°$, shown in Figure 4.32. By EDS these particles were identified to be molybdenum. There were many fine particles, which disperse uniformly on the $CaZrO_3$ matrix, shown in Figure 4.33. The twin structure in the $CaZrO_3$ matrix was shown in Figure 4.34.

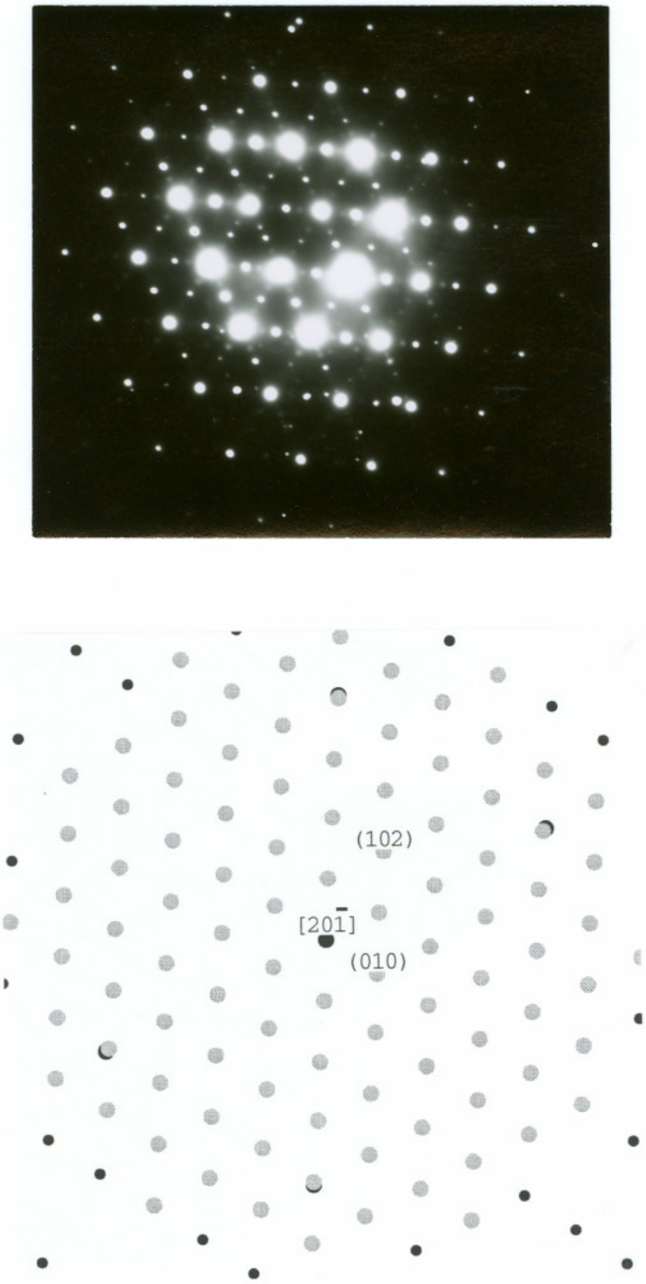

Figure 4.27 Electron diffraction pattern of $SrZrO_3$ matrix at [20-1] orientation.

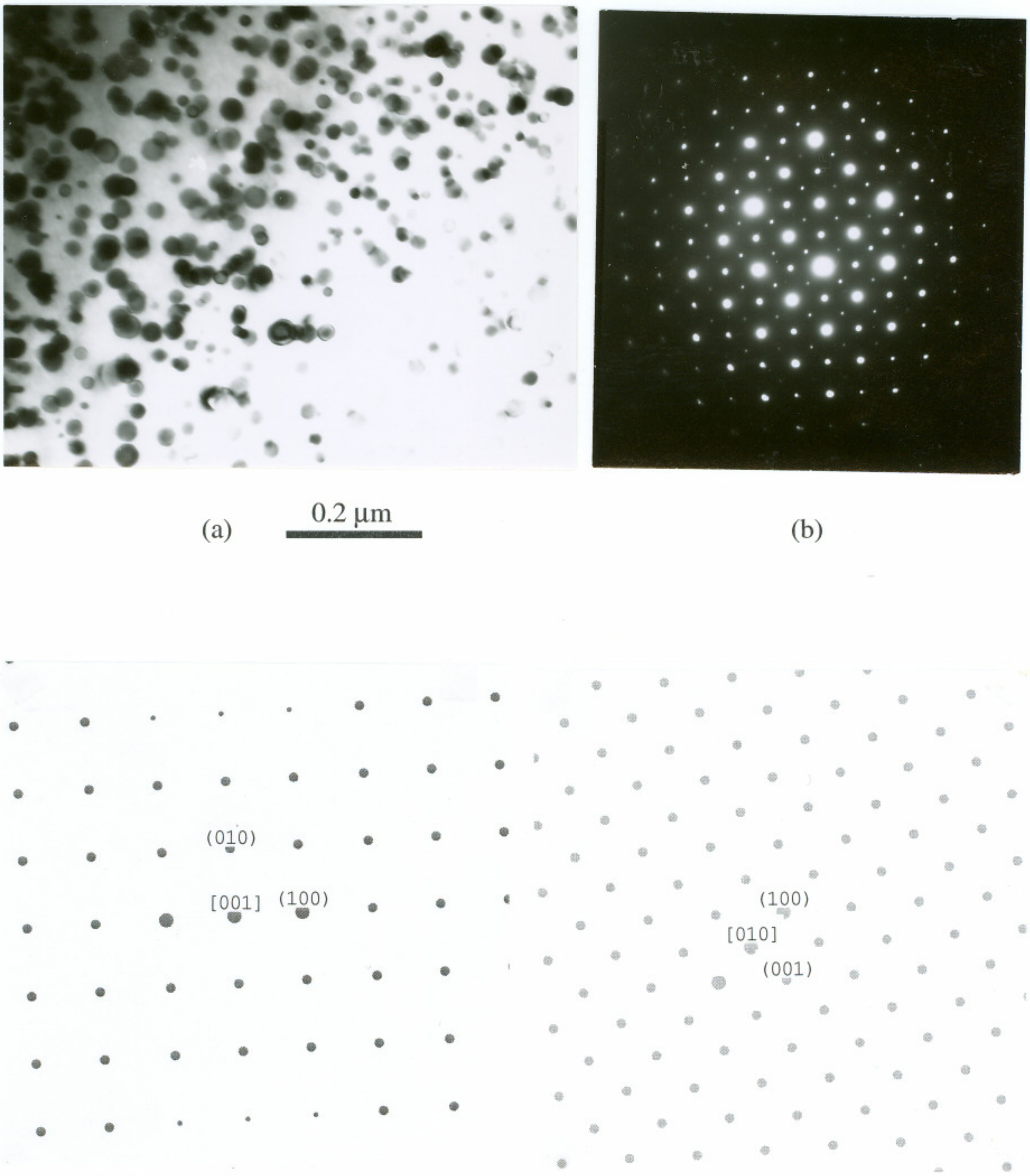

(a) (b)

(c) (d)

Figure 4.28 Bright-field TEM image of $SrZrO_3$ matrix and coarse precipitates, and its electron diffraction pattern. (a)the image, (b) the diffraction pattern, (c) index of matrix and (d) index of precipitate.

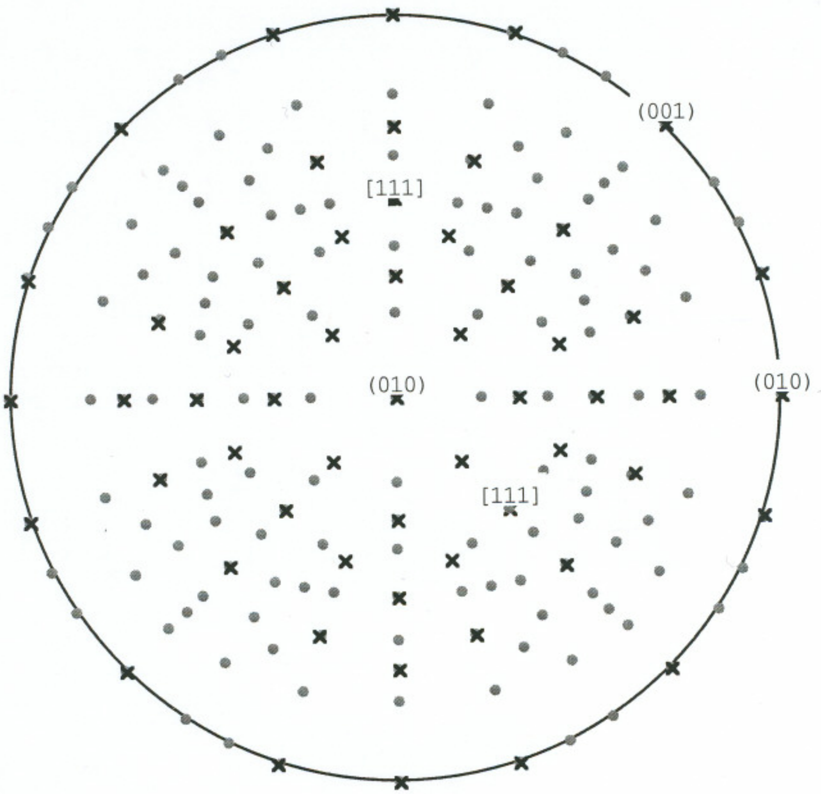

• matrix x precipitate

Figure 4.29 Stereographic projection of orientation relationships between $SrZrO_3$ matrix and coarse precipitate.

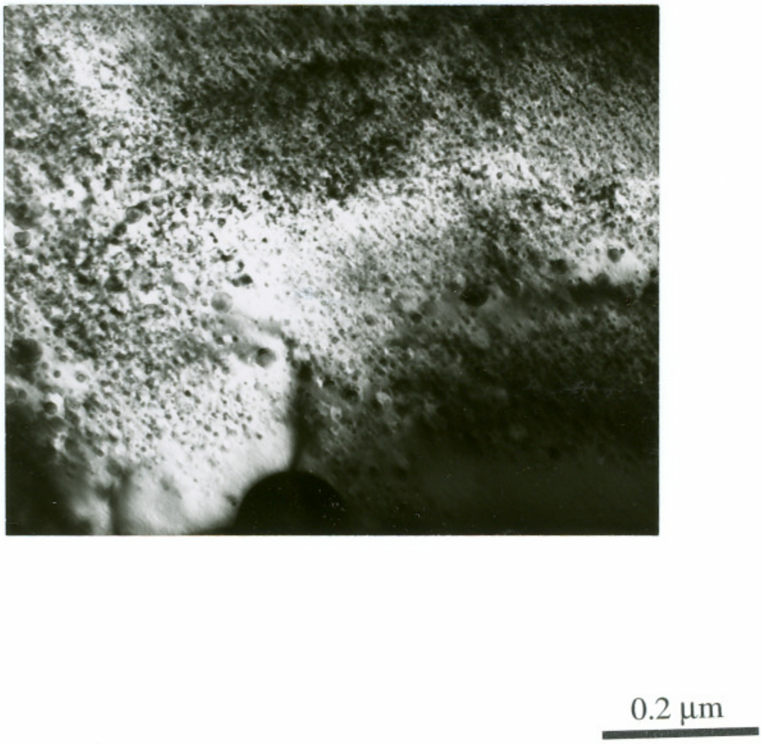

Figure 4.30 Bright-field TEM image of fine precipitates in the $SrZrO_3$ coating.

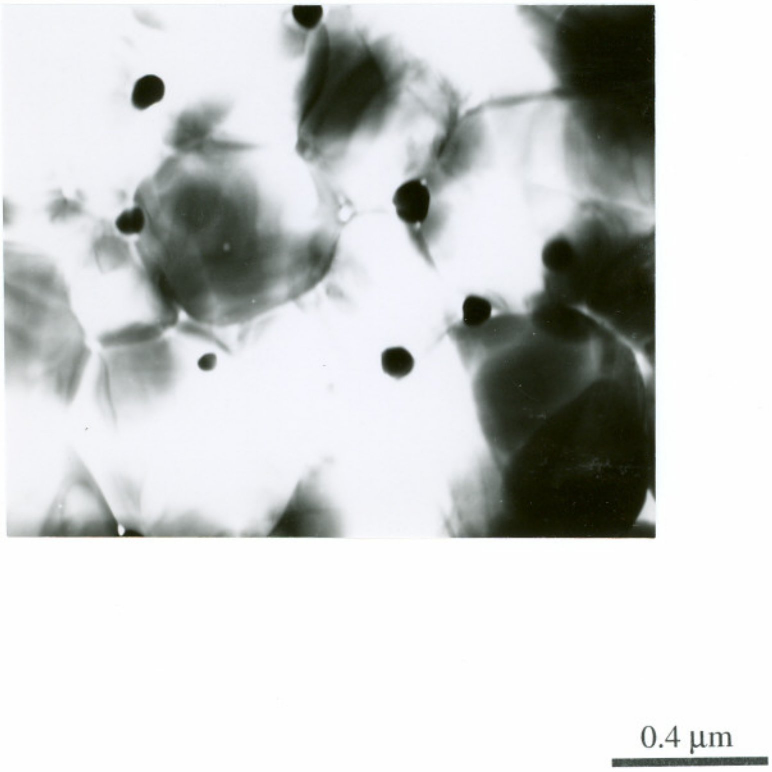

Figure 4.31 Bright-field TEM micrograph of $CaZrO_3$ coating after $CaZrO_3$ crucible was heated at 1510°C for 30 minutes.

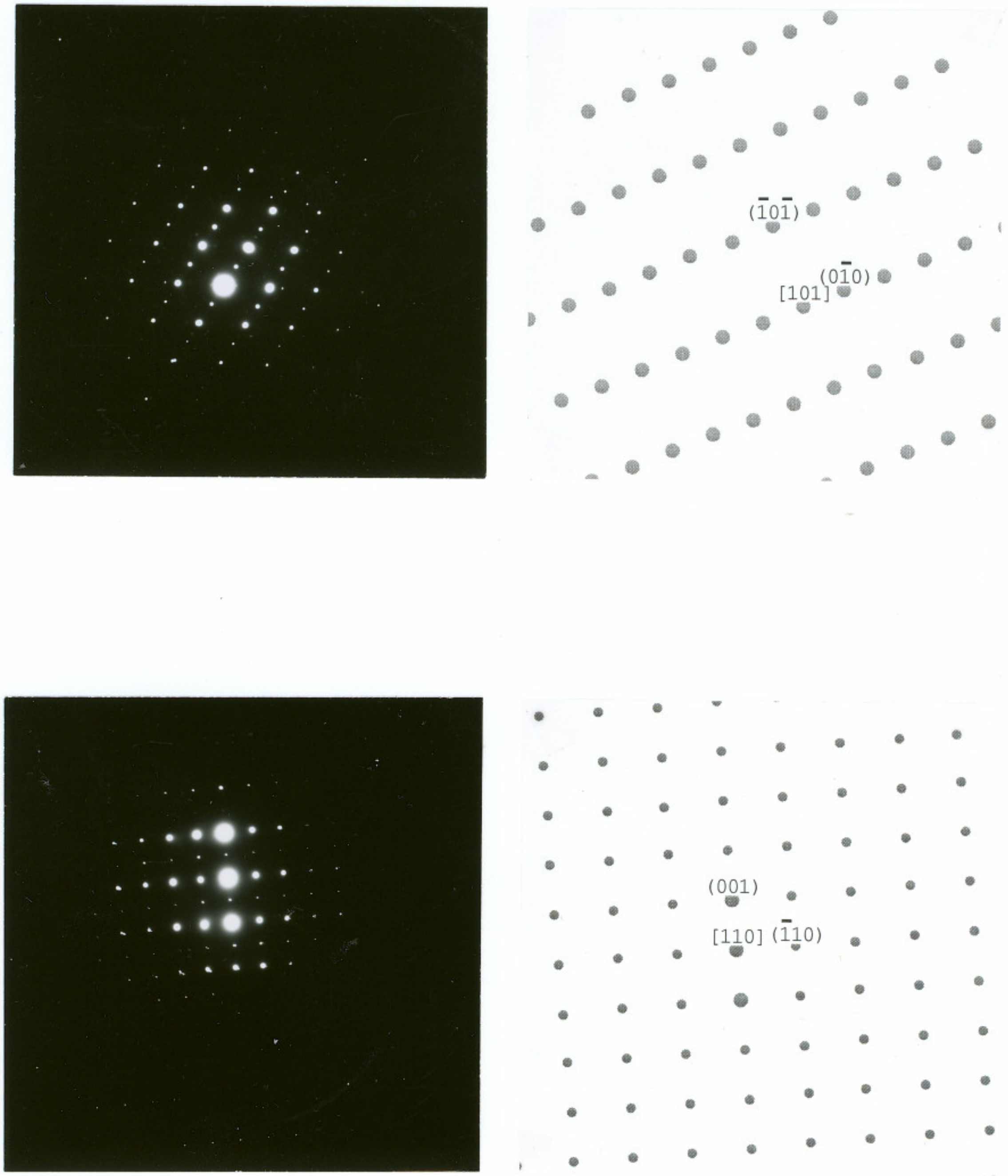

Figure 4.32 Electron diffraction patterns of $CaZrO_3$ matrix at [101] and [110] orientations.

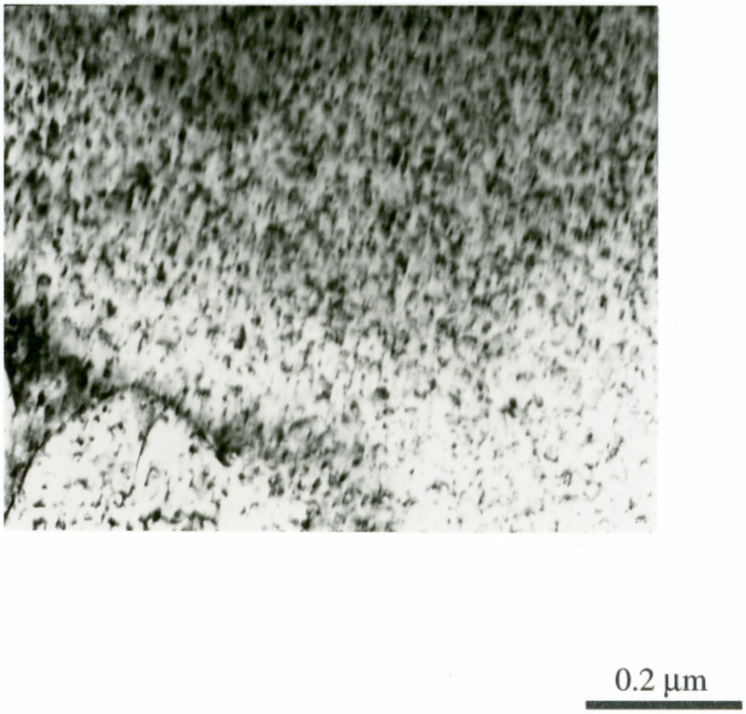

Figure 4.33 Bright-field TEM micrograph of fine precipitates in the $CaZrO_3$ matrix.

Figure 4.34 Bright-field TEM micrograph of twin structure in the $CaZrO_3$ matrix and its electron diffraction pattern.

CHAPTER 5

THERMODYNAMIC STUDY RESULTS AND DISCUSSION

SOLUBILITY OF SINGLE OXIDES IN MOLTEN TITANIUM

In the previous chapters, several types of single or complex oxides had been chosen and tried for containment of molten Ti. The experimental results need to be interpreted by their influencing factors, such as free energy, solubility in molten Ti, melting temperature, etc. Most of the researchers could only use the free energy of refractory compounds to explain their experimental results because solubility data of refractory compound in molten Ti were difficult to find. However, the above approach disregards the need to consider solution effects. Many experiments have shown that the level of contamination in liquid titanium from refractory oxides may not only be related to thermodynamic stability of the refractory material but may be influenced by its solubility in the titanium, which means that the solubility of ceramic compound in molten pure titanium is also a key factor to choose and evaluate crucible coating ceramics. A more refined approach is to calculate the solubility of the ceramic basic metal and the ceramic compound.

With titanium's large solubility and great affinity for interstitial elements, the driving force for reaction can better be evaluated by considering the partial molar free energies of solution for interstitials in titanium.(8) Using values averaged from literature,(59,60) the variation with temperature of partial molar free energies of several solutions was plotted. The variation of free energies of formation for refractory oxides with temperature was then superimposed on the earlier plot and materials rated. At 1400°C, the free energy of formation of ZrO_2 is more negative than any titanium oxygen phase, but comparison of this with titanium-10 atomic percent oxygen solution indicates a driving force for dissolution of the zirconia. This is well illustrated by the Ti-ZrO_2 line in the Ti-Zr-O ternary system where, at 1400°C, oxygen-deficient zirconia is in equilibrium with a Ti-Zr-O solution containing about 30 wt% ZrO_2.(61) Therefore, oxides such as Al_2O_3 and SiO_2 are not compatible with titanium, even at relatively low temperatures. A candidate oxide crucible should be able to coexist with a very dilute titanium-oxygen solution at temperature higher than melting point. This strict requirement eliminates most refractory with the possible exception of CaO, ThO_2, the trivalent rare earth (Y_2O_3) and perhaps a few others. This approach can explain some experimental results, but the data it needs is still hard to be found, and it can not give quantitative results to compare potential compounds and interpret the test results. The solubility of compounds is very important not only to explain present experimental results but also to select the potential refractory compounds in the future. So it is very necessary to try to get the data by some method.

Thermodynamic calculations have been carried out to determine solubility of single oxides in molten pure titanium.(28,62) Based on the standard Gibbs energy of formation of Y_2O_3 and Gibbs energy of solution of oxygen and yttrium in liquid titanium, the solubility product of Y_2O_3 in molten titanium has been evaluated by Hoch(62) as

$$(wt\ pct\ Y)(wt\ pct\ O)^{1.5} = exp(-(19.9/T)+8.325) \tag{1}$$

where T is temperature in kilo-Kelvin (kK).

Based on the assumption of ideal mixing of Zr in Ti in the liquid state, the solubility of ZrO_2 had been calculated by Saha et al (28)

$$(wt\ pct\ Zr)\cdot(wt\ pct\ O)^2 = exp(-(2.1639/T)+8.8755) \tag{2}$$

However, no such evaluation has been done for other potential refractory oxides, specially for complex oxides, and until now no work has explored the controlling factors for solubility of oxides in molten Ti. In this chapter, thermodynamics will be employed to evaluate the solubility of single and complex oxides in molten Ti, and influencing factors will be discussed in detail.

Based on the previous results,(28,62) the solubility of CaO, ThO_2 and HfO_2 in molten Ti will be calculated respectively, and CaO is used as an example.

Solubility of CaO in molten titanium

solubility of CaO in molten Ti is governed by Eq. (3):

$$Ca(s)+\frac{1}{2}O_2(g)\rightarrow CaO(s) \tag{3}$$

The standard free energy for this reaction is list below(20)

$$\Delta G^\circ = -792.3+192.83T\ \ kJ/mol \tag{4}$$

or $= -RT\ lnK$

where T is temperature in kilo Kelvin. Rearranging Eq. (4),

$$lnK = -\frac{\Delta G^\circ}{RT} = 792.3/RT - 192.83/R \tag{5}$$

where K is the equilibrium constant for Reaction (6).

The dissolution of CaO in liquid titanium is given by

$$\underline{Ca}+\underline{O}\rightarrow CaO \tag{6}$$

where the underlined values for $\underline{Ca}$ and $\underline{O}$ denote the activity of Ca and O in liquid titanium, respectively. From the equilibrium constant,

$$K = (\frac{a_{CaO}}{a_{\underline{Ca}} \cdot a_{\underline{O}}}) \tag{7}$$

where $a_{CaO} = 1$, Eq. (7) can be rewritten as

$$\ln K = -\ln a_{\underline{Ca}} - \ln a_{\underline{O}} \tag{8}$$

Based on the Hoch's results, following relationship can be given$^{(62)}$

$$\ln a_{\underline{O}} = \ln (wt\, pct\, O) - (65.27/T) + 9.528 \tag{9}$$

where the activity of dissolved oxygen is expressed with reference to the diatomic gas as the standard state.

For calcium

$$Ca\,(s) \rightarrow Ca\,(l) \tag{10}$$

If the heat capacities of the liquid and solid metal are the same ($\Delta C_p = 0$) then from thermodynamics we know that the enthalpy and entropy changes upon freezing are independent of temperature. The average value of ΔC_p for melting of Zr, Hf and Th is less than 1 %. Hence, to a good approximation we may take ΔH and ΔS constant with temperature, as ΔH_f and ΔS_f, and $\Delta H_f - T_f \Delta S_f = 0$,

$$\Delta G^\circ(11) = \Delta H_f - T\Delta S_f = \Delta H_f(1 - \frac{T}{T_m}) \tag{11}$$

where ΔH_f is the heat of fusion (8.36 kJ/mol for Ca) at the melting point, T_m (1.123 kK for Ca). However, for Ca this approximation is not suitable, for example, the average value of ΔC_p for melting of Ca is about 36%. The additional change in Gibbs free energy should be calculated when Ca is heated from its melting point to Ti melting temperature. The free energy change is

$$\begin{aligned}\Delta G_{ad} = \Delta H - T\Delta S &= \int_{1.123}^{T}(C_{pl} - C_{ps})dT - T\int_{1.123}^{T}\frac{C_{pl} - C_{ps}}{T}dT \\ &= \int_{1.123}^{T}(30.93 - 42.09)dT - T\int_{1.123}^{T}\frac{30.93 - 42.09}{T}dT \\ &= -11.16T + 12.53 + 11.16T\ln\frac{T}{1.123}\end{aligned} \tag{12}$$

where C_{pl} and C_{ps} are the molar heat capacities for liquid and solid forms of metal constituents, respectively.

Substituting ΔH_f and T_m values in Eq (11), we get

$$\Delta G^\circ(11) = 8.36 - 7.53T \tag{13}$$

So the total free energy change is

$$\begin{aligned}\Delta G &= \Delta G_{ad} + \Delta G(11) = -11.16T + 12.53 + 11.16T\ln\frac{T}{1.123} + 8.36 - 7.53T \\ &= -18.69T + 20.89 + 11.16T\ln\frac{T}{1.123}\end{aligned} \tag{14}$$

Assuming ideal mixing of Ca in liquid state,

$$Ca\ (l) \rightarrow Ca\ (alloy) \tag{15}$$

$$\Delta G_{Ca} = RT\ln X_{Ca} \tag{16}$$

Therefore, for the reaction

$$Ca\ (s) \rightarrow Ca\ (alloy) \tag{17}$$

$$\begin{aligned}\Delta G^\circ(17) = RT\ln a_{Ca} &= \Delta G^\circ(14) + \Delta G^\circ(16) \\ &= -18.69T + 20.89 + 11.16T\ln\frac{T}{1.123} + RT\ln X_{Ca}\end{aligned} \tag{18}$$

where X_{Ca} = [wt pct Ca/(100 atom wt Ca)] x atom wt Ti = wt pct Ca · (47.90/4008) for dilute solution of Ca in Ti.

Therefore,

$$\ln X_{\underline{Ca}} = \ln(\text{wt pct Ca}) - 4.427 \tag{19}$$

Substituting for X_{Ca} in Eq. (18) and dividing the whole expression by RT,

$$\ln a_{Ca} = \ln(\text{wt pct Ca}) - 4.427 - \frac{18.69}{R} + \frac{20.89}{RT} + \frac{11.16}{R}\ln\frac{T}{1.123} \tag{20}$$

Substituting values of ln $a_{\underline{O}}$ (Eq. 19) and ln $a_{\underline{Ca}}$ (Eq. 20) in Eq. (21) and combining it with Eq. (7), we get

$$\begin{aligned} \ln K = -\ln(\text{wt pct Ca}) + 4.427 + \frac{18.69}{R} - \frac{20.89}{RT} - \frac{11.16}{R}\ln\frac{T}{1.123} - \ln(\text{wt pct O}) \\ + (\frac{65.27}{T}) - 9.528 = \frac{792.3}{RT} - \frac{192.83}{R} \end{aligned} \tag{21}$$

Rearranging Eq. (21), one gets

$$\begin{aligned} \ln(\text{wt pct Ca}) + \ln(\text{wt pct O}) = 4.427 + \frac{18.69}{R} - \frac{20.89}{RT} - \frac{11.16}{R}\ln\frac{T}{1.123} \\ + (\frac{65.27}{T}) - 9.528 - \frac{792.3}{RT} + \frac{192.83}{R} \end{aligned} \tag{22}$$

where R is the gas constant (8.314 KJ/mol kK).

$$\ln(\text{wt pct Ca}) + \ln(\text{wt pct O}) = 20.34 - \frac{32.54}{T} - 1.342\ln\frac{T}{1.123} \tag{23}$$

The solubility product of CaO is

$$(\text{wt pct Ca})(\text{wt pct O}) = \exp(20.34 - \frac{32.54}{T} - 1.342\ln\frac{T}{1.123}) \tag{24}$$

(The solubility of CaO equals weight percentage of calcium in molten Ti times weight percentage of oxygen in molten Ti).

The solubility products of HfO_2 and ThO_2 are also calculated and listed below.

$$(wt\ pct\ Th)(wt\ pct\ O)^2 = exp(13.338 - (24.86/T)) \tag{25}$$

$$(wt\ pct\ Hf)(wt\ pct\ O)^2 = exp(9.43 - (4.06/T)) \tag{26}$$

Using the same strategy, the solubility product of Y_2O_3 in molten Ti is obtained

$$(wt\ pct\ Y)\ (wt\ pct\ O)^{1.5} = exp(8.281 - \frac{16.993}{T} + ln\frac{T}{1.803}) \tag{27}$$

Assume that all of the solubility product come from the dissolution of oxide coatings, the following relationships between solubility of oxides in molten titanium and melting temperature can be obtained:

$$(wt\ pct\ Y_2O_3)^{2.5} = 12.91exp(8.281 - \frac{16.993}{T} + ln\frac{T}{1.803}) \tag{28}$$

$$(wt\ pct\ ThO_2)^3 = 77.7exp(13.338 - (24.86/T)) \tag{29}$$

$$(wt\ pct\ CaO)^2 = 4.904exp(20.34 - \frac{32.54}{T} - 1.342ln\frac{T}{1.123}) \tag{30}$$

$$(wt\ pct\ HfO_2)^3 = 51.04exp(9.43 - (4.06/T)) \tag{31}$$

$$(wt\ pct\ ZrO_2)^3 = 20exp(-(2.1639/T) + 8.8755) \tag{32}$$

The results, sketched in Figures 5.1 and 5.2, show that solubility of Y_2O_3 in molten titanium is the lowest, which is the one of several main reasons that many experiments(8,9,27) showed Y_2O_3 is the most stable compound containing molten Ti. Another advantage is that its solubility is not pronouncedly dependent on melting temperature, suggesting that Y_2O_3 can be used in large superheat for Ti melting.

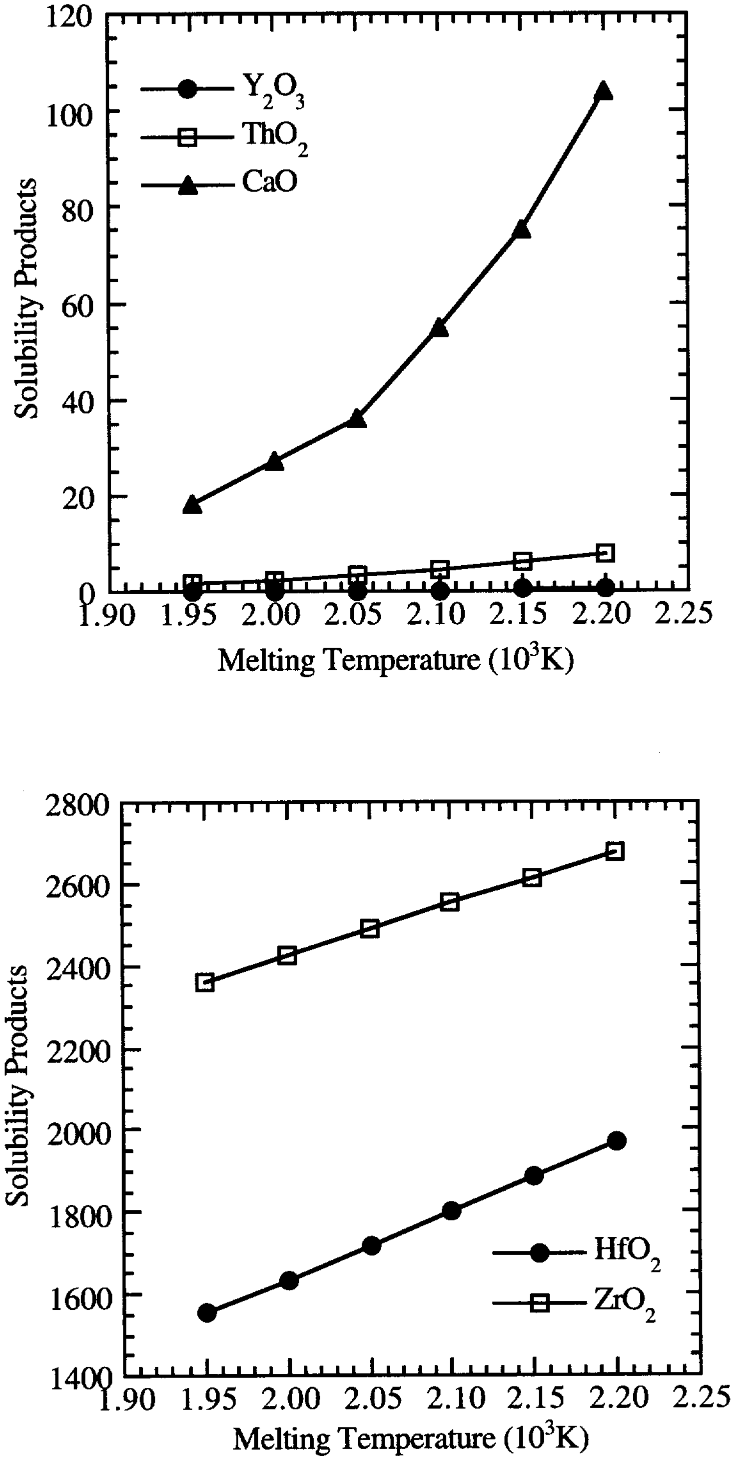

Figure 5.1 Solubility products of single oxides in molten titanium: Y_2O_3, ThO_2, CaO, HfO_2 and ZrO_2.

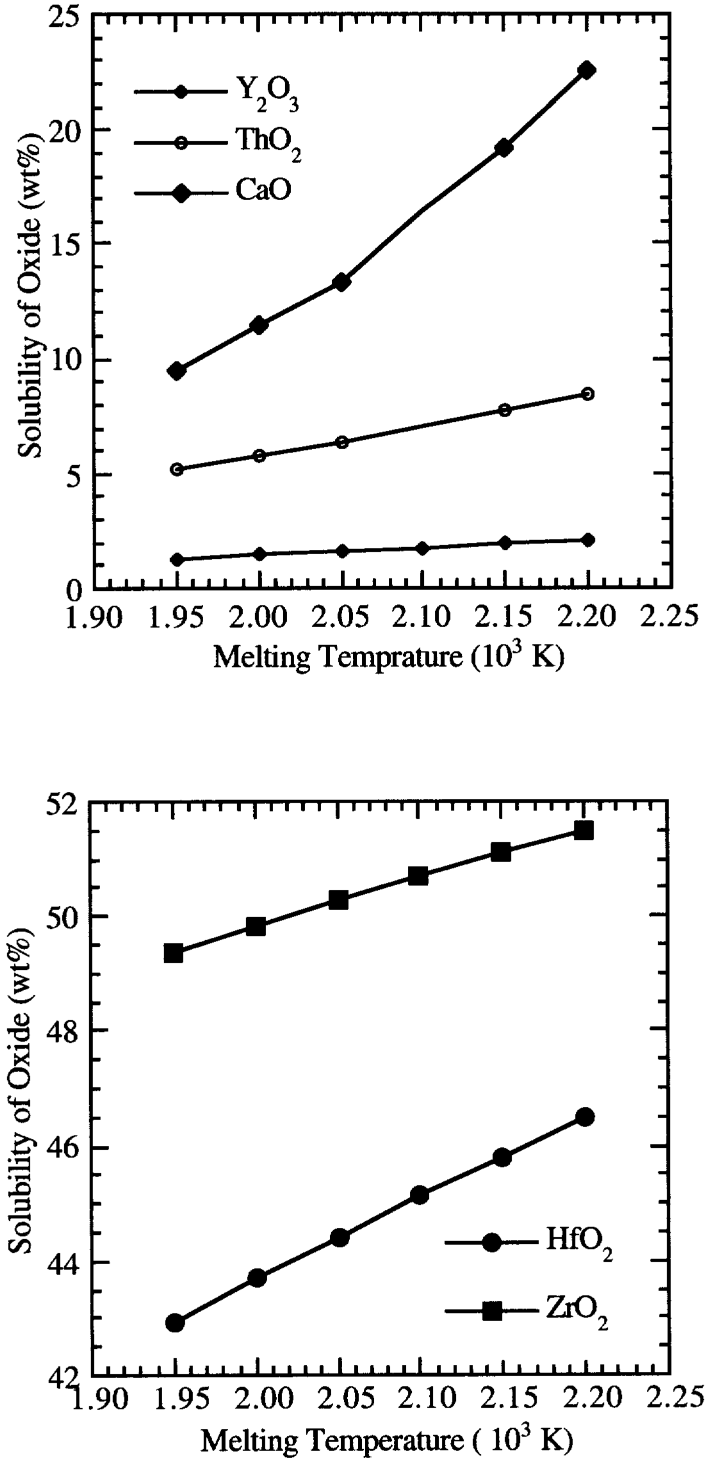

Figure 5.2 The solubility of single oxides in molten titanium at different melting temperatures: Y_2O_3, ThO_2, CaO, HfO_2 and ZrO_2.

Although Th element has a high solubility in molten Ti (up to 86.5% wt pct), ThO_2 is the second lowest, which is why prior to recognition of Y_2O_3 thorium oxide (ThO_2) was generally considered the most stable refractory oxide in contact with molten titanium,(9) but unfortunately it is radioactive and can not be used in industry. Solubility of CaO is the third lowest, only concern is that its solubility increases rapidly with melting temperature. Two experiments(21,63) showed that the oxygen contamination of Ti using CaO crucible is very low, perhaps because dissolution rate of CaO is slow. Those of ZrO_2 and HfO_2 are very high, which will seriously contaminate molten Ti. Domagala et al(56) found that the maximum solubilities of ZrO_2 in ß-Ti and α-Ti are about 17 and 40 %wt respectively.

SOLUBILITY OF COMPLEX OXIDES IN MOLTEN TITANIUM

In this experiment, complex-oxides are also evaluated for containing molten Ti. Because thermochemical properties of complex oxides are difficult to be found, many data such as free energy of complex oxide formation and free energy of formation from the constituent oxides have been calculated based on several handbooks(64-67) about thermochemical properties of inorganic substances and shown in Tables 5.1 and 5.2.

Table 5.1 Free energy of formation of complex oxides for one mole oxygen

Temperature (k)	$CaTiO_3$ -ΔG(kJ/mol)	$CaZrO_3$ -ΔG(kJ/mol)	$SrZrO_3$ -ΔG (kJ/mol)
1700	793.51	852.34	860.61
1800	769.41	828.35	836.54
1900	745.60	803.82	812.60
2000	721.44	779.40	788.80
2100	697.24	755.10	764.90

The relationships between free energy of formation and temperature are listed below:

$$\Delta G_{CaTiO3} = 239.85\ T - 1201.14 \quad (33)$$

$$\Delta G_{CaZrO3} = 244.75\ T - 1268.9 \quad (34)$$

$$\Delta G_{SrZrO3} = 238.7\ T - 1266.2 \quad (35)$$

Table 5.2 Free energy of formation from the constituent oxides to complex oxides

Temperature (k)	$CaTiO_3$ -ΔG (kJ/mol)	$CaZrO_3$ -ΔG (kJ/mol)	$SrZrO_3$ -ΔG (kJ/mol)
1700	90.0 (60.0)	43.68 (29.12)	90.68 (60.45)
1800	90.1(60.07)	38.58 (25.72)	90.53 (60.35)
1900	90.1 (60.07)	38.80 (25.86)	90.42 (60.28)
2000	90.1(60.07)	39.04 (26.02)	90.38 (60.26)
2100	90.12(60.08)	39.24 (26.16)	90.28 (60.19)

Values in ( ) denote the free energy for one mole oxygen

When complex oxides dissolve in molten Ti, there may exist in several existing forms such as $[Sr][Zr][O]^3$, $[SrO][Zr][O]^2$ and $[SrO][ZrO_2]$ for $SrZrO_3$ ($SrO \bullet ZrO_2$). $[SrO][Zr][O]^2$ is of importance because ZrO_2 contributes most of complex oxide solubility in molten titanium.

(1) Decomposition of $SrZrO_3$ to [SrO], [O] and [Zr] (Mode I)

At this decomposition mode, the solubility of $SrZrO_3$ is governed by following equation:

$$Zr + O_2 + SrO \rightarrow ZrO_2 + SrO \rightarrow SrZrO_3(SrO \bullet ZrO_2) \quad (36)$$

The standard free energy is

$$\Delta G^o = -90.38 - 1084 + 179.5T = -1174.38 + 179.5T \ kJ/mol \quad or = -RT \ lnK \tag{37}$$

where T is temperature in kilo Kelvin. Rearranging equation (37),

$$ln\,K = -\frac{\Delta G^o}{RT} = \frac{1174.38}{RT} - \frac{179.5}{R} = ln\frac{1}{a_{\underline{Zr}}a_{\underline{O}}^2a_{\underline{SrO}}} \tag{38}$$

where $\underline{Zr}$, $\underline{O}$ and $\underline{SrO}$ denote Zr, O and SrO in molten Ti, and $a_{SrZrO3} = 1$.

For dissolution of ZrO_2 in molten Ti, the following equation can be gotten from derivation below.

$$lna_{\underline{Zr}} + 2\ lna_{\underline{O}} = ln(wt\ pct\ Zr) + 2\ ln(wt\ pct\ O) - \frac{128.21}{T} + 12.74 \tag{39}$$

For SrO,

$$SrO(s) \rightarrow SrO(l) \tag{40}$$

$$\Delta G(36) = \Delta H_f - T\Delta S_f = \Delta H_f(1 - \frac{T}{T_m}) = 75.312 - 25.63T \tag{41}$$

where ΔH_f is the heat of fusion of SrO (75.312 KJ/mol) and T_m is the melting point of SrO (2.938 kK).

Also assuming ideal mixing of SrO in molten Ti,

$$SrO(l) \rightarrow SrO(alloy) \tag{42}$$

$$\Delta G_{SrO}(38) = RT\ ln\ X_{SrO} \tag{43}$$

Therefore, for the reaction

$$SrO(s) \rightarrow SrO(alloy) \tag{44}$$

$$\begin{aligned}\Delta G(40) &= RT\ ln\ a_{SrO} = \Delta G(36) + \Delta G_{SrO}(38) \\ &= (75.312 - 25.63T) + RT\ ln\ X_{SrO}\end{aligned} \quad (45)$$

where X_{SrO} = [wt pct SrO/100 at wt SrO)] x atom wt Ti = wt pct SrO (47.90/10362) for dilute solution of SrO in Ti.

$$ln\ X_{SrO} = ln\ (wt\ pct\ SrO) - 5.377 \quad (46)$$

So the following equation can be gotten

$$ln\ a_{\underline{SrO}} = ln(wt\ \text{pct SrO}) - 8.46 + \frac{9.058}{T} \quad (47)$$

Combining equations (42) , (43) and (47), we can get

$$\begin{aligned}&ln\ K = -ln(wt\ pct\ Zr) - 2\ ln(wt\ pct\ O) + \frac{128.21}{T} - 12.74 - ln(wt\ pct\ SrO) \\ &+8.46 - \frac{9.058}{T} = \frac{1084 + 90.38}{RT} - \frac{179.5T}{RT} = \frac{141.25}{T} - 21.59\end{aligned} \quad (48)$$

Rearranging equation (48), one gets

$$(wt\ pct\ SrO)(wt\ pct\ Zr)(wt\ pct\ O)^2 = exp(17.31 - \frac{22.10}{T}) \quad (49)$$

Solubility of $CaZrO_3$ and $CaTiO_3$ in molten Ti is also calculated and shown below

$$(wt\ pct\ CaO)(wt\ pct\ Zr)(wt\ pct\ O)^2 = exp(16.624 - \frac{16.422}{T}) \quad (50)$$

$$(wt\ pct\ CaO)(wt\ pct\ Ti)(wt\ pct\ O)^2 = exp(15.721 - \frac{5.057}{T}) \quad (51)$$

Also assume that all of the solubility come from the dissolution of complex oxide coatings, the following relationships between solubility of complex oxides in molten titanium and melting temperature can be obtained:

$$(wt\ pct\ SrZrO_3)^4 = 273.82 exp(17.31 - \frac{22.10}{T}) \tag{52}$$

$$(wt\ pct\ CaZrO_3)^4 = 478.46 exp(16.624 - \frac{16.422}{T}) \tag{53}$$

$$(wt\ pct\ CaTiO_3)^4 = 123.81 exp(15.721 - \frac{5.057}{T}) \tag{54}$$

(2) Decomposition of $SrZrO_3$ to [SrO] and [ZrO_2] (Mode II)

At this decomposition mode, the reaction should be:

$$SrO + ZrO_2 \rightarrow SrZrO_3 \tag{55}$$

The free energy for this reaction is given by the table above

$$\begin{aligned}\Delta G^\circ &= -90.382 \text{ KJ / mol (reaction temperature} > 1900 \text{ k)} \\ &\text{or} = -RT\ ln\ k\end{aligned} \tag{56}$$

Using same strategy used above, following equations will be gotten

$$ln\ a_{\underline{SrO}} = ln(wt\ pct\ SrO) - 8.46 + \frac{9.058}{T} \tag{57}$$

$$ln\ a_{\underline{ZrO_2}} = ln(wt\ pct\ ZrO_2) - 9.10 + \frac{10.47}{T} \tag{58}$$

$$ln\ k = ln\ a_{\underline{SrO}} + ln\ a_{\underline{ZrO_2}} = -\frac{\Delta G^\circ}{RT} \tag{59}$$

$$(wt\ pct\ ZrO_2)(wt\ pct\ SrO) = exp(17.56 - \frac{30.382}{T}) \tag{60}$$

For other complex oxides, we can get

$$(wt\ pct\ CaO)(wt\ pct\ ZrO_2) = exp(16.847 - \frac{24.72}{T}) \tag{61}$$

$$(wt\ pct\ CaO)(wt\ pct\ TiO_2) = exp(16.645 - \frac{28.438}{T}) \qquad (62)$$

The solubility of complex oxides in equations (49-54) is given in Figures 5.3 and 5.4, where the solubility products of solute weight percentages are plotted against the melting temperatures. When decomposition is from $SrZrO_3$ to [SrO], [O] and [Zr], from $CaZrO_3$ to [CaO], [O] and [Zr], and from $CaTiO_3$ to [CaO], [O] and [Ti], the solubility of $SrZrO_3$ is the lowest, that of $CaTiO_3$ is the highest and the difference between solubility of $SrZrO_3$ and $CaTiO_3$ is very large, shown in Figures 5.3 and 5.4. $SrZrO_3$ is used as an example to discuss the effect of some parameters on its solubility. Like single oxides, the solubility of complex oxides is dependent on free energy of formation of ZrO_2, heat of fusion of Zr , melting point and atomic weight of Zr. It is also dependent on the free energies of formation of complex oxides $SrZrO_3$ from the constituent oxides ZrO_2 and SrO. The free energy of formation of ZrO_2 and free energies of formation of complex oxides $SrZrO_3$ from the constituent oxides ZrO_2 and SrO have a dominant effect on the solubility in molten Ti. The lower the total of the two free energies, the lower the solubility in molten Ti. The lower free energy of formation of $SrZrO_3$ from ZrO_2 and SrO (90 KJ/mol) compared to the formation of $CaZrO_3$ from CaO and ZrO_2 (40 KJ/mol) makes $SrZrO_3$ have lower solubility than $CaZrO_3$. The highest free energy of TiO_2 makes $CaTiO_3$ have the highest solubility in molten Ti, although there is a lower free energy of formation of $CaTiO_3$ from CaO and TiO_2 (90 kJ/mol).

The solubility of complex oxides in equations (60 - 62) is given in Figure 5.5. At this decomposition mode, $SrZrO_3$ and $CaTiO_3$ have very similar lower solubility in molten Ti, but $CaZrO_3$ has the highest solubility, shown in Figure 5.5. On assumption of this decomposition mode, only free energy of formation of complex oxides from constituent oxides exerts an effect on its solubility in molten Ti. Both $SrZrO_3$ and

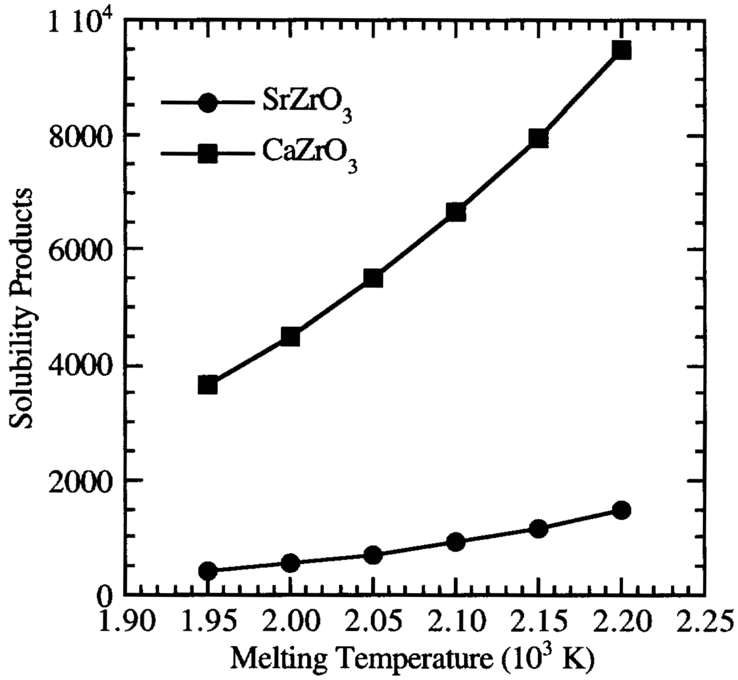

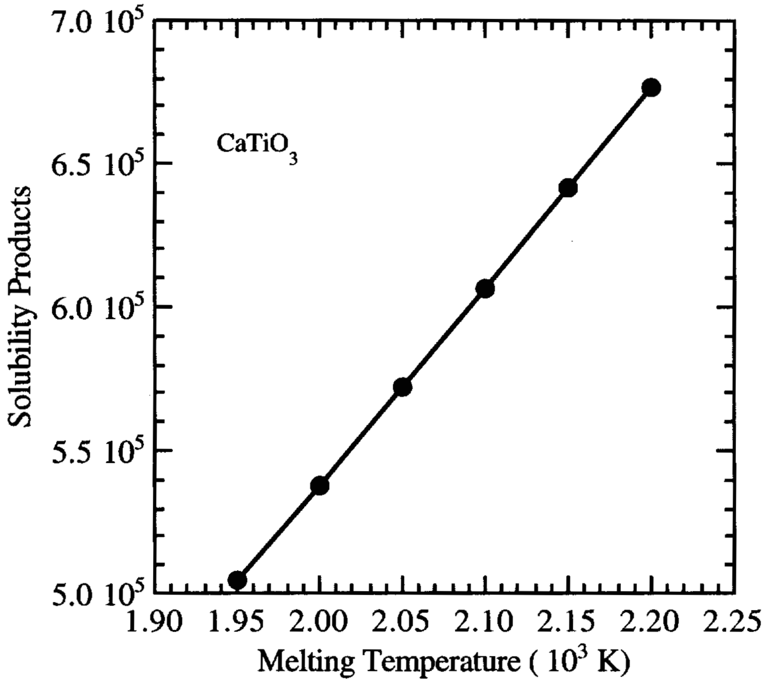

Figure 5.3 Solubility products of $SrZrO_3$, $CaZrO_3$ and $CaTiO_3$ in the form of [SrO] [Zr] $[O]^2$, [CaO] [Zr] $[O]^2$ and [CaO][Ti]$[O]^2$.

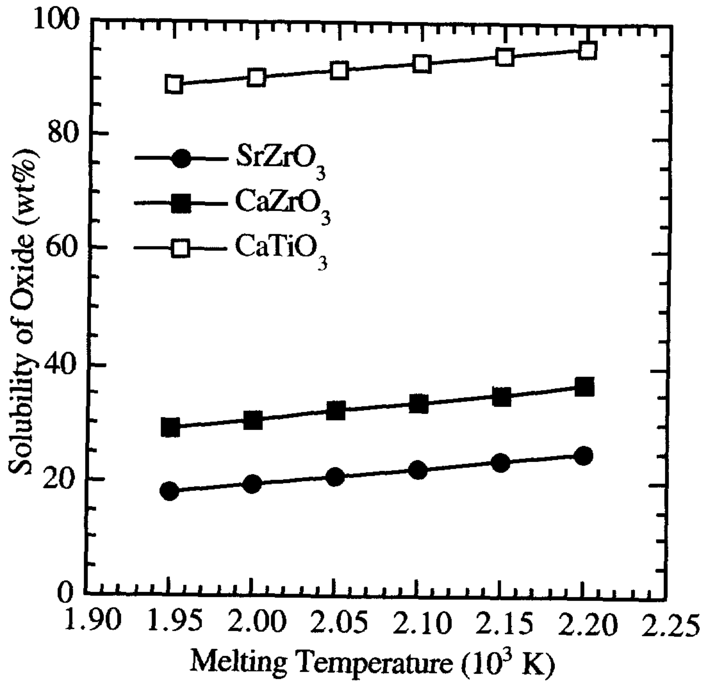

Figure 5.4 Solubility of complex oxides in molten titanium at different melting temperatures: $SrZrO_3$, $CaZrO_3$ and $CaTiO_3$.

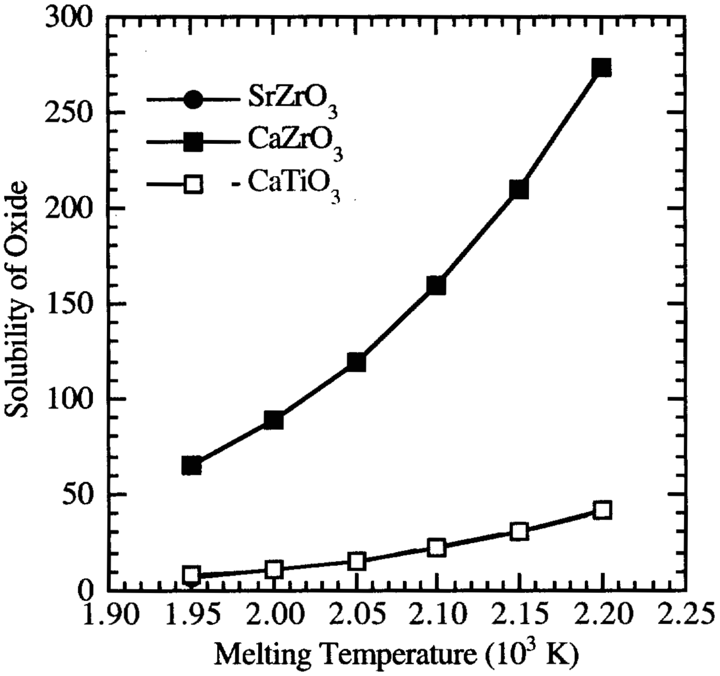

Figure 5.5 Solubility products of $SrZrO_3$, $CaZrO_3$ and $CaTiO_3$ in the form of [SrO][ZrO_2, [CaO] [ZrO_2] and [CaO][TiO_2].

$CaTiO_3$ have a lower free energy than $CaZrO_3$, which make the former two oxides have a lower solubility at this decomposition mode.

THE OXYGEN ACTIVITY DEPENDENCE OF INTERFACE REACTION BETWEEN MOLTEN TITANIUM AND OXIDE

There are three types of coating degradation mechanisms: dissolution, reaction and erosion. The dissolution mechanism has been studied by evaluating the solubility of single and complex oxides in liquid titanium. For the reaction mechanism, in order to study a balanced complex-oxide formation reaction between liquid Ti and CaO, the oxygen activity dependence of complex oxide formation at the liquid Ti/CaO interface was explored further by equilibrium thermodynamic calculations. The overall reactions are:

$$Ti\ (l) + 2\underline{O}_{Ti(l)} + CaO = CaO{\bullet}TiO_2(l) \qquad (63)$$

$$Ti\ (l) + O_2\ (g) + CaO = CaO{\bullet}TiO_2(l) \qquad (64)$$

where $2\underline{O}_{Ti(l)}$ denotes oxygen in solution in liquid Ti and O_2 (g) denotes oxygen in furnace atmosphere.

The standard free energy of formation of $CaO{\bullet}TiO_2$ involving gaseous reactant oxygen is shown below:

$$Ti\ (s) + O_2\ (g) + CaO = CaO{\bullet}TiO_2\ (s) \qquad (65)$$

$$\Delta G_{65} = -1030350 + 177.41\ T \qquad (J/mol) \qquad (66)$$

The activity coefficient of oxygen in liquid titanium are not available from direct experimental measurement. However Hu et al,(68) and Liang and Schuster(69) analyzed the deoxidization equilibrium in Fe-Ti-O, Co-Ti-O and Ni-Ti-O and recommended the standard free energy of solution of oxygen in molten Ti:

$$O_2\ (g) = 2\underline{O}_{Ti(l)} \qquad (67)$$

$$\Delta G_{67} = -1098000 + 170.2\ T \qquad (68)$$

$$Ti(s) = Ti\ (l) \qquad (69)$$

$$\Delta G_{69} = \Delta H_f - T\ \Delta S_f = \Delta H_f\ (1 - T/T_m) = 17500 - 9.02\ T \quad (J/mol) \qquad (70)$$

where ΔH_f is the heat of fusion of Ti (17.5 kJ/mol) and T_m is the melting point of Ti (1943 k).

Because reaction (63) is equal to reaction (65) - reaction (67) - reaction (69)

$$\Delta G_{63} = \Delta G_{65} - \Delta G_{67} - \Delta G_{69} = 50150 + 16.43T \qquad (71)$$

From reaction (63) the CaO and $CaO{\bullet}TiO_2$ are in their standard status and thus have unit activity. The molten Ti is also assigned unit activity although its solubility for oxygen is high (Raoultian limit). At equilibrium the standard free energy of reaction (63) can expressed in terms of an equilibrium constant, which is the reciprocal activity of oxygen dissolved in the molten Ti

$$\Delta G_1 = -RT\ln K = -RT\ \ln\ (\ a_{CaO{\bullet}TiO2} \,/\, a_{CaO}\ a_{Ti(l)}\ a^2_{\underline{o}}) = 2RT\ \ln\ a_{\underline{o}} \qquad (72)$$

Solving for $a_{\underline{o}}$ with equations (71) and (72) yields the equilibrium oxygen activity for $CaO{\bullet}TiO_2$ formation during Ti melting in CaO crucibles, expressed in at. %

$$(at\ \%)\ a_{\underline{o}} = \exp\ (3016/T + 0.988) \qquad (73)$$

For a CaO crucible used for Ti melting, the equation (73) and Figure 5.6 indicate that there is a threshold oxygen activity, which decreases with increasing melting temperature. Below a threshold activity, oxygen-containing Ti is stable, and no crucible and molten Ti reaction occurs. Above the threshold the $CaTiO_3$ is stable, molten Ti will react with CaO to form $CaTiO_3$.

Figure 5.6 also shows that the threshold oxygen activity is very high, about 13 at% at the titanium melting point (1943 k). At present industrial and laboratory melting conditions, CaO will not react with molten Ti, which is supported by several experiments.(21,63) On the other hand, when $CaTiO_3$ is used as a crucible coating for Ti melting, it will decompose to single oxides CaO and TiO_2. Because TiO_2 has very high solubility in molten Ti, it will contaminate molten Ti seriously. The experimental work has proved this prediction.

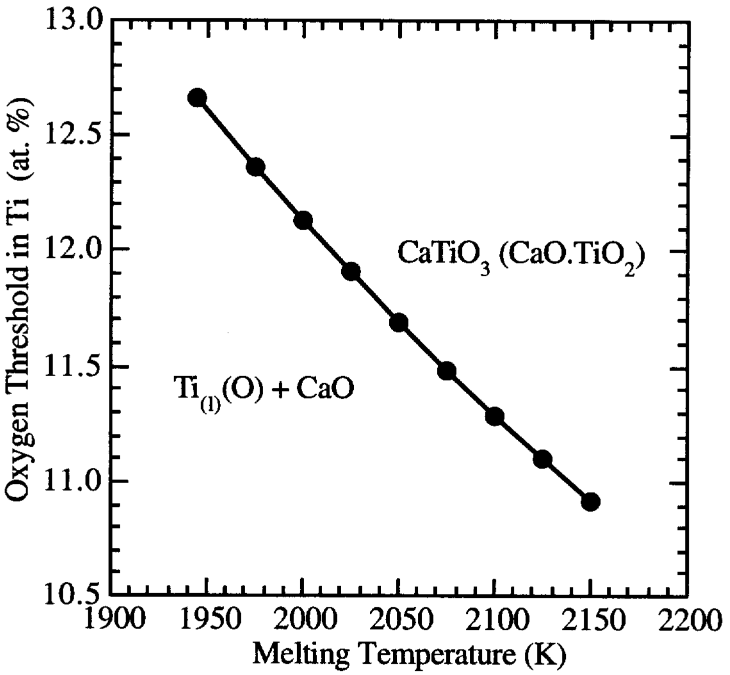

Figure 5.6 Plot showing the calculated threshold oxygen activity dependence of $CaTiO_3$ formation at the molten titanium and CaO coating interface.

CHAPTER 6

COMPARISON OF EXPERIMENTAL RESULTS AND THEORETICAL ANALYSIS AND DISCUSSION

DISCUSSION OF THERMODYNAMIC ANALYSIS

When titanium is melted in yttrium oxide crucibles, the liquid titanium will be saturated with yttrium oxide. The solubility product can be calculated from the oxygen and yttrium contents after melting and compared with the Hoch's work (equation (5.1)) and current work (equation (5.27)). The pertinent data are shown in Table 6.1.

Table 6.1 Experimental and theoretical results of solubility product of Y_2O_3 in liquid titanium

Conditions	Composition after Melting		Solubility Product in Liquid Ti		
	O ppm	Y wt%	Exp.	Equ. 5.1	Equ. 5.27
A-55 Rod (200 g), Induction-susceptor melted in fully oxidized Y_2O_3 for 1 min. at 2003 k under 1/3 atm helium(5)	2900	0.9	0.141	0.196	0.906
A-55 Rod (200 g), Induction-susceptor melted in partially reduced Y_2O_3 for 1 min. at 2003 k under 1/3 atm helium(5)	2800	0.9	0.134	0.196	0.906
A-55 Rod + 1.2% Y (200 g). Arc-cast in water-cooled copper 2.5 min. under 1.3 atm helium (1943 k)(5)	1550	1.2	0.074	0.147	0.677
A 200 g charge in Y_2O_3 by a vacuum arc furnace for 5 min. furnace at 1963 k under 0.5 atm.(28)	1100	0.05	0.0577	0.163	0.748
A 30 g charge in fully oxidized Y_2O_3 for 5 min. at 1998 k in a resistance heated furnace under 1 atm Ar.(9)	5608	1.92	0.806	0.195	0.886
in Y_2O_3 by a resistance heated vacuum furnace for 10 min. at 2045 k(27)	6200	0.72	0.352	0.245	1.102

For a very short melting time (1 minute), the solubility product of current theoretical work is higher than Hoch's and is slightly higher than the experimental data. For a little bit long time (5 or 10 minutes), the experimental data is lower than current theoretical calculation, but higher than Hoch's calculation, shown in Table 6.1. Although there are some differences between current calculations and experimental data, an order of magnitude agreement has been achieved. This is a very good agreement, and several reasons can be used to explain the difference. First, 5 or 10 minutes is not sufficient for dissolving the equilibrium concentration of the Y_2O_3 oxide, and longer melting makes the better match, shown in Table 6.1. Griesenauer(5) showed that longer melting (from 1 to 8 minutes) can significantly help the dissolution of Y_2O_3 oxide in liquid Ti (also in Table 6.1). Second, it should be pointed out that the oxygen contents reported for the melted samples were obtained by vacuum fusion techniques and considered to be below actual levels. The fusion bath temperature of 1950°C is probably too low to take all the Y_2O_3 particles into solution for reduction by carbon. This theory was substantiated by analyses of high purity metal having known levels of oxygen by intentional additions of Y_2O_3 particles, found to contain far less oxygen than intentionally added.(5) So the solubility equations can be used to predict the solubility of oxides in liquid Ti.

According to Equation (5.22), Table 2.8 and Figures 5.1 and 5.2, compared to heat of fusion, melting point and atomic weight of metal constituent, etc., the free energy of formation of single oxide is a dominant influencing factor on its solubility in molten Ti. The lower the free energy of formation of oxide, the lower its solubility is. We shall see that this feature is extremely useful, which makes the selection of single refractory oxide straight-forward. However when the free energy of two oxides is similar, other factors including heat of fusion, melting point and atomic weight of metal constituent have to be considered. If the rate of dissolution of oxides is very slow, the compound still can be considered as potential candidate, even although it has a little high solubility.

In molten Ti the solubility of the single oxide is not always consistent with that of its metal constituent. For example, thorium has a high solubility in molten titanium, maximum is about 86.5% wt. However, ThO_2 has very low solubility in molten titanium, as shown in Figures 5.1 and 5.2. The reason is that the solubility of a metal in a liquid is dependent on its heat of fusion (ΔH_f), melting temperature (T_m) and the difference between the heat capacities of solid and liquid forms of the metal (ΔC_p).(70) A metal having a higher melting point and/or lower heat of fusion is less soluble at given temperatures than one having a lower melting point. However the solubility of its oxide in this liquid is dependent on not only heat of fusion, melting temperature (T_m) and the difference between the heat capacities of solid and liquid forms of the metal constitute, but also mainly free energy of formation of the oxide.

The larger difference between the molar heat capacities (C_{pl} and C_{ps}) for metal constituent in liquid and solid states also can exert some effect on the solubility of single oxide. For CaO, if the difference is not considered, the relationship between solubility and melting temperature is

$$(wt\,pct\,Ca)(wt\,pct\,O) = exp(18.99 - 31.03/T) \qquad (1)$$

The difference between Equations 5.24 and 6.1 is about 20%. So in some cases, for greater accuracy, we may consider the difference between the molar heat capacities (C_{pl} and C_{ps}) for metal constitutes in liquid and solid forms.

THERMODYNAMIC ANALYSIS IN SINGLE OXIDE CRUCIBLES

Of all the oxides tested in the experiments, Y_2O_3 demonstrated the greatest potential as the most possible containment material for molten Ti. It has excellent degradation resistance (stability) based on low solubility, low reactivity and mechanical strength at temperature. No degradation of Y_2O_3 coating was observed. Analysis of the titanium matrix with EDS analysis showed no detectable contamination of yttrium and the its oxygen contamination to titanium is the lowest. The thermodynamic analysis in Table 2.8 shows that of all the oxides, Y_2O_3 has the lowest free energy. Figures 5.1 and 5.2 indicated that Y_2O_3 has the lowest solubility in molten titanium. Y_2O_3 has all the properties a refractory material needs to have for effective containment of molten titanium:

- The lowest free energy
- Very low solubility of Y_2O_3 and Y in molten Ti
- High melting point

These outstanding characteristics make Y_2O_3 the most stable oxide. Many experiments showed that Y_2O_3 has the highest stability against molten Ti in all the studied crucible compounds.(2,5,9,28) Figures 5.1 and 5.2 showed that the solubility of Y_2O_3 increases very slowly with melting temperatures, which is the sign that overheating will not affect the contamination very much. However, in ceramic crucibles, at high superheats (> 100°C) under conditions where the crucible temperature is equal to or greater than liquid temperature, yttria reacted and contaminates liquid titanium.(8) Further study is needed to give the maximum reacted overheating for plasma-sprayed Y_2O_3 crucibles. All the experimental results confirmed that the thermodynamic approach was reasonable.

The disadvantage of Y_2O_3 is its low thermal shock resistance and the potential for mechanical instability due to inappropriate processing. Based on experimental work, it should be possible to effectively eliminate or minimize these potential problems. Through increased densification and heat treatment mechanical strength, thermal shock resistance can be improved. Also, proper heating and cooling of the crucible will help to minimize the thermal shock.

The experimental results showed that Y_2O_3-stabilized ZrO_2 coating degraded completely and titanium was contaminated severely. Therefore Y_2O_3-ZrO_2 can not be used as a container material. In current tests, CaO-stabilized ZrO_2 faired better than Y_2O_3 stabilized ZrO_2. For CaO stabilized ZrO_2 crucible there was a 0.3 - 0.4 mm Zr contamination zone in titanium, which was thinner than that in the Y_2O_3-ZrO_2 crucible This phenomenon is difficult to explain using thermodynamic analysis because both compounds have similar free energy, composition and melting point, and the only differences are the stabilizing compounds Y_2O_3 and CaO. However, the CaO stabilized ZrO_2 coating was also degraded. EDS elemental analysis showed a high Ti content in most of the CaO stabilized ZrO_2 coating. The experiments showed that CaO-ZrO_2 coating may be used as a molten Ti container material, but not for long duration and/or higher melting temperatures. Additional experiments would be needed to determine precise limits and degradation rates. In both CaO-ZrO_2 and Y_2O_3-ZrO_2 coatings, the degradation mechanism was dissolution.

Table 2.8 indicated that of all studied oxides ZrO_2 has higher free energy, which only little bit lower than that of $CaTiO_3$. Of all single oxides, ZrO_2 has the highest solubility in molten titanium, and it increases fast with melting temperature, shown in Figures 5.1 and 5.2. These are the thermodynamic reasons that ZrO_2 degraded by dissolution mechanism. Domagala et al(56) found that the maximum solubilities of ZrO_2 in ß-Ti and α-Ti are about 17 and 40 %wt respectively, and the solubility of Ti in ZrO_2 at 1700°C is about 5 %wt. Rue reported that Ti contents up to 4 atomic % were retained in substitutional solid solution in ZrO_2, ZrO_2 contents up to approximately 10 mole % were retained in solid solution in Ti, and no evidence of compound formation was observed at any composition.(19) Previous experiments also showed that ZrO_2 crucibles in contact with molten titanium degraded quickly and seriously contaminate titanium.(28,56,64) The current and previous experimental results are in agreement with the thermodynamic analyses.

Degawa et al(21) reported that the oxygen contamination of Ti using calcia crucibles was caused by the reaction of molten titanium and low grade oxides, especially Fe_2O_3 and SiO_2. Contamination of Ca in titanium was about 0.002 - 0.005 %wt. The application of high purity fused calcia crucibles enabled the melting of titanium with less contamination by reducing the oxygen content in Ti below 0.2%. Prigent and Debuigne(63) reported that oxygen contamination of titanium cast in calcia crucibles could not be quantified by traditional methods of investigation such as metallography, micro-hardness and EPMA examination. The thermodynamic analysis above can also provide theoretical evidence for the results. The Table 2.8 and Figures 5.1 and 5.2 demonstrate that CaO has relatively lower free energy and a lower solubility in molten titanium, and is the third in the most potential compounds, following Y_2O_3 and ThO_2. Solubility of calcium in molten titanium is very low, only 0.0033 %wt. The thermodynamic analysis in chapter 5 also showed that because the threshold oxygen activity needed for reaction of CaO and molten titanium is very high (about 13% at), shown in Figure 5.6, CaO will not react with molten titanium. It is very difficult for a high purity CaO coating to degrade due to dissolution and reaction at normal industrial and laboratory melting conditions. No reaction and dissolution was found on the wall of a high purity CaO crucible after melting pure titanium, only a Ti penetration of approximately 1 mm into the wall was found.(21) The previous experiments showed that the dissolution rate of CaO appeared to be very slow. Thus a high purity CaO crucible has a high potential to contain molten titanium. Only concern is that, compared with Y_2O_3 and ThO_2, solubility of CaO in molten titanium increases a little bit faster with melting temperatures. Overheating of the melt must be carefully controlled so that the contamination can always be tolerated.

Prigent et al(63) reported that, in an induction melting system, a sample of titanium (5g) was placed inside a CaO crucible and to 1700°C. No reaction due to temperature increase was observed until 1660°C. Above this temperature, an important release of vapor was noted, with a bubbling of metal in the crucible. Holding times of 1, 2 and 3 minutes in the molten state have shown a hardness increase of about 50 HV for each additional minute of holding time. Molten titanium reduces calcium oxide, then oxygen diffuses into the liquid metal. The solubility of calcium in molten titanium is very low, and these atoms are in free states at temperatures above its boiling point (1440°C). This causes vapor releasing from the sample. Calcium hydroxide has been identified by X-Ray analysis of chamber deposits. The product of reaction between calcium and moisture air is calcium hydroxide.

However, for this experiment, several things have to be mentioned. According to the photos in the paper(63), the quality of crucibles appears poor. The failure of the Pr/Pt.Rh.10% thermocouple at the melting point of the titanium prevented a precise recording of the temperature of molten titanium. Due to the thermocouple being on the bottom of the crucible, measured temperatures could be lower than the actual. Vacuum conditions (vacuum or inert gas protection) was not mentioned in the paper. Even with these questions and problems, the experimental results are still useful in verifying the thermodynamic analysis in Chapter 5. Overheating of the CaO must be controlled; overheating will damage a CaO crucible and contaminate molten titanium. Second, the solubility of CaO in molten titanium is relatively low, but is still higher than that of Y_2O_3 and ThO_2, long holding times will increase the contamination in molten titanium. A short holding time is strongly recommended for a CaO crucible.

THERMODYNAMIC ANALYSIS IN COMPLEX OXIDE CRUCIBLES

Previous experimenters have concentrated on single metallic oxides as potential crucible candidates. This is because it is more difficult to find or calculate the free energy of formation of multicompounds and their solubility in molten titanium. In this experiment, multicompounds have been evaluated. It was decided to expand into multicompounds because of several reasons. The calculations in Table 2.8 indicate that some multicompounds have lower free energy, and higher melting temperatures (except for $CaTiO_3$). Figures 5.3 and 5.4 indicated that some of complex oxides such as $SrZrO_3$ have a much lower solubility in molten titanium than HfO_2 and ZrO_2 although the solubility of $SrZrO_3$ is still higher than those of Y_2O_3, ThO_2 and CaO. Additional considerations include the lower solubilities of some constitute elements such Sr and Ca in titanium, 0.011% wt for Sr, which can lower dissolution potential of zirconium for multicompounds like $SrO{\cdot}ZrO_2$ ($SrZrO_3$) and $CaO{\cdot}ZrO_2$ ($CaZrO_3$).

Of all of the multicompounds, $SrZrO_3$ performed best in contact with molten titanium and is another potential candidate. At 1760°C for 30 minutes, there was a little coating degradation in $SrZrO_3$ coatings. Titanium only penetrated into $SrZrO_3$ coating 0.04 mm, which could be improved by decreasing the coating porosity. Its oxygen contamination to titanium was the second lowest in all tested refractory compounds. Its degradation was a dissolution of the compound, and mainly zirconium and oxygen diffused into molten titanium. Like Y_2O_3, the performance of $SrZrO_3$ can be attributed to not only its lower free energy (Table 2.8), lower solubility (Figures 5.3 and 5.4) and higher melting point (2973 K), but also lower free energy of formation from the constituent oxides to complex oxides (Table 5.2). Of all the complex oxides, $SrZrO_3$ has lowest solubility in molten titanium, and it has lower free energy that only trails that of Y_2O_3, ThO_2 and CaO. In addition, a low zirconium content in the compound and the low solid solubility of titanium in strontium (SrO) and of strontium in titanium may partly account for the observed superiority of $SrZrO_3$ over $CaTiO_3$ and $CaZrO_3$, Y_2O_3 -ZrO_2 and CaO-ZrO_2. Previous material selection(8,21) was only based on simple thermodynamic stability considerations. Recently, both thermodynamic stability of compounds and solubility were utilized in the compound selection. However, only the solubility of the metallic species in molten titanium was used. The solubility of titanium in ceramic coating is also an important factor. If this solubility is high, coating melting temperature will decrease severely, and the coating will peel off and degradation will be stimulated. In practice, the titanium solubilities in ceramic compounds are difficult to be found or calculated, so solid solubility of titanium in the metallic species are usually used as the basis for compound selection.

Of three complex oxides, $CaTiO_3$ had the worst performance. Several reasons were responsible to this experimental result. Firstly its high free energy (Table 2.8) and high solubility (Figures 5.3, 5.4 and 5.5) make $CaTiO_3$ dissolve into molten titanium. Secondly, the thermodynamic analysis in chapter 5 (Figure 5.6) showed that in such melting conditions, $CaTiO_3$ would react with molten titanium and decompose into CaO, Ti and O. Both of mechanisms made $CaTiO_3$ coating degrade very fast, and it contaminated titanium severely. No doubt its low melting point (2248 K) is another factor.

For $CaO \cdot ZrO_2$ ($CaZrO_3$), the coating degradation was also relatively severe, and dissolution was the main mechanism because its solubility is high (Figures 5.3 and 5.4) and the free energy of formation of $CaZrO_3$ for its component binary oxides CaO and ZrO_2 is high (Table 5.2). However, the $CaZrO_3$ performed better than $CaTiO_3$ and Y_2O_3-ZrO_2 due to a lower free energy and lower zirconium content in the compound. Despite this it can not be used to contain molten titanium.

For melting of TiAl compounds, although the melting temperature only increase from 1785 to 1870 K, the $CaZrO_3$ crucible still contaminated TiAl compound severely. Many inclusions could be found in the TiAl sample (Figure 4.24), high zirconium content was detected by EDS (Figure 4.25); $CaZrO_3$ coating began to peel off and went into melt. Because the melting point of aluminum is only about 870 K, melting temperature 1785 K is very high for aluminum, and can make aluminum ions very reactive and susceptive to oxidation. $CaZrO_3$ coatings are not stable enough to resist high reactivity of TiAl compound.

DEGRADATION MECHANISMS OF CRUCIBLE COATINGS

In general, there were three degradation mechanisms: erosion, reaction and dissolution. In a Brew high temperature controlled atmosphere furnace, only a stagnant melt pool was obtained, so erosion was not a factor. Experiments showed that between the other two mechanisms, dissolution is the primary degradation mechanism. In most cases, at elevated temperatures, coating compounds will dissolve to different degrees, depending on their free energy of formation, melting temperatures, holding times and vacuum conditions. The oxygen and metal components of coating compounds will diffuse into molten active metals. The diffusion coefficient of oxygen in molten titanium is very high. If high contents of oxygen and metal components in molten reactive metals or alloys, inclusions will be found,(5,23) usually the compositions of inclusion are similar to that of coating compound. Molten reactive metals will also diffuse into coatings through porosity. So the coatings with higher density, lower porosity are preferred. For CaO crucibles, the situation is little different. The solubility of calcium in molten titanium is low (0.0033 %wt at 1067 K, shown in Table 2.8) and its boiling point is only 1440°C. Unlike the oxidation of titanium in the solid state, the crucible reaction is almost entirely interfacial, with a rapid elimination of the reaction products: oxygen by dissolution into the molten titanium and calcium by vaporization.(63) All of these experiments showed that solubility factors are very important for selection of refractory materials, especially for similar free energy of formation of oxides.

For some compounds with higher free energy of formation, such as $CaTiO_3$, reaction mechanism also played a role in degradation of coatings. $CaTiO_3$ has a very high solubility in molten titanium, as shown in Figures 5.3, 5.4 and 5.5. Figure 5.6 also shows that at the melting temperature of titanium $CaTiO_3$ is not stable and will decompose, which will worsen degradation process of coatings.

A GENERAL APPROACH FOR SELECTION OF REFRACTORY COMPOUND

The experimental results and discussions show that a thermodynamic analysis can explain experimental results. More importantly, it can be used to choose potential crucible compounds for a specific reactive metal. Selection procedure should first examine the free energy of formation of refractory compounds which must be lower than those of corresponding phases of the specific reactive metal (oxides, nitrides, borides and carbides), depending on types of refractory compounds. The free energy data is the most important factor for selection of potential compounds. The lower the free energy, the better the stability. However, because the stability does not fully follow the free energy data,(28) other important factors have to be considered. Secondly, solubility of refractory compounds in the molten reactive metal need to be calculated. The lower the solubility of refractory compounds, the better their stability and lower contamination level in the molten reactive metal. Finally for reasons of mechanical stability, the melting point of the compound should be higher than the temperature of the superheated titanium. The higher the melting point, the more stable the compound. Generally, this procedure can be used for all the reactive metals.

COMMERCIALIZATION OF CONTINUOUS CASTING OF REACTIVE METALS

Due to reactivity, high melting point and the high viscosity of molten titanium, and other reactive metals, the primary concern with continuous casting of titanium and other reactive metals is the ability of crucible materials to withstand the rigors of prolonged exposure needed for processing the molten metal. A stable, mechanically sound and low contamination crucible is required for long duration production while a low erosion rate ensures proper chemistry control which is important for ultimate properties of the material.(1) Crucible material selection and crucible fabrication are critical bases for the transfer of continuous casting from steel industry to reactive metals industry. In this respect, the experimental results were extremely encouraging. The Y_2O_3 and $SrZrO_3$ compounds showed potential to be the sufficiently stable crucible materials to withstand the rigors of the application. Plasma spraying technology could fabricate Y_2O_3 and $SrZrO_3$ compounds into useful shapes, and enable fabrication of large crucibles.

In commercialization of continuous casting of reactive metals, both induction melting and plasma melting can be chosen as a local heat source. The major advantage of induction melting is the continuous stirring process which helps to bring undesirable volatile elements to the surface and thereby facilitates the refining process.(71) The main advantage of plasma melting is that it minimizes the loss of volatile alloy elements.(71) Plasma melting is used for making titanium-alloy ingots, nickel-based powders, niobium-based superconducting alloys and a number of other special metal applications. Plasma melting also provides an effective method for recovering machine turnings of titanium alloys and other special metals. Contamination by cutting oil and by fragments of tool bits can be effectively removed by plasma hearth melting.(72) No matter in what kind of design, the measurement and control of the temperature of molten reactive metals will be important and necessary. It is desirable to have a melting design approach with good control of temperature and low contact time of molten reactive metals with the crucible material. Crucible material selection and crucible fabrication, several critical questions(1) need to be answered before the technology will be ready for commercialization. An effective model needs to be developed which will allow the technology to move economically into different forms (plate, sheet, tubes, etc.) and different reactive metals materials. Monitoring and controlling process is critical so that smooth and continuous operation will be guaranteed for a commercial scale process. Finally, demonstration of the technology on a sufficient scale is needed to insure the viability of the concept.

FUTURE WORK

In spite of a great deal of progress during this experiment, a number of issues still needed to be addressed in the future:

1. Consistent experimental conditions are still difficult to achieve. This problem can be attributed primarily to the effect of secondary contamination from graphite base material. it is imperative to eliminate the graphite crucible. The suggested method would be to use a reusable refractory metal such as molybdenum or tungsten as the backing material.

2. Some work is needed to improve thermal shock resistance of several potential crucible compounds, namely Y_2O_3 and $SrZrO_3$. This will become an increasingly important issue as the size of the crucible is scaled to production.

3. The actual mechanisms of degradation are still open to analysis, the degradation rates of Y_2O_3 and $SrZrO_3$ at different melting temperatures should be measured.

For some tolerable contamination limits in the reactive metals, the maximum melting temperature and holding time should be explored.

CHAPTER 7

CONCLUSIONS

1. A general thermodynamic procedure has been developed to choose potential crucible compounds for molten reactive metals, using free energy of compounds and their solubility in molten reactive metals as the most important factors for selection. The experimental results verified that the thermodynamic analyses can be used to not only choose potential compounds, but also explain experimental results.

2. Plasma spraying technology has been developed and implemented which effectively allows the rapid evaluation of a wide range of crucible materials. In addition, this coating technology can allow to exploration of the use of alloy additions to strength and resist both mechanical and chemical degradation of molten titanium during real process conditions.

3. Experimental results and thermodynamic analysis showed that Y_2O_3 has the highest stability and lowest oxygen contamination for contact with molten titanium, which confirmed the importance of Y_2O_3 as a containment material. Its disadvantage is a lower thermal shock resistance.

4. A new compound, $SrZrO_3$, was identified as another potential candidate that showed real possibility for containment of molten titanium. At 1760°C for 30 minutes, a low zirconium content but no detectable strontium were found in titanium, and the oxygen contamination was the second lowest. Titanium

penetrated into $SrZrO_3$ coating only 0.04 mm, which can possibly be improved by increasing coating density.

5. CaO-stabilized ZrO_2, Y_2O_3-stabilized ZrO_2, $CaTiO_3$, and $CaZrO_3$ crucibles were eliminated as candidates because these compounds severely contaminated titanium.

6. Three degradation mechanisms of ceramic coating in contact with molten titanium or titanium aluminide were identified: dissolution, reaction and erosion; with dissolution causing the greatest damage.

7. A bond layer of molybdenum provided an effective barrier to carbon diffusion, and showed potential to replace the graphite base material which can contaminate titanium and its alloys.

REFERENCES

1. Oregon Metallurgical Corporation, *A New Process for the Continuos Casting of Reactive Metals*, Albany, OR, (1993).

2. Schuyler D. R., J. A. Petrusha, W. R. Keu, *Development of Titanium Alloy Casting Technology, AFML-TR-76-80*, Scientific Press, Princeton, NJ, (1976).

3. Degawa T., T. Ototani, "Refining of High Purity Ni-Base Superalloy Using Calcia Refractory," *Journal of Iron & Steel Institute of Japan*, 73, 1691-1697 (1987).

4. Degawa T., "Recent Development of High Purity Advanced Metal and Alloys Using Calcia Refining Process," *Proceedings of the Tenth International Conference on Vacuum Metallurgy,* p.54-64, Fu J., Ed., Metallurgical Industry Press, Beijing, China, (1990).

5. Griesenauer N. M., S. R. Lyon, C. A. Alexander, "Vacuum Induction Melting of Titanium," *J. Vac. Sci. Technol.*, 9 (6), 1351-1355 (1972).

6. Weber B. C., W. M. Thompson, H. O. Beilstein, M. A. Schwartz, "Ceramic Crucible for Melting Titanium," *Journal of the American Ceramic Society*, 40 (11), 363-373 (1957).

7. Finlay W. L., J. A. Snyder, "Effects of Three Interstitial Solutes (Nitrogen, Oxygen, and Carbon) on Mechanical Properties of High-Purity Alpha Titanium," *J. Metals*, 188, 277- 286 (1950).

8. Lyon R. L., S. Inouye, A. Alexander, D. E. Niesz, "The Interaction of Titanium with Refractory Oxides," *Titanium Science and Technology, Proceedings of the 2nd International Conference,* p.271-284, Jaffe R. I., H. M. Brute, Eds., Plenum Press, New York, NY, (1973).

9. Helferich R. L., C. A. Zanis, *An Investigation of Yttrium Oxide as a Crucible Material for Melting Titanium, AD-754 092*, Naval Research and Development Center, Annapolis, Maryland, (1973).

10. Garnier M., I. LeClercq, P. Paillere, J. F. Wadier, "The Cold Crucible Continuous Casting," *Proceeding of the Sixth International Iron and Steel Congress*, p.260-266, Iron and Steel Institute of Japan, Nagoya, Japan, (1990).

11. Gaspar T. A., L. E. Hackman, "Direct Cast Titanium Alloy Strip," *Sixth World Conference on Titanium,* p.739-743, Les Editions de Physique, Cannes, France, (1988).

12. Eastwood L. W., C. M. Craighead, *Refractories for Melting Titanium,* AFML-TR-6218, Part I, Air Force Materials Laboratory, OH, (1950).

13. Eiseuberg M., J. Stavrolakis, *Investigation of Refractories Suitable for Melting Titanium and Its Alloys*, U.S. Air Force, Air Research and Development Command, WADC Tech. Report, (1953).

14. Crandall W. B., K. D. Scheffer, C. H. McMurtry, R. B. Burdick, *Exploratory Research in Field of Container Materials for Titanium*, Watertown Arsenal Report (Final Report), AD 60587, (1955).

15. Parker D. W., G. L. Kutner, "HVOF Moves into the Industrial Mainstream," *Advanced materials & Processes*, 146 (7), 31-35 (1994).

16. Weber B. C., H. J. Garrett, F. A. Mauer, M. A. Schwartz, "Observation on the Stabilization of Zirconia," *Journal of the American Ceramic Society*, 39, 197-207 (1956).

17. Garfinkle M., H. M. Davis, " Reaction of Liquid Titanium with Some Refractory Compounds," *ASM Trans.*, 48 (4), 520-530 (1965).

18. Eastman E. D., L. Brewer, L. A. Bromley, P. W. Gilles, N. L. Lofgren, "Preparation and Tests of Refractory Sulfide Crucibles," *ASM Trans.*, 34 (4), 128-134 (1951).

19. Ruh R., "Reactions of Zirconia and Titanium at Elevated Temperatures," *Journal of the American Ceramic Society*, 46, 301-307 (1963).

20. Koch R. K., J. L. Hoffman, M. L. Transue, R. A. Beall, *Casting Titanium and Zirconium in Zircon Sand Molds*, Bureau of Mines, Washington, (1977).

21. Degawa T., K. Kamata, Y. Yoneda, "Melting and Precision Casting of Pure Titanium Using Calcia," *Sixth World Conference on Titanium,* p.707-713, Les Editions de Physique, Cannes, France, (1988).

22. Nakamura T., T. Togaya, S. Tani, K. Ida, T. Degawa, "High Temperature Wetting of Molten Pure Ti on Several Ceramic Crucible Materials for Dental Casting," *Proceedings of International Congress on Dental Materials,* p.328-329, The Metallurgical Society, Honolulu, (1989).

23. Degawa T., K. Kamata, Y. Nagashima, "The Effect of Oxygen Content and Surface Contamination on Mechanical Properties of TiAl Precision Castings," *Proceedings of International Symposium on Intermetallic Compounds (JIMIS- 6),* p.1003-1008, The Japan Institute of Metals, Semdai, Japan, (1991).

24. Sikka V. K., "Commercialization of Nickel Aluminides," *High Temperature Aluminides and Intermetallics*, p.505-520, Wang S. H., C. T. Liu, D. P. Pope, J. O. Stiegler, Eds., The Minerals, Metals & Materials Society, (1990).

25. Sordelet D. J., T. W. Ellis, "Evaluation of Plasma Arc Sprayed Refractory Metal Crucible Coatings for Containing Molten Ceramic Oxides," *Proceedings of the 1993 National Thermal Spray Conference*, p.643-648, ASM International, Anaheim, CA, (1993).

26. Zanis C. A., R. L. Helferish, *Investigation of Coated Graphite Crucibles for Induction Melting of Titanium*, Report 8-949, Navy Ship Research and Development Center, (1971).

27. Holcombe C. E., T. R. Serandos, "Consideration of Yttria for Vacuum Induction Melting of Titanium," *Metallurgical Transactions*, 14B (9), 497-499 (1983).

28. Saha R. L., T. K. Nandy, R. D. K. Misra, K. T. Jacob, "On the Evaluation of Stability of Rare Earth Oxides as Face Coats for Investment Casting of Titanium," *Metallurgical Transactions*, 21B (6), 559-566 (1990).

29. Koger J. W., C. E. Holcombe, L. G. Banker, "Coatings on Graphite Crucibles Used in Melting Uranium," *Thin Solid Films*, 39, 297-303 (1976).

30. Bird E. L., C. E. Holcombe, "Investigation of Plasma-Sprayed Laminates for High Temperature Melting Operations," *Thermal Spray: International Advances in Coatings Technology, Proceedings of the International Thermal Spray Conference*, p.625-629, Berndt C., Ed., ASM International, Materials Park, OH, (1992).

31. Verhoeven J. D., W. A. Spitizig, F. A. Schmidt, P. D. Krotz, E. D. Gobson, "Processing to Optimize the Strength of Heavily Drawn Cu-Nb Alloys," *J. Mat. Sci.*, 24, 1015-1020 (1989).

32. Ellis T. W., D. J. Sordelet, F. C. Laabs, "Evaluation of Plasma Sprayed Crucible Coatings for Melt Processing Copper-Refractory Metal Alloys," *Proceedings of the International Thermal Spray Conference & Exposition*, p.631-636, ASM International, Orlando, (1992).

33. Frazier W. E., J. S. J. Chen, "The Melt Spinning of Gamma Titanium Aluminides," *JOM*, 44, 52-55 (1992).

34. Brown R. A., "Making Investment Shell Molds Inhibited against Reaction with Molten Reactive and Refractory Casting Metals," *U. S. Patent No. 3,743,003 (CI. 164/16 B22C),* Rem metals corporation, Albany, OR, (1973).

35. Waldron R. D., "Solid Solution Ceramic Materials," *U. S. Patent No. 4,014,706 (CI. 106-55, CO 4B 35/000),* Research Enterprises Corporation, Phoenix, AZ, (1977).

36. Moreau C., M. Lamontague, P. Cielo, "Influence of the Coating Thickness on the Cooling Rate of Plasma-Sprayed Particles Impinging on a Substrate," *Thermal Spray Coatings: Properties, Processes and Applications, Proceedings of the Fourth National Thermal Spray Conference*, p.237-243, Berneki T. F., Ed., ASM International, Materials Park, OH, (1991).

37. Smith R. W., R. Knight, "Thermal Spraying I: Powder Consolidation - from Coating to Forming," *JOM*, 47, 32-39 (1995).

38. Kushner B. A., E. R. Novinski, "Surface Treatments and Castings for Friction and Wear Control," *ASM HANDBOOK, Vol. 18, Friction, Lubrication and Wear Technology*, p.829- 833, Henery S. D., Ed., ASM International, Materials Park, OH, (1992).

39. Clare J. H., D. E. Crawmer, "Thermal Spray Coatings," *Metals Handbook,* Vol. 5, p. 361-374, Wood W. G., Ed., ASM International, Metals Park, OH, (1994).

40. Murray J. L., *Phase Diagrams of Binary Titanium Alloys*, ASM International, Metals Park, OH, (1987).

41. Ingham H. S, A. P. Shepherd, "Plasma Flame Process," *Flame Spray Handbook,* Vol. III, p.5-15, Metco Inc., (1965).

42. Nakahira H., Y. Harada, K. Tani, "Influence of Microstructure on the Morphology of Mirror-Finished Thermally Sprayed Coatings," *Thermal Spray Research and Applications, Proceedings of the Third National Thermal Spray Conference*, p.581-586. Berneki T. F., Ed., ASM International, Materials Park, OH, (1990).

43. "Thermal Spraying," *Welding Handbook,* Vol. 3, p.368-393, Kearnsm W. H., Ed., American Welding Society, Miami, FL, (1994).

44. Steffens H. D., K. H. Busse, G. Matthaus, " Arc Spraying of Steel and Cored Wires," *Advances in Thermal Spray, Proceedings of the Eleventh International Thermal Spray Conference,* p.457-466, Pergamon Press, Welding Institute of Canada, Montreal, Canada, (1986).

45. Smith R. G., "The Basic Principles of Detonation Coating," *Science and Technology of Surface Coatings*, p.271-297, Chapman B. N., Ed., Academic Press, London, (1974).

46. Kharlamov Y. A., "Detonation Spraying of Protective Coatings," *Materials Science and Engineering*, 93, 1-37 (1987).

47. Mc Murchie D., *Development of A 1080 Steel Plasma Sprayed Coating for Slide/Roll Wear Condition*, Ph.D. Thesis, Oregon Graduate Institute, Portland, OR, (1996).

48. "Plasma Deposition Processing," *Plasma Processing of Materials*, p.79-104, National Materials Advisory Board, Commission on Engineering and Technical Systems, (1994).

49. Ingham H. S., A. J. Fabel, "Comparison of Plasma Flame Spray Gases," *Welding Journal*, 54 (2), 101-105 (1975).

50. Scholl M., P. Clayton, "Abrasive and Erosive Wear of Some Hypervelocity Air Plasma Sprayed Coatings," *Thermal Spray Coatings: Properties, Processes and Applications, Proceedings of Fourth National Thermal Spray Conference,* p.39-52, Berneki T. F., Ed., ASM International, Materials Park, OH, (1991).

51. Scholl M., P. Clayton, E. Elmore, J. Wooten, "Sprayforming by High-Power High-Velocity Plasma Spraying," *Thermal Spray Coatings: Properties, Processes and Applications, Proceedings of the Fourth National Thermal Spray Conference,* p.281-288, Berneki T. F., Ed., ASM International, Materials Park, OH, (1991).

52. Nightingale R. E., "Various Forms of Carbon," *Fundamentals of Refractory Compounds*, p.203-228, Hausner H. H., M. G. Bowman, Eds., Plenum Press, New York, (1968).

53. Nightingale R. E., H. H. Yoshikawa, H. H. W. Losty, "Physical Properties," *Nuclear Graphite*, p.117-194, Nightingale R. E., Ed., Academic Press, New York and London, (1962).

54. Condon J. B., C. E. Holcombe, "Kinetics of the Yittria-Carbon Reaction," *High Temperature Science*, 18, 79-95 (1984).

55. Stanley J. T., *Development of Containment Material for the Reactive Metal Industry*, Report to Oregon Metallurgical Corporation, Albany, OR, (1994).

56. Domagala R. F., S. R. Lyon, R. Ruh, "The Pseudobinary Ti-ZrO_2," *Journal of the American Ceramic Society*, 56 (11), 584-587 (1973).

57. Ahtee A., M. Ahtee, A. M Glazer,, A. W. Hewat, "The Structure of Orthorhombic SrZrO3 by Neutron Powder Diffraction," *Acta Cryst.*, B32, 3243-3246 (1976).

58. Ahtee M., A. M. Glazer, A. W. Hewat, "High-Temperature Phases of $SrZrO_3$," *Acta Cryst.*, B34, 752-758 (1978).

59. Kubaschewski O., W. A. Dench, "The Free-Energy Diagram of the System Titanium-Oxygen," *Journal of the Institute of Metals*, 82, 87-91 (1953).

60. Komarek K. H., M. Silver, *Thermodynamics of Nuclear Materials*, International Atomic Energy Agency, Vienna, (1962).

61. Gingerich K. A., "Gaseous Metal Nitrides II: The Dissociation Energy, Heat of Sublimation, and Heat of Formation of Zirconium Mononitride," *J. Chem. Phys.*, 49, 14-18 (1968).

62. Hoch M., "Solubility of Y_2O_3 in Liquid, Solid Ti and Commercial Ti Alloys," *Titanium Science and Technology*, p.1431-1438, Lutjering G., V. Zwicker, W. Bunk, Eds., Deutsche Gesellschaft Fur Metallkunde, Oberursel, Federal Republic of Germany, (1984).

63. Prigent S., J. S. Debuigne, "A New Calcia Technology for Investment Casting of Titanium Alloys with the Lost Wax Process," *Titanium'92 Science and Technology*, p.1519-1526, Froes F. H., I. Captan, Eds., TMS, San Diego, CA, (1992).

64. Barin I., O. Knacke, *Thermochemical Properties of Inorganic Substances*, Spsenger-Verlag, New York, Berlin, Heidelberg, (1977).

65. *JANAF Thermochemical Tables*, U.S. National Bureau of Standards, Michigan, (1971).

66. *The Oxide Handbook*, IFI/Plemum Data Corporation, New York, (1973).

67. Wicks C. E., F. E. Block, *Thermodynamic Properties of 65 Elements - Their Oxides, Halides, Carbides, and Nitrides*, Bureau of Mines, Albany, OR, (1963).

68. Hu D. C., W. W. Liang, E. S. McCormick, "On the Solubility of Oxides in Liquid Alloys Containing Titanium," *Proceedings of Fourth International Conference on Titanium*, p.3019-3029. Kimura H., O. Izumi, Eds., The Metallurgical Society of AIME, Warrendale, PA, (1980).

69. Liang W. W., W. Schuswter, "Solubility of Oxides in Liquid Alloys Containing Titanium and Zirconium," *Trans. Japan Inst. Metals*, 23, 368-377 (1982).

70. Hildebrand J., R. L. Scott, *The Solubility of Nonelectrolytes*, Dover Publications Inc., New York, (1964).

71. Sen S., D. M. Stefanescu, "Melting and Casting Process for High-Temperature Intermetallics," *JOM*, 43, 30-31 (1991).

72. Eschenbach R. C., "Plasma Arc System for Waste Treatment and Metal Recovery," *JOM*, 48, 49-52 (1996).

BIOGRAPHICAL NOTE

The author was born on October 13, 1963 in Jilin, People's Republic of China. He graduated from Northeast University of Technology with a Bachelor of Engineering degree in Materials Science in 1984 and a Master of Engineering degree in Materials Science in 1987. He worked as an Assistant Professor and Instructor at Northeast University of Technology from 1987 to 1992. He then joined the Department of Materials Science and Engineering of Oregon Graduate Institute of Science & Technology to pursue a Ph.D. degree.